Support structure of an aluminium offshore wind turbine development of a conceptual design

Ritoe, S.R.

Award date:
2016

Support Structure of an Aluminium Offshore Wind Turbine

Development of a conceptual design

Master's Thesis

Student:	Stephany Ritoe Department of the Built Environment Architecture, Building and Planning - Structural Design
Graduation committee:	prof. dr. ir. J. Maljaars ir. B.W.E.M. van Hove dr. ir. H. Hofmeyer
Date:	03-08-2016

A thesis of S.R.Ritoe for completing the Master phase at the Department of the Built Environment, Eindhoven University of Technology. Graduating as a Structural Engineer at the unit Architecture, Building and Planning - Structural Design.

A – 2016.147

Name	Stephany Ritoe
Address	Frederiklaan 175E
	5616 NG Eindhoven
Phone nr	+31 642356191
E-mail	s.r.ritoe@student.tue.nl
ID-nr	0715906
Date	03-08-2016
Graduation committee	prof. dr. ir. J. Maljaars
	ir. B.W.E.M. van Hove
	dr. ir. H. Hofmeyer

Abstract

The support structures of wind turbines are mostly made of steel. However, there is a trend towards lighter weight systems. So far, only research has been done to lightweight rotors and nacelle, since this weight is multiplied throughout the wind turbine (SAPA, 2013). Though, the weight of the support structure is also significant since it exists of 60% of the weight of the wind turbine (Ancona D. and McVeigh J., 2001). A steel support structure may not be the most optimal solution, therefore an alternative is considered in this thesis, namely a structure assembled from aluminium extruded sections. Besides being lightweight, aluminium is also less sensitive to corrosion than steel, has a high end-of-life value, is easy to recycle and provides design flexibility by making use of extrusion technique. Of course, there are also downsides of using aluminium for offshore support structures assembled from extruded sections. For example, higher sensitivity to stability problems and ower fatigue strength.

The aim of this Master's thesis is to develop a conceptual design for a support structure of an aluminium offshore wind turbine and determining if this is a more optimal solution for offshore wind turbines than one made of steel. An 8MW steel offshore wind turbine with a height of 125m is analyzed, located in the Dutch sector of the North Sea, which has a water depth of approximately 20 meters. The location is outside any sailing routes and earthquake, snow and ice loads are not relevant here. The mono pile is a suitable structure for this water depth. The aluminium alternative will be located at this site, therefore the same loads are applied, making a proper comparison possible. The tower should have a design life of 20 year, and must have adequate fatigue strength to reach this design life.

In order to achieve an optimal design, some design limits are stated. The conceptual design was reduced to the design of the tower component of the wind turbine. Besides, applying extrusion technique leads to a limit on the dimensions of the extruded parts.

The overall structural form of the aluminium tower is a conical tube, which has become the predominant form for wind towers over the past decade. To realize this conical shape, small parts are cut off diagonally of either side of the extruded parts. When assembled, the radius at the top will be smaller than at the bottom. The horizontal cross-section is radially divided into 30 extruded parts, connected by welding and mechanical fastening.

A tower with a diameter of 6m at the bottom satisfies the unity checks, although resonance will occur. Several solutions are suggested. To determine which material provides the most optimal solution, a comparison is made between the steel and the aluminium design on the following aspects: (1) structural weight, (2) manufacturing process, (3) weld volume, (4) material usage, (5) resonance behavior and (6) fatigue strength.

A conclusion can be drawn that an aluminium tower does not lead to a more optimal solution for offshore wind turbines. It appears that the aluminium design does satisfy the bearing capacity, but will fall short in terms of fatigue.

Preface

This report is the result of a Master's thesis on the 'development of a conceptual design for a support structure of an aluminium offshore wind turbine' at Eindhoven University of Technology.

I would like to take this opportunity to thank all those who supported me and contributed directly or indirectly to this thesis.

First of all, I would like to express my appreciation to my graduation committee: Prof. dr. ir. J. Maljaars, ir. B.W.E.M. van Hove and dr. ir. H. Hofmeyer for their guidance, advice, time and most of all patience. Their knowledge and feedback (often online) have played an important role in the completion of this thesis.

Additionally, I would like to thank my fellow students who became my closest friends over the years who stood by me during the ups and downs. Special thanks to Lin Luu, for being 'my person', for her moral support and especially for her patience during the last few months. Furthermore, I thank Benny Ng for his constant flow of advice, concerning everything. And last but not least, I want to express my sincere gratitude to my mother and sister for their support and understanding during my whole study career.

Table of contents

List of symbols

A_{eff}	effective section area	[mm²]
A_{haz}	area of HAZ	[mm²]
A_{rotor}	swept area	[mm²]
A_V	shear area	[mm²]
b_{haz}	extent of HAZ	[mm]
C_D	static drag coefficient	[-]
C_D'	dynamic drag coefficient	[-]
$C_D{}^*$	drag coefficient in breaking waves	[-]
C_I	inertia coefficient	[-]
C_p	power coefficient	[-]
C_T	thrust coefficient of the rotor	[-]
C_w	coefficient dependent on the shape of the object	[-]
$C_{w,tower}$	shape drag coefficient	[-]
d	water depth	[m]
DAF	Dynamic Amplification Factor	[-]
D_{bottom}	diameter at the bottom	[mm]
D_{top}	diameter at the top	[mm]
D_{rotor}	diameter of the rotorblades	[mm]
E	modulus of elasticity	[N/mm²]
f_0	characteristic value of 0,2% proof strength	[N/mm²]
$f_{0,haz}$	0,2% proof strength in the HAZ	[N/mm²]
f_u	characteristic value of ultimate tensile strength	[N/mm²]
$f_{u,haz}$	ultimate tensile strength in HAZ	[N/mm²]
$f_{v,haz}$	limiting shear strength of HAZ	[N/mm²]
f_w	limiting strength weld metal	[N/mm²]
fs	eddy changes frequency	[Hz]
f_{1P}	rotor frequency	[Hz]
f_{3P}	blade passing frequency of three-bladed turbine	[Hz]
F_{blades}	dead load blades	[N]
$F_{breaking\ wave}$	breaking wave force	[N]
$F_{current}$	current load	[N]
F_{tower}	weight of the tower	[N]
F_w	resistance force of an object in a flowing medium	[N]
F_{wave}	wave load	[N]
$F_{wind,rotor}$	horizontal load exerted by the rotor blades	[N]
H	wave height	[mm]
H_b	breaking wave height	[mm]
i	radius of gyration about the relevant axis	[mm]
I	moment of inertia	[mm⁴]
l_e	embedded part of the tower	[mm]
l_t	total height of the tower	[mm]

l_s	submerged part of the tower	[mm]
K_D	correction coefficient for extent of drag force	[-]
K_I	correction coefficient for extent of inertia force	[-]
$M_{current}$	moment as a result of $F_{current}$	[Nmm]
M_{Ed}	design value of the bending moment	[Nmm]
M_{Rd}	design bending moment resistance	[Nmm]
M_{top}	moment as a result of the rotor blades	[Nmm]
M_{wave}	moment as a result $F_{breaking\ wave}$	[Nmm]
$M_{wind,rotor}$	moment as a result of $F_{wind,rotor}$	[Nmm]
$M_{wind,tower}$	moment as a result of $q_{wind,tower}$	[Nmm]
N_{Ed}	design value of the axial compression	[N]
N_{Rd}	design resistance for uniform compression	[N]
N_{cr}	elastic critical force for the relevant buckling mode	[N]
$q_{wind,tower}$	horizontal line load on tower as a result of wind	[N/mm]
R	rotor radius	[mm]
R_e	Reynolds number	[-]
rpm	revolutions per minute	[-]
S	number of Strouhal	[-]
S_d	correction factor for the position of $F_{breaking\ wave}$	[-]
$t_{towerwall}$	tower wall thickness	[mm]
t_w	wall thickness	[mm]
u	velocity of undisturbed current	[m/s]
v_r	rated wind speed	[m/s]
v_c	cut-out wind speed	[m/s]
V_{Ed}	design value of the shear force	[N]
V_{Rd}	design shear resistance	[N]
V_{tip}	the tangential speed of the tip of a blade	[m/s]
V_w	the actual velocity of the wind	[m/s]
W_{el}	the elastic modulus of the gross section	[mm^3]
$W_{el,haz}$	effective elastic modulus of the gross-section	[mm^3]
W_{net}	the elastic modulus of the net section allowing for holes and HAZ softening	[mm^3]

a	axial induction factor	[-]
α	imperfection factor	[-]
β	slenderness ratio	[-]
$\beta_1, \beta_2, \beta_3$	limits for slenderness parameters	[-]
ξ	damping ratio relative to critical damping	[-]
ε	strain	[%]
ϕ	value to determine the reduction factor χ	[-]
γ_f	load factor	[-]
γ_m	resistance factor	[-]
κ	factor to allow for the weakening effects of welding	[-]
λ	tip-speed ratio	[-]

λ_c	relative slenderness	[-]
λ_0	limit of the horizontal plateau of thee buckling curves	[-]
ρ	density	[kg/m^3]
ρ_{air}	density air	[kg/m^3]
ρ_{water}	density water	[kg/m^3]
$\rho_{0,haz}$	ratio between 0,2% proof strength in HAZ and in parent material	[-]
$\rho_{u,haz}$	ratio between ultimate strength in HAZ and in parent material	[-]
ν	kinematic viscosity	[m/s]
ω	rotor rotational speed	[r/s]
ω_0	factor for section with localized weld	[-]
χ	reduction factors for relevant buckling mode	[-]
Ω	ratio between applied and natural frequency	[-]

1. Introduction

1.1 Offshore wind

Wind energy has been utilized by humans for more than two thousand years. Windmills are a well-known example in the Netherlands, used for pumping water or grinding grain. Nowadays, energy demands are growing, making wind energy a mainstream source of energy. Converting wind energy into electrical energy is primarily done through the use of wind turbines. They operate as follows: as the wind blows, it flows over the airfoil-shaped blades, causing them to spin. The blades are connected to a drive shaft that turns a generator to produce electricity (BOEM, 2016).

Wind energy generating onshore meets part of the energy needs. Due to growing demands of renewable energy sources, it is becoming more and more difficult to find suitable onshore locations which are not already occupied. This made the relocation of wind turbines to offshore sites a natural step.

An advantage of offshore sites is the strong, consistent wind that can be found over the oceans. The potential energy produced from wind is directly proportional to the cube of the wind speed. This results in a significantly larger amount of electricity when the wind speeds are increased with only a few meters per second. For example, a turbine at a site with an average wind speed of 7m/s would produce 50% more electricity than at a site with the same turbine and average wind speeds of 2m/s. Pursuing offshore wind energy resources is therefore interesting for developers (BOEM, 2016). However, offshore wind turbines also have disadvantages, for example they are less accessible than onshore installations, which raises the operations and maintenance costs and possibly increases the downtime of the machines. Other advantages and disadvantages are mentioned in *Paragraph 2.2* of the *Literature Survey.*

1.2 Objective of this thesis

In this thesis a conceptual design for a support structure of an aluminium offshore wind turbine will be developed, located in the North Sea as shown in Figure 1.1 with a red dot. The IJ-geul Munitiestortplaats 1 is the most nearby measuring station where Rijkswaterstaat measures wind and waves. Site specific data is shown in Table 1.1.

The most common type of support structure so far is the mono pile. This is also the most suitable structure with a water depth of 20m. Therefore, the mono pile is the main focus point in this thesis. The support structures of wind turbines are nowadays mostly made of steel. However, also in this field there is a trend toward lighter weight systems. So far, only research has been done to lightweight rotors and nacelle, since the top mass dictates the necessary support structure and thus a reduction in this mass will have a direct impact on the total turbine cost. On the other hand, the weight of the support structure is also significant because it exists of 60% of the weight of the wind turbine (Ancona D. and McVeigh J., 2001). Moreover, roughly a quarter to a third of the costs of an offshore wind farm is in the support structure. Among that cost share, weight has a moderate direct contribution since also manufacturing and especially transportation and installation are of importance (Kühn, 1997).

Figure 1.1 Selected location in the North Sea (Wijngaarden, M., 2013)

Table 1.1 Water, wind, wave and current data for selected location (Wijngaarden, M. van, 2013)

Water depth (MSL)	20	[m]
HAT (high astronomical tide)	1.04	[m+ MSL]
MSL (mean sea level)	0.00	[m+ MSL]
LAT (low astronomical tide)	-1.03	[m+ MSL]
Storm surge 50 yr.	1.00	[m+ MSL]
Mean wave height	1.25	[m+ MSL]
Wave height 50 yr.	14.9	[m+ MSL]
Wave height 5 yr.	12.61	[m+ MSL]
Wave period 50 yr.	10.99	[s]
Wave period 5 yr.	10.02	[s]
Wind speed 50 yr.	42.04	[m/s]
Wind speed 5 yr.	35.95	[m/s]
Current velocity 50 yr.	2.1	[m/s]
Current velocity 5 yr.	1.0	[m/s]
Top transition piece	13.23	[m+ MSL]
Hub height	93.23	[m+ MSL]

So, a steel support structure may not be the most optimal solution; an alternative should be considered, for example a structure assembled from aluminium extruded sections.

An aluminium alternative may have the following advantages:

- Aluminium is less sensitive to corrosion than steel. Untreated aluminium has very good corrosion resistance in most environments, because it forms a thin but effective oxide layer

that prevents further oxidation. However, aluminium presents a greater risk of galvanic corrosion.

- High end-of-life value and easy to recycle due to the homogeneous composition, the low melting temperature and lack of paint, thus compensating for the relatively high initial energy cost (SAPA, 2013).
- Ease of inspection, since it is rust-free and does not need to be painted.
- The use of extrusions reduces the weld volume in comparison to full wall sections. It may be possible to use the friction stir welding process for at least large parts of the structure.
- The low self-weight of the structure eases installation.
- It may enhance the possibility of floating structures in deep see (this will not be researched in this thesis).
- Aluminium provides design flexibility by making use of extrusions through (SAPA, 2013):
  - Complex profile cross-section: allowing different parts and features to be integrated into the same profile.
  - Fewer parts and fewer production steps in assembly.

Of course, an offshore support structure made from aluminium extruded sections also has disadvantages:

- In case of cyclic loading, the low modulus of elasticity E (see Table 1.2) is responsible for the lower fatigue strength of aluminium, circa one-third of steel. This means that fatigue design should be considered more carefully than with steel structures (Höglund T. et al., 2014).
- The low Young's modulus E and low density ρ (see Table 1.2) make aluminium structures susceptible to vibrations and in these cases the dynamic behavior for the structure has to be considered (Höglund T. et al., 2014).
- The low Young's modulus E also causes a higher sensitivity to stability problems (Höglund T. et al., 2014).
- Creating a structure which is conical by means of extruded sections could be challenging. A good method to assemble this type of structure from aluminium extruded sections ought to be developed.

Table 1.2. Material properties aluminium and steel (Höglund T. Et Al., 2014)

		Aluminium	Steel
Density, ρ	kg m^{-3}	2,700	7,800
Young modulus, E	N mm^{-2}	70,000	210,000
Shear modulus, G	N mm^{-2}	27,000	81,000
Poisson ratio, v		0.33	0.3
Coefficient of linear thermal expansion, α	K^{-1}	23×10^{-6}	12×10^{-6}

So the problem that will be looked into this thesis is as follows:

How will a support structure from aluminium extruded sections be designed and is this a more optimal solution for offshore wind turbines than one made of steel?

To be able to give an answer to this question, the possibilities of using aluminium for an offshore wind turbine has to be researched. This is done by firstly reviewing the extrusion limits and frequency limits in *Chapter 2 Design limits*. The limits for extrusion profiles have to be determined in which the profile ought to be designed. The frequency limit includes both the excitation and natural frequencies. When the natural frequency approaches an excitation frequency, the lifetime of the structure will be influenced since the damage as a result of fatigue will be larger.

Then in *Chapter 3 Concept variants* possibilities concerning the overall tower design, as well as the profile section design will be looked into.

Finally, in *Chapter 4 Conceptual design*, a final design will be made for the 8.0MW wind turbine with the most optimal tower, profile and joint design. The loads acting on the support structure will be calculated, namely the wind loads that act on the tower, the wind loads exerted by the rotor blades, the current load and the wave load. Then the unity checks will be performed and the resonance behavior will be discussed. The last part of this chapter concerns the elaboration of two types of joints.

Chapter 5 Conclusion and discussion gives a brief summary and discusses the results.

In the final chapter recommendations will be suggested for further research.

2. Design limits

2.1 Components

First, a short description of an offshore wind turbine will be given. The five main components of the horizontal axis wind turbine are shown in Figure 2.1, which are the rotor, the nacelle, the tower, transition piece and mono pile. The tower, substructure and foundation together form the support structure. In this thesis, emphasis is placed on the tower. The dimensions for the mono pile are assumed, based on the tower's dimensions.

- The rotor consists of the rotor hub and the blades. The hub is the connection between the rotor blades and the rotating bar that goes into the nacelle.
- The nacelle holds all the turbine machinery. It must be able to rotate to follow the wind direction; it is therefore connected to the tower via bearings.
- The tower of wind turbine must absorb the huge static loads caused by the varying power of the wind.
- The transition piece connects the tower with the mono pile.
- The mono pile supports the nacelle and transfers all the loads to the seabed.

The components are explained in more detail in *Paragraph 2.1* of the *Literature Survey*.

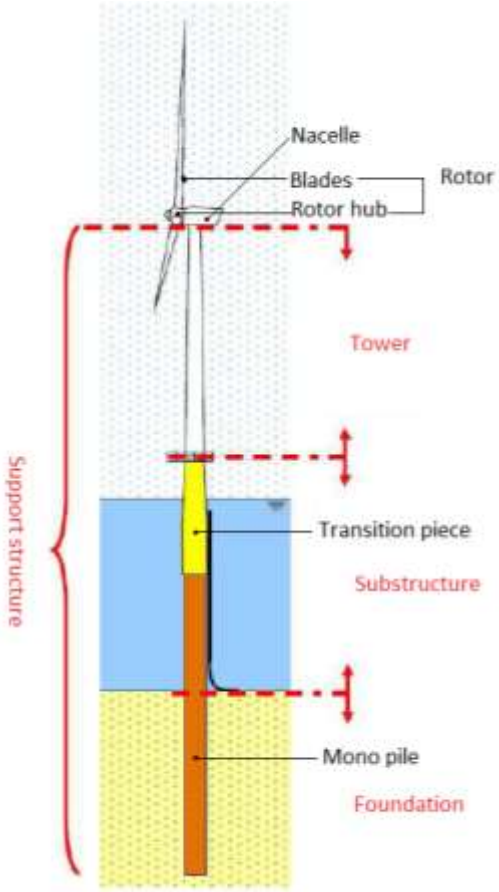

Figure 2.1 Components wind turbine

2.2 Extrusion technique

Now the possibilities of the profile section will be looked into. It is important to take the limits of extrusion technique into account. There are several suppliers which produce large extrusion profiles. Three suppliers (SAPA, Nedal Aluminium and one located in Qingdao, China) are featured in *Paragraph 3.3* of the *Literature Survey*.

When choosing an extrusion press and making an optimal design, transportation limits should be taken into account. For transportation on road, diameters up to 4,25m are possible and lengths up to 30m (with a trailer) (Gerritsen, 2015). When the tower is produced in Qingdao, China (near the seacoast), overseas transport is required. In this case, the dimensions are not limited. However, this is an expensive option. The best choice would be the using the 55MN extrusion press from Nedal Aluminium. The diameter of the tower can obviously not be extruded at once; the cross-section has to be divided in multiple equal extruded parts, connected radially as depicted in Figure 2.2. Figure 2.3 shows the extrusion press mouth limits. A profile width of 650mm to a corresponding height of 200 with extrusion lengths of 30m requires the least connections to manufacture the tower's cross-section.

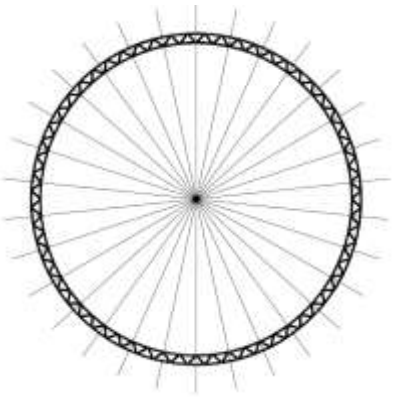

Figure 2.2 Tower cross-section divided radially for extrusion

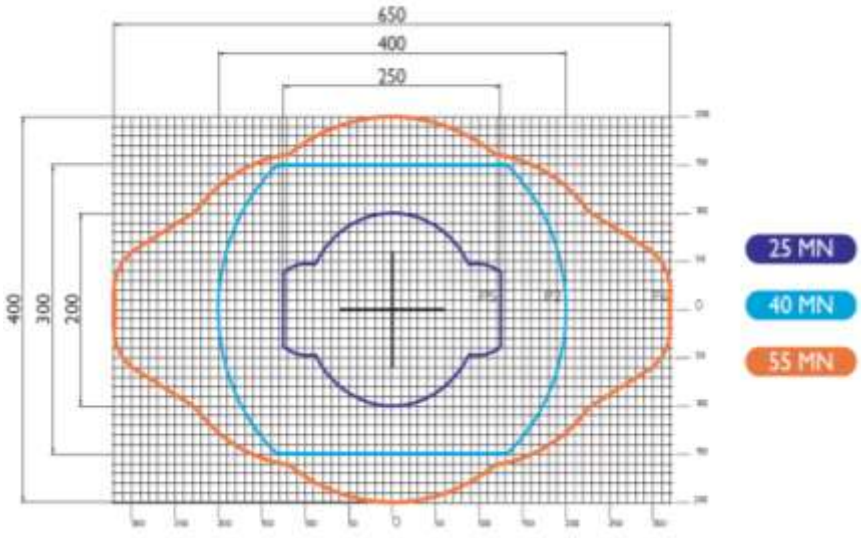

Figure 2.3. Limits for the extrusion press mouth (Nedal, 2015)

The extruded parts can be joined by adhesive bonding, mechanical fastening (bolts, rivets, etc.) or by using features that are integrated in the profile (snap-fits, hinges, etc.). Another way of joining two aluminium parts is by fusion welding or Friction Stir Welding. A combination of joining methods is also possible, the so called hybrid connections. The different methods are explained in the *Literature Survey*. There, the conclusion was made that the best method for joining aluminium parts for the wind turbine tower would be MIG welding in combination with integrated features. However, after the dimensions were optimized, only welding is a more suitable joining method for the extruded parts. This is explained in more detail in *Paragraph 4.5.1*.

2.3 Excitation and natural frequency

Excitation frequencies affect the dynamic response of the wind turbine. In order to prevent resonance, the natural frequencies of the structure should stay well away from the excitation frequencies. There are three different loads which cause four fundamental dynamic excitation frequencies:

- Current 0.0003Hz to 0.04 Hz
- Wind:
    - Rotor 0.08Hz to 0.203Hz
    - Blade passing 0.24Hz to 0,609Hz
- Waves 0.05Hz to 0.2Hz

2.3.1 Excitation frequencies as a result of currents

Since the support structure is located in a flowing medium, there is the possibility that the structure will vibrate as a result of fluctuating swirls (time-dependent turbulences) which arise behind the structure. This occurs when the Reynolds number is between 300 and $3 \cdot 10^5$ which is commonly applied for hydraulic structures. Due to the fluctuating swirls behind the object, a varying load

perpendicular to the current is applied on the object. The frequency of these eddy changes is (Aalst, W. van, 1984):

$$fs = \frac{uS}{D} \tag{2.1}$$

Where:

u	velocity of undisturbed current	[m/s]
S	number of Strouhal, describing the oscillation of liquids. With the aid of a graph and the Reynolds number $Re = \frac{U \cdot D}{\nu}$, the number of Strouhal can be determined. It can also be approached with the following formula: $S = 0{,}21 \cdot C_D^{-0{,}75}$	
D	characteristic diameter of the cylinder	[m]

If the excitation frequency, in this case the frequency as a result of the maximum current velocity, is larger than the natural frequency, resonance could occur.

The occurrence of swirls can be prevented by making the backside of the structure streamlined (provided that the current always has the same direction) or by making the section irregular so that the Strouhal number varies over the height (Aalst, W. van, 1984). This would also affect the current and wind loads.

2.3.2 Excitation frequencies as a result of the rotor and blades

The rotor frequency f_{1P}, also referred to as 1P, occurs as a result of the eccentricity of the rotor hub, see Figure 2.4. This means that the center of gravity is not situated exactly in the middle in relation with the axis, resulting in a dynamic force when the rotor rotates. The eccentricity could be a consequence of a small deviation in the rotor blades.

The blade passing frequency $f_{3P} = N_B \cdot f_{1P}$, occurs when a rotor blade passes the tower at a certain frequency which is N_B times larger than the rotor frequency. N_B represents the number of rotor blades.

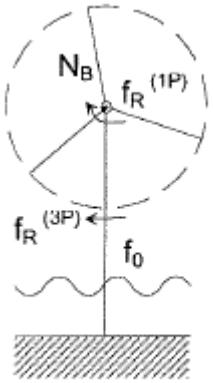

Figure 2.4 Rotor and blade passing frequency (Ginhoven, J. van, 2006)

The rotor frequency and blade passing frequency can be determined with the following formula (Tempel, 2006):

$$f_{1P} = \frac{\lambda V_w}{\pi D_{rotor}} = \frac{V_{tip}}{\pi D_{rotor}} = \frac{rpm \cdot \pi \cdot D_{rotor}}{60 \cdot \pi \cdot D_{rotor}} = \frac{rpm}{60} \tag{2.2}$$

$$f_{3P} = 3 \cdot f_{1P} \tag{2.3}$$

Where:

rpm	revolutions per minute	[-]
D_{rotor}	the diameter of the rotor blades	[m]
λ	Tip-speed ratio = $\frac{V_{tip}}{V_w} = \frac{\omega R}{V_w}$	[-]
	V_{tip} the tangential speed of the tip of a blade	[m/s]

V_w	the actual velocity of the wind	[m/s]
ω	the rotor rotational speed	[r/s]
R	rotor radius	[m]

The smallest frequencies are obtained during startup (3m/s), then the frequency increases until the wind velocity has reached the nominal wind velocity. From this moment on, the frequency is maximal and remains unchanged until eventually the cut out wind speed (25m/s for the 8.0MW) is reached (Ginhoven, J. van, 2006).

The rpm's for the 8.0 MW wind turbine are in the range of 4.8-12.2. Filling in these values in formulas (2.2) and (2.3) gives the following frequency ranges, which are also shown in Figure 2.6:

$$f_{1P,min} = \frac{rpm}{60} = \frac{4{,}8}{60} = 0{,}08Hz$$

$$f_{1P,max} = \frac{rpm}{60} = \frac{12{,}2}{60} = 0{,}203Hz$$

$$f_{3P,min} = 3 \cdot f_{1P} = 3 \cdot 0{,}08 = 0{,}240Hz$$

$$f_{3P,max} = 3 \cdot f_{1P} = 3 \cdot 2{,}03 = 0{,}609Hz$$

The most occurring wind velocity V_w gives a 1P frequency that must be known in order to calculate the Dynamic Amplification Factor (*Paragraph 4.4.2*), which will be calculated with the first part of formula (2.2). The tip speed ratio λ depends on the power coefficient C_p as can be seen in Figure 2.5. For the development of a conceptual design, a maximum power coefficient will be assumed, which leads to a tip speed ratio of 8.

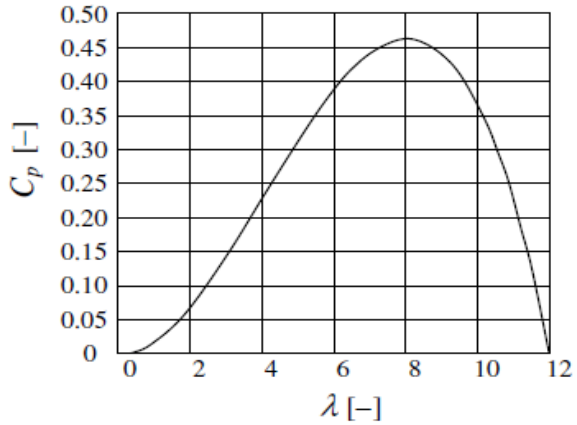

Figure 2.5 Typical C_p- λ curve (Tempel, J. van Der, 2006)

Now the rotor frequency f_{1P} can be calculated:

$$f_{1P} = \frac{\lambda V_w}{\pi D_{rotor}} = \frac{8 \cdot 10{,}61}{\pi \cdot 164} = 0{,}165Hz$$

And thus:

$$f_{3P} = 3 \cdot f_{1P} = 3 \cdot 0{,}165 = 0{,}495Hz$$

2.3.3 Excitation frequencies as a result of waves

Waves come with different frequencies; in general in a range in the 1P frequency range of the wind turbine. The frequency of this range is around 0,05Hz to 0,2Hz as indicated in Figure 2.6 with the blue curved line (Bhattacharya, S., 2014).

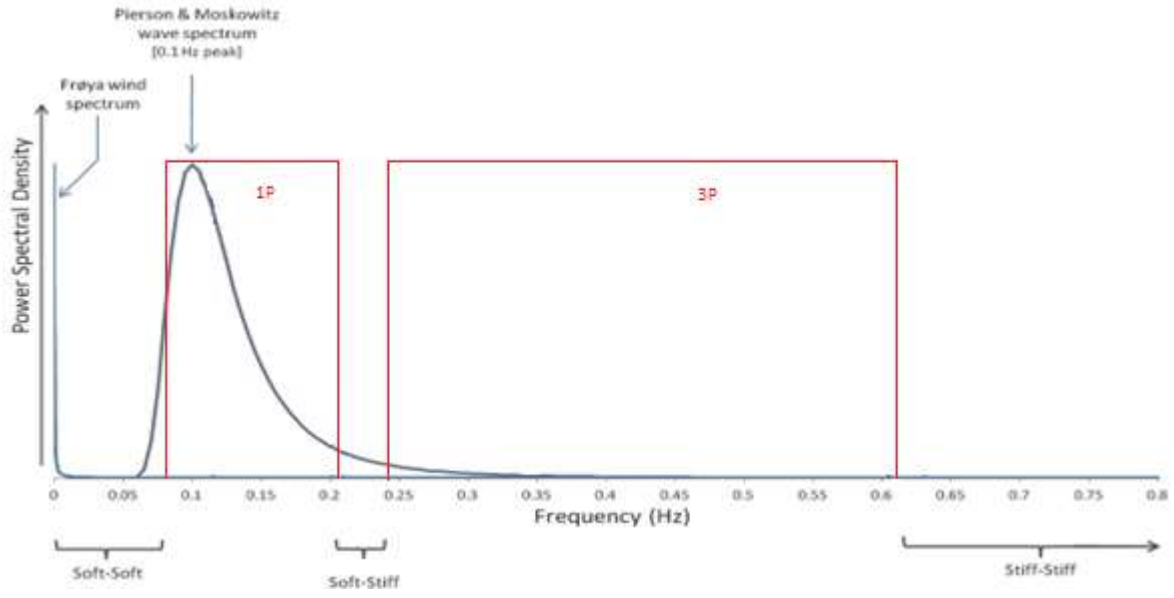

Figure 2.6 Frequency ranges of a wind turbine and waves (Bhattacharya, S., 2014 - edited)

2.3.4 Natural frequency

The support structure is likely to fail due to the large sinusoidal deformations resulting in fatigue. To avoid resonance, the structure should be designed in such a way that its natural frequency does not coincide with either 1P or 3P frequencies. As discussed in the *Literature Survey*, this creates three possible intervals and therefore three possible structures; a very stiff structure with a high natural frequency greater than 3P (stiff-stiff), a structure with a natural frequency between 1P and 3P (soft-stiff) and a very soft structure with a frequency less than 1P (soft-soft) (Kühn, 2001). These intervals are indicated in Figure 2.6 below the horizontal axis. In literature, the term soft is commonly used for flexible turbine systems.

Stiff-stiff structures are problematic due to the increase of wind induced fatigue. According to Kühn (1997) for this type of structure at least in the upper part flexibility should be introduced. Soft-stiff support structures should be possible for most sites, but not for all generic concepts. Problems may occur if the design range between the 1P and 3P frequencies is not large enough or the overall height is too large for the considered concept and stiffness. Soft-soft designs are economically interesting but susceptible to wave fatigue thus careful design is required. Relatively high stiffness in the foundation and submerged part of the support structure and a gradual decrease in stiffness from towards the top seem to be a possibility, certainly for locations with a moderate wave regime (Kühn, 1997).

3. Concept variants

Concept variants concerning the overall tower design and the profile sections design will be developed and optimized.

3.1 Tower variants

As mentioned in the *Literature Survey*, most steel towers are designed as conical circular beams. When a uniform cross-section along the length of the tower is applied, the unity check at the top is obviously lower than the check at the bottom due to the length-depending bending moment. Therefore, it would be more material efficient if the top has a smaller diameter than the bottom. Thus, for the aluminium alternative, a tubular design will be developed with a decreasing diameter towards the top.

In *Paragraph 2.2* it was mentioned that extruded parts with lengths up to 30m are possible. Therefore, it would be efficient if the tower is manufactured in several parts with this length. If the tower is cut into four parts, the total tower would be 120m high. To obtain the required height of 125m, the tower should be divided into five parts of 25m. This would not be cost-effective, so from here on a tower with a height of 120m is assumed.

The following two designs for a conical tower with a smaller diameter at the top could be considered (see Figure 3.1):

- A telescopic design, see left drawing in Figure 3.1. Here, the tower is divided into four parts with different diameters. Each part consists of multiple extruded profiles connected radially as seen from a horizontal section, see Figure 3.2. The jumps in diameter require extra attention, since a loss of strength is undesirable. For this alternative, calculations have been be made, which can be found in Appendix A.
- The obvious design here is a conical one, depicted on the right of Figure 3.1. Here each of the four parts also consists of multiple extruded profiles connected radially. However, the periphery formed at the top is lower than at the bottom of each of the four parts. This can be realized by cutting off small parts diagonally of either side of the extruded parts, see Figure 3.3. In this figure the extruded part is viewed enlarged for clarity.

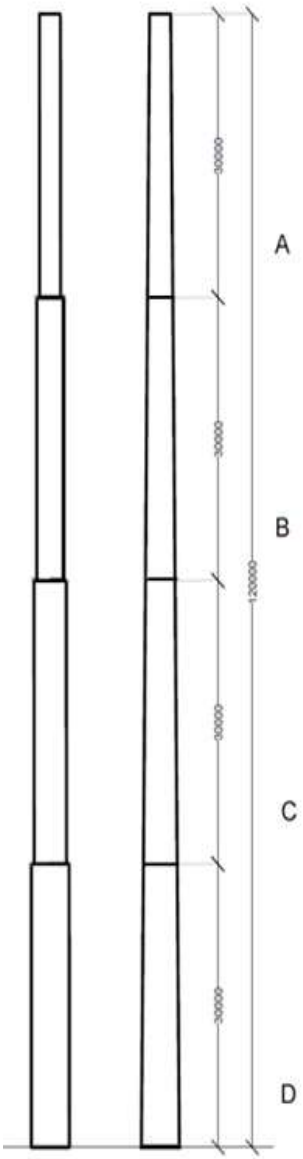

Figure 3.1 Tower designs; telescopic and conical

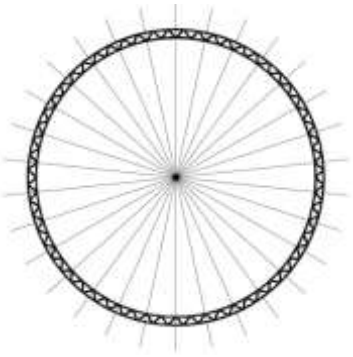

Figure 3.2 Tower cross-section divided radially for extrusion

Figure 3.3 extruded part with the to be removed part indicated (enlarged)

3.2 Profile variants

The most simplistic solution for the tower wall cross-section would look like the two variants shown in Figure 3.5; the masses should be moved to the outsides as much as possible. Since only a small part of the perimeter is depicted in this figure, the profiles are drawn straight. A possible connection between the tower walls can be realized by means of three-point connections in the structure, see Figure 3.4. When creating profile variants, it must be kept in mind that the profile should be dimensionally stable.

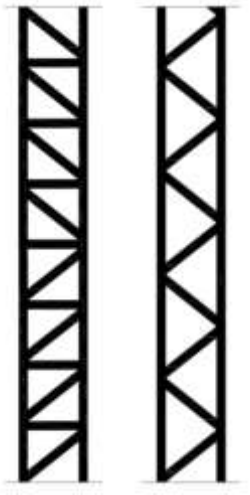

Figure 3.4 Two variants of the tower's cross -section

It is also possible to abandon the idea of a circular tower. A study has been done by Umut, O., Akbas B. and Shen J. (2011) to investigate the use of square cross-sections for wind turbine towers for different thickness and height as an alternative to circular cross-sections. It appears that it might be a possible alternative to commonly used circular cross-sections.

Another option is a Y-shaped profile like the floor plan of the Burj Khalifa, which provides an efficient structure, see Figure 3.5. The Burj Khalifa is an 828m high skyscraper located in Dubai. The hexagonal core, with six columns and structural walls made from high-performance concrete, serves to resist torsion due to heavy wind loads. Corridor walls extend from the central core to near the end of each wing, terminating in thickened hammer head walls. These corridor walls and hammer head walls behave similar to the webs and flanges of a beam to resist the wind shear and moments. Furthermore, perimeter columns and flat plate floor construction complete the system. This system can be used as a guideline to design a new profile section for the wind turbine tower (Baker, W.F. and Pawlikowski, J.J., 2009).

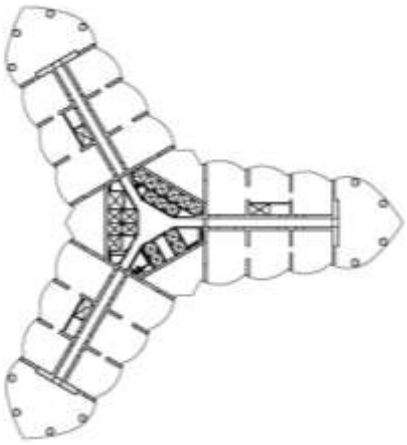

Figure 3.5 Y-shaped floor plan of the Burj Khalifa (Baker, W.F. and Pawlikowski, J.J.,

Figure 3.6 shows several basic alternatives for the wind turbine tower's cross-section, based on the floor plan of the Burj Khalifa. The profiles most likely need extra features in order to fulfill the desired requirements, for example a second wall and a connection between the two walls, in the same way as in Figure 3.4. These types of profiles will be studied further in order to determine whether they can be considered as a serious alternative. If this is the case, one conceptual design will be developed and calculations will be made to make sure the profile fulfills the requirements.

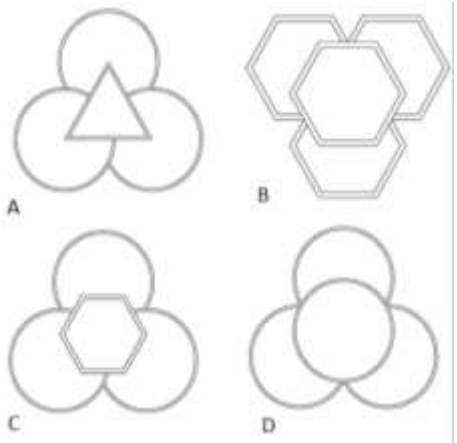

Figure 3.6 Basic alternatives for the tower's cross-section

3.2.1 Cross-sectional study

Based on the profiles of Figure 3.6, a profile is designed and compared with the initial cross-section (Figure 3.7A) for the 8.0MW wind turbine, see Figure 3.7B. The triangular connection between the two walls is not illustrated for convenience. The alternative design started with the cross-section of Figure 3.6D, consisting of three circular parts around the middle circle. Now extra circular parts are added. Each circle has a wall thickness of 50mm and a radius of 0,3 meter which is the maximum extrudable radius. In this case, only the circular parts have to be connected with each other, making a total of 16 connections. This cross-section can obviously not compete with the circular double walled cross-section which has a radius of 2,3m.

Figures 3.7 C and D shows cross-sections where an extra wall is added with an overall thickness of 25mm and 50mm respectively. This still is insufficient to fulfil the stiffness requirements, see Table 3.1. Adding even more circular parts will not be material efficient, since a lot of material is not situated at the outer side of the cross-section. A lot of material would be necessary to obtain a similar stiffness and also lots of connections will be necessary.

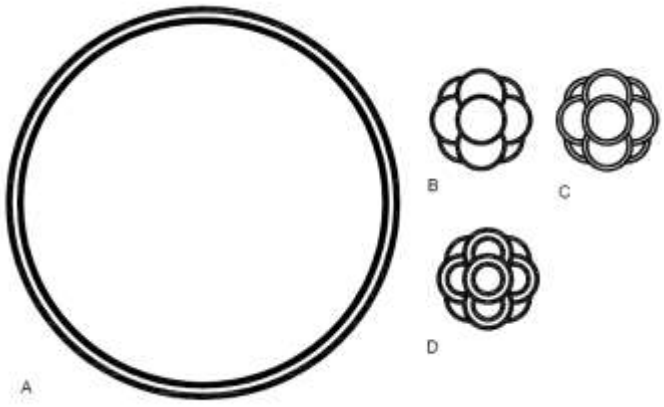

Figure 3.7 Alternative cross-sections (extrusion efficient)

Table 3.1 Comparison cross-sections of Figure 24

Cross-section	I [m⁴]	A [m²]
A	4,70	1,94
B	0,041	0,36
C	0,037	0,34
D	0,053	0,54

When this type of cross-section is enlarged, a more equal profile section will be obtained. However, the main reason for applying this type of profile is efficiency in the extrusion process. When the radius of the circles is increased to 2m, it is not possible to extrude a circle part at once. With the dimensions of Figure 3.8 B, more extrusion parts and therefore more connections will be necessary. The two profiles in Figure 3.8 do not have the same stiffness, see Table 3.2. Thus, the overall dimensions of cross-section B would exceed the dimensions of cross-section A to obtain the same stiffness. In conclusion, cross-section A is still the most suitable profile for further designs.

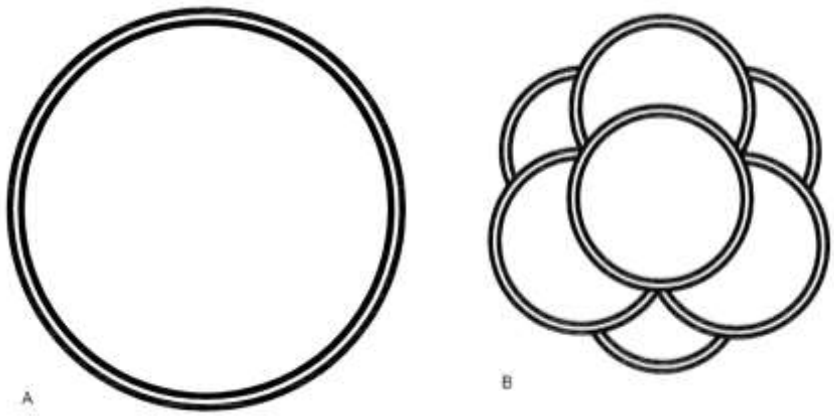

Figure 3.8. Alternative cross-section enlarged

Table 3.2. Comparison cross-sections of Figure 25

Cross-section	I [m^4]	A [m^2]
A	4,70	1,94
B	3,24	2,40

4. Conceptual design

In this chapter, a conceptual design for the 8MW aluminium offshore wind turbine will be developed. Based on the previous chapters, the design has the following starting points:

- Conical tower
- Circular hollow cross-section
- Double-walled
- Overall tower wall thickness of 200mm, which is the maximum possible with extrusion
- A total height of 120m
- Tower divided into four parts of 30m

Primary, some simplified calculations were done in order to achieve global dimensions.

First a design was made for a 3.6MW wind turbine to explore the possibilities in aluminium. A steel 3.6MW wind turbine from manufacturer Siemens was analyzed, see Table 4.1. The same height of this steel tower and rotor dimensions were appointed to the aluminium variant. It is important to mention here that only static calculations were made. The stresses at the top and bottom of the tower were checked. It showed possible to realize such a structure in aluminium, see Appendix B for the elaboration.

Thereafter, an aluminium design for an 8MW wind turbine was made. Also for this wind turbine, first an 8MW steel design from supplier Vestas was analyzed. This was done globally at first in order to get an idea of what kind of dimensions we are dealing with, see Appendix C. Afterwards, more accurate calculations were made, taking into account the Dynamic Amplitude Factor (DAF). When the overall dimensions were known, they were optimized. How this was done will be explained in *Paragraph 4.1*, which include a detailed description of the design. In *Paragraph 4.2* the cross-sections are classified. In *Paragraph 4.3* the loads are calculated. *Paragraph 4.4* gives the unity checks performed for the ultimate limit state and serviceability limit state and the resonance check. *Paragraph 4.5* discusses several joints of the wind turbine.

Table 4. 1 Data offshore wind turbine (Ginhoven, J. van, 2006)

Rated power	3.6	8.0	[MW]
Rpm range	8.0-13.0	4.8-12.2	[-]
Rotor diameter	100	164	[m]
Swept area	7854	21124	[m^2]
Hub height	70	125	[m]
Rotor, hub and nacelle mass	227	492	[ton]
Tower mass	335	480	[ton]
Diameter tower top	2.8	4.7	[m]
Diameter tower bottom	4.6	6.0	[m]
Wall thickness	54	75	[mm]
Annual mean wind speed	14	11	[m/s]
Cut-out wind speed	30	25	[m/s]

4.1 Optimization

A study has been done to optimize the dimensions of the tower. Four different tower diameters at the bottom were considered, namely 5, 6, 7 and 8 meters. The tower wall thickness is held constant at 200mm, since this is the maximum possible with extrusion. A requirement was the fulfillment of the flexural buckling check with a value around 0,9. Appropriate wall thicknesses were sought to satisfy this requirement. Now the different obtained designs are compared on the following criteria, see also Table 4.2:

- The first natural frequency, which should preferably be not located in the 1P frequency range
- The volume of the aluminium tower
- The area of the welds in one horizontal cross-section

Table 4.2 Comparison of different tower diameter, wall thicknesses and overall tower wall

D,bottom	5	**6**	7	8	[m]
t,towerwall	200	**200**	200	200	[mm]
t,w	50	**35**	25	20	[mm]
F.B check	0,90	**0,90**	0,91	0,87	[-]
Frequency f_1	0,111	**0,126**	0,134	0,147	[Hz]
Volume materal	124,41	**100,28**	81,05	72,38	[m^3]
Area of welds	0,1	**0,08**	0,07	0,06	[m^2]

A small diameter is desired to limit the amount of connections and in view of transportation; therefore the 5m and 6m will be compared. The tower with a diameter of 6m has a lower material volume. More welds are needed, but with a lower welded area since the wall thickness is smaller. Both natural frequencies are located in the 1P frequency range. Although, they do not conflict with the main applied frequency, which is 0,165Hz, resonance still arises for less occurring wind velocities. Several solutions are given in *Paragraph 4.5.2* So, a diameter of 6m seems to be the best choice, see Figure 4.1, which is also the diameter of the steel tower. Thus, an appropriate comparison can be made.

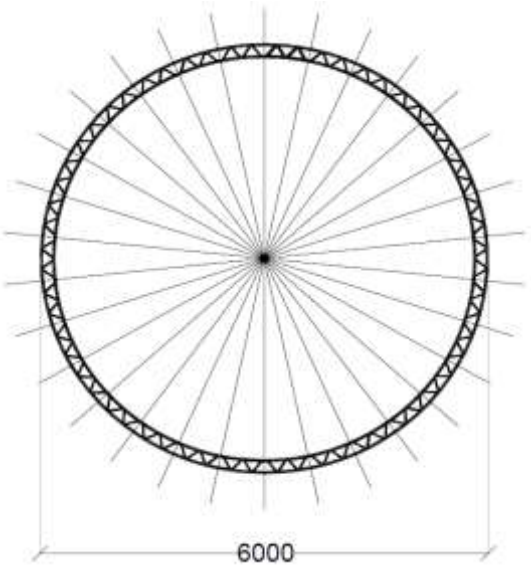

Figure 4.1 Horizontal cross-section of the 8MW wind turbine tower

While the dimensions of the extruded parts are constant, each tower part (see Figure 4.2) has a different diameter and thus exists of a different number of extruded parts, see Table 4.3.

Table 4.3 Number of extruded parts per tower part

Tower part	Diameter top [mm]	Number extruded parts
A	3000	19
B	3750	22
C	4500	26
D	5250	30

Figure 4.3 and 4.4 show an extruded at the top and bottom of part D respectively. The vertical lines indicate the boundaries of the extruded part. Figure 4.3 shows that at the top the parts are connected with the triangular parts, fitting well together. This is in contrast to Figure 4.4, where the triangles of each extrusion part are not fluently connected to each other. This is done to ensure that the tower has a conical shape, as explained in *Paragraph 3.1*. A distance of 40mm has to be removed of both sides of an extruded part at the top, as indicated in Figure 4.4.

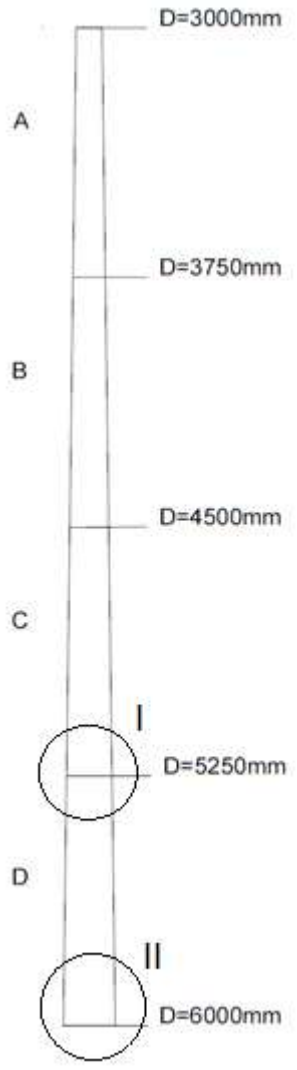

Figure 4.2 Tower view with indicated the top and bottom diameters of the four extruded parts

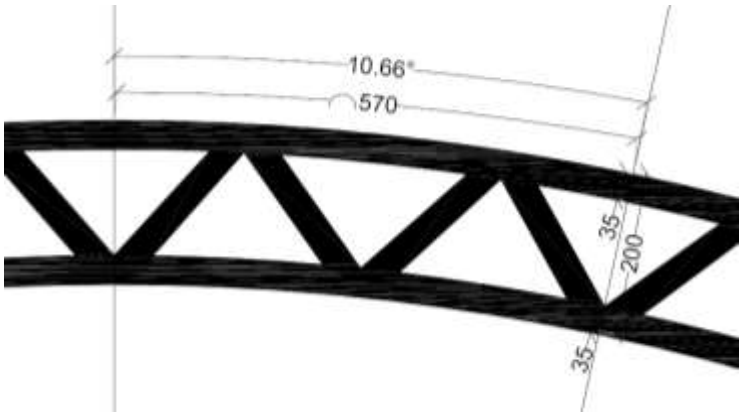

Figure 4.3 Close-up of one extruded part in a horizontal cross-section at the height of I as indicated in Figure 4.2

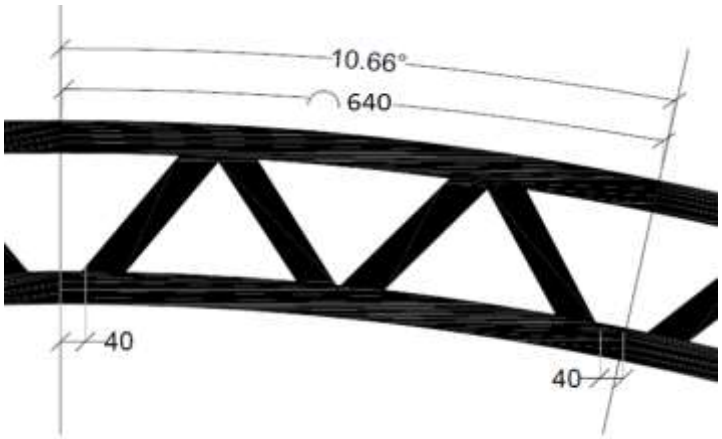

Figure 4.4 Close-up of one extruded part in a horizontal cross-section at the height of II as indicated in Figure 4.2

The steel 8MW wind turbine tower also has a bottom diameter of 6m. A disadvantage of a tower with a large diameter is the transportation. Although there are restrictions on the dimensions during transport, three years ago in Denmark they have managed to transport an 8MW wind turbine tower with a diameter of 6,5m by road.

4.2 Classification of cross-section

The resistance of a cross-section part in compression is generally limited by local buckling. The buckling load depends on the slenderness of the cross-section. The slenderness ratio is normally determined by the ratio of the width, in this case the diameter, divided by the thickness

$$\beta = \frac{d}{t} \tag{4.1}$$

The behavior of a cross-section part in compression depends on the slenderness ratio, see Figure 4.3.

a. If the slenderness ratio of the cross-section part is small ($\beta \leq \beta 1$) no buckling occurs. The average stress is equal to or even larger than the ultimate strength of the material in tension.

b. If the slenderness ratio is somewhat larger ($\beta 1 < \beta \leq \beta 2$) buckling occurs after the compressed cross-section part has been plastically deformed to a strain, which is more than about twice the strain corresponding to the $f_{0,2}$ ($\varepsilon \approx 1\%$) .

c. If the slenderness ratio is further increased ($\beta 2 < \beta \leq \beta 3$), buckling occurs once the 0,2% proof strength has been reached and plastic deformation has started. See figure 3.01c.

d. If the slenderness ratio is large ($\beta > \beta 3$), then buckling occurs before the average stress in the compressed part of the section has reached the 0,2% proof strength.

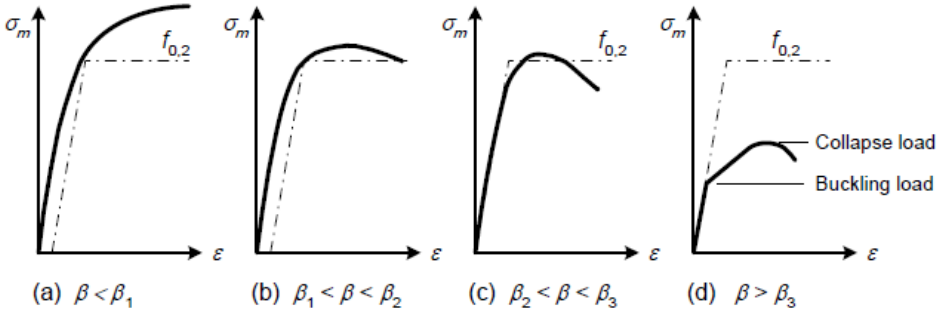

Figure 4.3. Principle relationship between mean stress σ_m and compression ε for different slenderness β (TALAT 2301, 2009)

The division of cross-sections into four classes for members in bending corresponds to the different behavior as above (EN 1999-1-1, 2007).

Class 1 cross-sections have compact cross-section parts that behave according to *a*. This type of cross-section can form a plastic hinge with the rotation capacity for plastic analysis without reduction of the resistance.

Class 2 cross-sections also have compact cross-section parts that behave according to *b*. This type of cross-section can develop their plastic moment resistance, but have limited rotation capacity because of local buckling.

Class 3 cross-sections have semi-slender cross-section parts and behave according to *c*. In this type of cross-section the calculated stress in the extreme compression fibre of the aluminium member can reach its proof strength, but local buckling is liable to prevent development of the full plastic moment resistance.

Class 4 cross-sections have one or more slender section parts that behave according to *d*. In this type of cross-section local buckling will occur before the attainment of proof stress in one or more parts of the cross-section.

First, the overall cross-section is classified. According to EN 1999-1-1 the susceptibility of a thin-walled round tube to local buckling, whether in uniform compression or in bending is defined by:

$$\beta = 3\sqrt{\frac{D}{t}} \tag{4.2}$$

Where:

D	diameter to mid thickness of the tower wall
t	thickness of the tower wall

The diameter of the tower decreases to the top. The diameter at the bottom (6m) will be used for the calculation since it has to deal with the heaviest loads. The total thickness of the tower wall is 200mm. Filling in these values in formula (4.2) gives the following susceptibility to local buckling:

$$\beta = 3\sqrt{\frac{5.8}{0{,}200}} = 16{,}16$$

The classification of parts of cross-sections is linked to the values of the slenderness parameters β as follows:

	$\beta \leq$	β_1	Class 1
$\beta_1 <$	$\beta \leq$	β_2	Class 2
$\beta_2 <$	$\beta \leq$	β_3	Class 3
$\beta_3 <$	β		Class 4

Values of β_1, β_2 and β_3 are given in Table 4.4. Before this table can be read, ε and therefore f_0 have to be known.

Table 4.4 Slenderness parameters β_1/ε, β_2/ε and β_3/ε (EN 1999-1-1, 2007)

Material classification according to Table 3.2	Internal part			Outstand part		
	β_1/ε	β_2/ε	β_3/ε	β_1/ε	β_2/ε	β_3/ε
Class A, without welds	11	16	22	3	4,5	6
Class A, with welds	9	13	18	2,5	4	5
Class B, without welds	13	16,5	18	3,5	4,5	5
Class B, with welds	10	13,5	15	3	3,5	4
$\varepsilon = \sqrt{250/f_o}$, f_o in N/mm^2						

Data corresponding for the aluminium alloy 7020 T6 is given in Table 4.5.

Table 4.5. Details alloy 7020 T6 (EN 1999-1-1, 2007)

Alloy EN-AW	Product form	Temper	Thick-ness t mm 1) 3)	f_o 1)	f_u 1)	A 5) 2)	$f_{o,haz}$ 4)	$f_{u,haz}$ 4)	HAZ-factor 4)		BC 6)	n_p 7)
				N/mm^2		%	N/mm^2		$\rho_{o,haz}$	$\rho_{u,haz}$		
7020	EP,ET,ER/B	T6	$15<t<40$	**275**	350	10	205	280	0,75	0,80	A	19

4) The HAZ-values are valid for MIG welding and thickness up to 15mm. For TIG welding strain hardening alloys (Aly) (3xxx and 5xxx) (Al) up to 6 mm the same values apply, but for TIG welding precipitation hardening alloys (6xxx and 7xxx) and thickness up to 6 mm the HAZ values have to be multiplied by a factor 0,8 and so the ρ-factors. For higher thickness – unless other data are available – the HAZ values and ρ-factors have to be further reduced by a factor 0,8 for the precipitation hardening alloys (6xxx and 7xxx) alloys and by a factor 0,9 for strain hardening alloys (3xxx, 5xxx and 8011A). These reductions do not apply in temper O.

Applying the value for $f_{0,haz}$ leads to $\varepsilon = \sqrt{\frac{250}{275}} = 0{,}953$.

Alloy 7020 T6 can be classified in buckling class A and for round tube profiles the ratios in Table 4.3 for 'internal part' should be used. Now ε is known, the following values for slenderness parameters can be determined.

$\beta_1 = 9 \cdot 0{,}953 = 8{,}59$
$\beta_2 = 13 \cdot 0{,}953 = 12{,}40$
$\beta_3 = 18 \cdot 0{,}953 = 17{,}16$

As calculated before, $\beta = 16{,}16$. Thus, $\beta_2 < \beta \leq \beta_3$. This means that the cross-section is classified in class 3.

The HAZ values are only valid for MIG welding and thickness up to 15mm. Note 4 under Table 4.3 claims that for higher thickness, the HAZ values and ρ-factors have to be further reduced by a factor of 0,8. Table 4.6 gives the new values.

Table 4.6 New HAZ values and ρ-factors

$f_{0,haz}$ [N/mm^2]	$f_{u,haz}$ [N/mm^2]	$\rho_{0,haz}$	$\rho_{u,haz}$
166,4	224	0,605	0,640

Now the cross-section of an extruded part will be classified in order to verify if a local buckling check must be carried out. According to EN 1999-1-1 (2007,) the susceptibility of an un-reinforced flat part to local buckling is defined by the parameter β. Formula (4.3) applies for flat internal parts with no stress gradient:

$$\beta = \frac{b}{t} \tag{4.3}$$

Filling in the values gives:

- For the flange

$$\beta = \frac{280}{35} = 8$$

- For the web

$$\beta = \frac{185}{35} = 5{,}29$$

For both applies: $\beta < \beta_1$, thus class 1 applies for the flange of an extruded part and therefore no local buckling needs to be checked.

4.3 Loads

4.3.1 Load and resistance factors

Table 4.7 shows load factors for the Ultimate Limit State, Serviceability Limit State and the Fatigue Limit State. Two load states are assumed for the ULS. Table 4.8 shows the resistance factors for the permanent loads (G) and environmental loads (E) for the three limit states.

Table 4.7 Load cases with related factors γ_f for the ULS, SLS and FLS (DNV, 2014)

Limit State			Load factors γ_f G	E
1	ULS	Extreme permanent loads and normal environmental loads	1,25	1,00
2	ULS	Normal permanent loads and extreme environmental loads	1,00	1,35
3	SLS		1,00	1,00
4	FLS		1,00	1,00

Table 4.8 Resistance factors γ_m for the ULS, SLS and FLS (DNV, 2014)

		Resistance factor γ_m
ULS		1,10
SLS		1,00
FLS	Depends on location of the element or joint	1,15

The DNV (2014) mentions 5 simplified environmental load combinations which are to be considered, including ice loads. However, these can be neglected regarding the location of the wind turbine. Therefore, three load combinations remain. These three will be taken into account in this thesis, see Table 4.9.

Table 4.9 Proposed load combinations for simplified load combinations (DNV, 2014)

Load combination for ULS	Environmental load type and return period to define characteristic value of corresponding load effect			
	Wind	Waves	Current	Water level
1	50 years	5 years	5 years	50 years
2	5 years	50 years	5 years	50 years
3	5 years	5 years	50 years	50 years

The loads for the first and second limit state have been calculated with the three load combinations. It appears that limit state 2 and load combination 2 are decisive, so further calculations are made with these values. In order to calculate the loads, the data shown in Table 4.1 is necessary.

4.3.2 DAF

The dynamic influence on the loads has to be taken into account. This can be done by making use of a dynamic amplification factor (DAF). The DAF is the factor by which static displacement responses are amplified due to the fact that the external force is dynamic, see Figure 4.4 (Gavin, H.P., 2014). The DAF is defined for harmonic excitation.

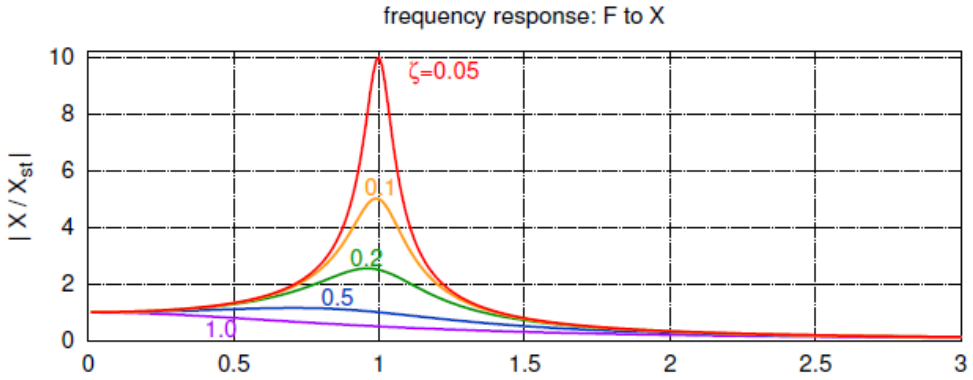

Figure 4.4 The dynamic amplification factor for external forcing (Gavin, H.P.)

According to the DNV (2014), when the natural period of the wind turbine, support structure and foundation is less than or equal to 2.5 sec, a DAF may be applied to the load on the structure, when the wind turbine, support structure and foundation are modelled as a single-degree-of-freedom (SDOF) system:

$$DAF = \frac{dynamic\ amplitude}{static\ deformation} = \frac{X}{X_{st}} = \frac{1}{\sqrt{(1-\Omega^2)^2 + (2\xi\Omega)^2}} \tag{4.4}$$

Where:

ξ	damping ratio relative to critical damping	[-]
Ω	ratio between applied frequency and natural frequency	[-]

When the natural period is greater than 2,5s, a time domain analysis should be carried out to determine the dynamic amplification factor.

Later on the natural frequency of the wind turbine is determined. This gives a natural period of $T = \frac{1}{f} = \frac{1}{0{,}126} = 7{,}9s$. Although a time domain analysis should be carried out and although the formula is only applicable for SDOF systems, it is still used to make a rough estimation of the DAF.

According to the DNV, the structural damping c_1 should be taken as 1% of the critical damping c_{crit}.

$$\xi = 1\% = 0{,}01$$

$$\Omega = \frac{applied\ frequency}{natural\ frequency} = \frac{0{,}165}{0{,}126} = 1{,}31 \tag{4.5}$$

Entering these two values in formula (4.4) leads to the following DAF:

$$DAF = \frac{1}{\sqrt{(1-\Omega^2)^2 + (2\xi\Omega)^2}} = \frac{1}{\sqrt{(1-1{,}31^2)^2 + (2 \cdot 0{,}01 \cdot 1{,}31)^2}} = 1{,}40$$

Excitation frequencies as a result of the current load only occur when the Reynold's number is between 300-300·10^5 (Ginhoven, J. van, 2006). For a cylindrical structural member of diameter D, the DNV (2014) gives the following definition:

$$R_e = \frac{(u_{max} \cdot D)}{\nu} \tag{4.6}$$

Where:

u_{max}	extreme current velocity	[m/s]
D	diameter tower at seabed level	[m]
ν	kinematic viscosity	[m/s]

Filling in the corresponding values in formula (4.6) gives:

$$R_e = \frac{(u_{max} \cdot D)}{\nu} = \frac{1 \cdot 6}{10^6} = 6{,}0 \cdot 10^{-6} < 300$$

This means that the current load causes no significant excitation frequency. The frequency of the waves is located between 0,05-0,2Hz, this also causes no significant excitation frequency (Ginhoven, J. van, 2006).

4.3.3 Wind loads

All objects located in a flowing medium such as wind or water are subject to a resistance force which generally can be written as follows (DNV, 2014):

$$F_w = \frac{1}{2} C_w \rho A v^2 \tag{4.7}$$

Where:

C_w coefficient dependent on the shape of the object; the more aerodynamic, the lower the value.
A area facing flow
v flow velocity of the medium

The wind load specifically consists of (DNV, 2014):

- Aerodynamic blade loads
- Aerodynamic drag forces on tower and nacelle

The aerodynamic behavior of wind turbines can be analyzed by considering the simplest model of a wind turbine, the so-called actuator disc model. In this model, the turbine is replaced by a circular disc through which the airstream flows with a velocity U_∞ and across which there is a pressure drop from p_u to p_d as illustrated Figure 4.5. The actuator disc model is based on the following ideal assumptions: no frictional drag, homogeneous, incompressible, steady state fluid flow, constant pressure increment or thrust per unit area over the disc, continuity of velocity through the disc and an infinite number of blades.

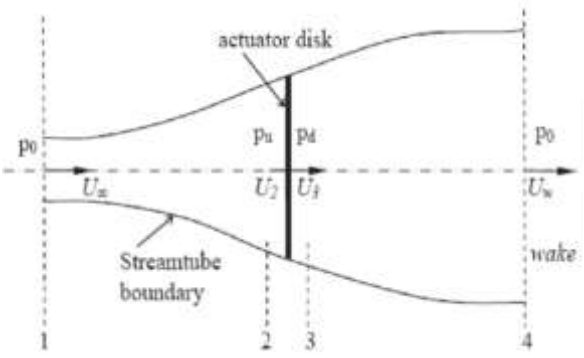

Figure 4.5 Actuator disc model (Kulunk, E. 2011)

The analysis of the actuator disc theory assumes a control volume in which the boundaries are the surface walls of a stream tube and two cross-sections. Four sections are made where the control volume is analyzed: 1) free-stream region, 2) just before the blades, 3) just after the blades, 4) far wake region. The mass flow rate remains the same throughout the flow. It is assumed that the velocity through the disc is continuous, thus: $U_2 = U_3 = U_R$ (Kulunk, E. 2011).

The thrust coefficient of the rotor C_T can be determined with the following equation (Kulunk, E. 2011):

$$C_T = \frac{T}{\frac{1}{2}\rho U^2 A} = \frac{2Aa\rho(1-a)U^2}{\frac{1}{2}\rho U^2 A} = 4a(1-a) \tag{4.8}$$

Where:

T thrust which is, under unideal conditions, dependent on the dimensions of the rotor and the aerodynamic design versus settings of the rotor blades.
a axial induction factor $a = \frac{U_\infty - U_R}{U_\infty}$, which represents the relative variation of the undisturbed wind speed from the free-stream region up to just after the blades.

The following applies under ideal conditions: $U_R = \frac{2}{3}U_\infty$, this leads to an induction factor of $a = \frac{1}{3}$. These values are inserted in formula (4.8), leading to a thrust coefficient C_T of (Ginhoven, J. van, 2006):

$$C_T = 4a(1-a) = 4 \cdot \frac{1}{3}\left(1 - \frac{1}{3}\right) = 0{,}89$$

Under non-ideal conditions, this value depends on the dimensions of the rotor and the aerodynamic design. The maximum drag coefficient is reached when the rated wind speed is assumed, and not the

cut-off wind speed. When the latter would be the case, the flow velocities would be larger which leads to a decrease in drag since the angle of attack of the rotor blades will be smaller to remain constant revolutions of the blades for a constant energy production.

Now the value for the horizontal load exerted by the rotor blades can be calculated with formula (4.9):

$$F_{wind,rotor} = \frac{1}{2} C_T \rho_{air} A_{rotor} {v_r}^2 \quad (4.9)$$

Where:

C_T	thrust coefficient of the rotor	[-]
ρ_{air}	density air	[kg/m³]
A_{rotor}	swept area	[m²]
v_r	annual mean wind speed	[m/s]

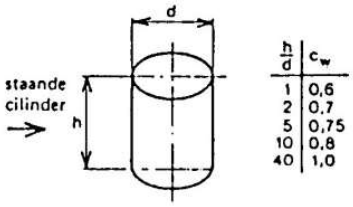

Figure 4.6 Drag coefficient for a cylinder (Hydromechanica 1, 2005)

Filling in the corresponding values from Table 4.1 in formula (4.9) gives the following design value for the horizontal load, see also Figure 4.6:

$$F_{wind,rotor,d} = \gamma_f \cdot \frac{1}{2} C_T \rho_{air} A_{rotor} {v_r}^2 = 1{,}35 \cdot \frac{1}{2} \cdot 0{,}89 \cdot 1{,}225 \cdot 21124 \cdot 11^2 = 1881kN$$

The corresponding moment will be:

$$M_{wind,rotor,d} = F_{wind,rotor,d} \cdot l_t = 1881 \cdot 120 = 225720kNm$$

Where:

$F_{wind,rotor,d}$	horizontal load exerted by the rotor blades	[kN]
l_w	length tower structure	[m]

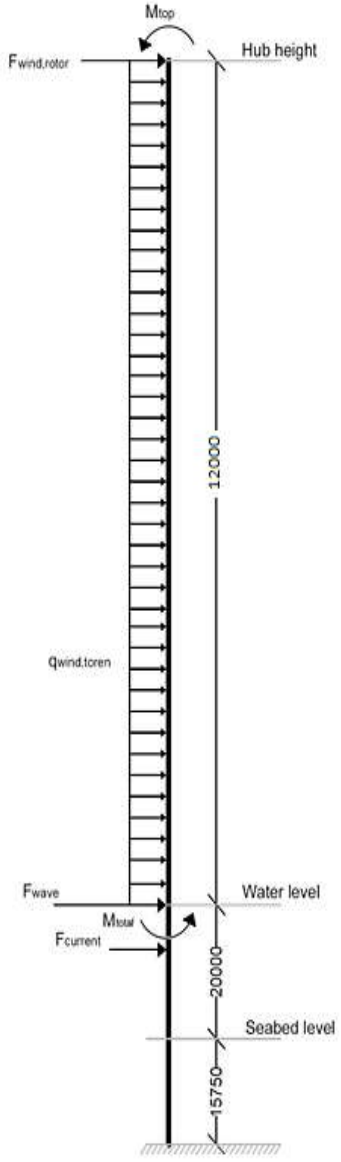

Figure 4.7 Forces acting on the support structure

The wind flow also exerts a force on the cylindrical tower. In order to calculate this force a value for the shape drag coefficient needs to be determined. This can be done with the aid of Figure 4.7: h/d = 70/4= 17,5. Interpolating gives a value for C_w of 0,85. The cut-out wind speed is the maximum wind velocity at which the turbine is still in operation. Above this wind speed the rotor blades are brought to rest to avoid damage from high winds. The cut-out wind speed results in the highest wind load on the tower, thus a wind speed of 30m/s is used for the calculation (see Table 4.1).
The horizontal line load on the tower as a result of the wind can be determined with the following formula:

$$q_{wind,tower} = \frac{1}{2} C_{w,tower} \rho_{air} A_{tower} {v_c}^2 \quad (4.10)$$

Where:

$C_{w,tower}$	shape drag coefficient	[-]
ρ_{air}	density air	[kg/m³]
A_{tower}	area facing wind flow($D_{av} \cdot l_{tower}$)	[m²]
v_c	cut-out wind speed	[m/s]

Now the coefficient is known, the horizontal line load on the tower as a result of the wind force can be determined, see Figure 4.7:

$$q_{wind,tower,d} = \gamma_f \cdot \frac{1}{2} C_{w,tower} \rho_{air} A_{tower} {v_c}^2 \cdot DAF = 1{,}35 \cdot \frac{1}{2} \cdot 0{,}85 \cdot 1{,}225 \cdot 4{,}0 \cdot 25^2 \cdot 1{,}4 = 2{,}46 kN/m$$

This load acts on the total height of the tower, which is 120m. The corresponding moment at the bottom of the tower will thus be:

$$M_{wind,tower} = q_{wind,tower,d} \cdot l_t \cdot \frac{1}{2} l_t = 2{,}46 \cdot 120 \cdot \frac{1}{2} \cdot 120 = 17725 kNm$$

Where:

$q_{wind,tower}$	horizontal line load on the tower as a result of the wind force	[kN/m]
l_t	total height of the tower	[m]

4.3.4 Current load

Although sea currents vary in space and time, they are generally considered as a horizontally uniform flow field of constant velocity and direction, varying only as a function of depth (IEC 61400-3, 2009). It will be highest at the surface level and zero at the seabed due to friction. Three basic current profiles over depth can be presented, illustrated by Figure 4.8, namely:

- the linear profile
- the bilinear profile
- the power law profile

(Tempel, J. van der, 2006)

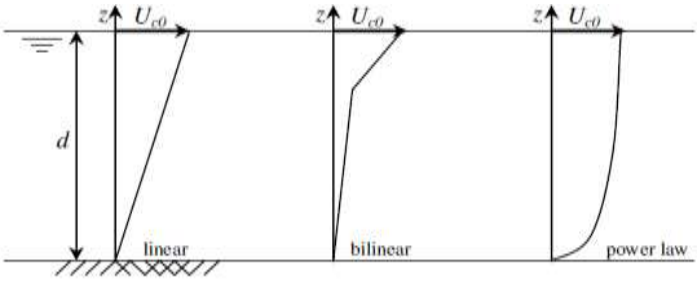

Figure 4.8 Different current distributions (Tempel, J. van der, 2006)

Due to lack of data, a linear distribution will be assumed. Therefore, the point where the current load is schematically applied is on 2/3 of the water depth, viewed from the bottom.

The current load can be derived using a formula for flow around slender structures, which consists of a static and a dynamic part of the drag force (Ginhoven, J.):

$$F_{current} = \frac{1}{2} \rho_{water} u^2 (C_D + C_D') A_{water} \quad (4.11)$$

Where:

ρ_{water}	density water	[kg/m³]
u	extreme current velocity	[m/s]
C_D	static drag coefficient	[-]
C_D'	dynamic drag coefficient	[-]
A_{water}	area facing water flow	[m²]

To determine the coefficients, first the Reynolds number has to be defined, which is, as calculated in *Paragraph 2.3.1*:

$$R_e = \frac{(u_{max} \cdot D)}{\nu} = \frac{1 \cdot 6}{10^6} = 6{,}0 \cdot 10^{-6}$$

It was also mentioned that excitation frequencies as a result of current only occur when the Reynolds number is between 300 and $3 \cdot 10^5$. So in this case, the current causes no significant excitation frequency.

From the C_D graph illustrated in Appendix A, a value of 0,7 can be obtained for the coefficient with the aid of the Reynolds number. The maximum dynamic drag coefficient C_D' is equal to: $0{,}25C_D = 0{,}175$. The values can now be inserted in formula (4.11), leading to the following current load, see also Figure 4.7:

$$F_{current,d} = \gamma_f \cdot \frac{1}{2}\rho_{water} u^2 (C_D + C_D')A = 1{,}35 \cdot \frac{1}{2} \cdot 1025 \cdot 1^2 \cdot (0{,}7 + 0{,}175) \cdot (20 \cdot 6) = 72{,}65kN$$

This load is applied on the support structure at a height of 2/3 of the water depth viewed from the bottom. The occurring moment will be:

$$M_{current} = F_{current,d} \cdot \left(\frac{2}{3} \cdot l_s + l_e\right) = 72{,}65 \cdot \left(\frac{2}{3} \cdot 20 + 15{,}75\right) = 2494kNm$$

Where:

$F_{current,d}$	current load	[kN]
l_s	submerged part of the tower	[m]
l_e	embedded part of the tower	[m]

4.3.5 Wave load

For the calculation of the wave load, the Morison formula should be used as proposed in the DNV Offshore Standard. This is a formula to calculate the hydrodynamic loads on slender members per unit length, consisting of two parts: an inertia part, which is quadratic in the structural diameter D and a drag part that is linear in D. The velocity and acceleration have a 90° phase difference, so inertia and drag loads will also be out of phase. This means that in general the maximum load is not equal to either maximum drag or maximum inertia load. For a conceptual design, the wave load can be defined as follows (DNV, 2014):

$$F_{wave} = F_I + F_D = C_I K_I H \rho_{water} g \pi \frac{D^2}{4} + C_D K_D H^2 \frac{1}{2} \rho_{water} g D \qquad (4.12)$$

Where:

C_I	inertia coefficient	[-]
C_D	drag coefficient	[-]
K_I	correction coefficient for extent of inertia force	[-]
K_D	correction coefficient for extent of drag force	[-]
H	wave height	[m]
ρ_{water}	density water	[kg/m^3]
D	pile diameter	[m]

The four coefficients depend on the water depth d, the wave period T and the wave height relative to the breaking wave height ($\frac{H}{H_b}$). The values for the first two parameters can be obtained from Table 1.2. Thus, the coefficients could be determined when the ratio of the wave height over the breaking wave height ($\frac{H}{H_b}$) is known. This ratio can be calculated with Figure 4.9, by entering the graph at the horizontal axis, and determine the value at the vertical axis (with H = breaking height of the wave) at the intersection with the 'breaking limit' line. When the breaking wave height is known, the ratio $\frac{H}{H_b}$ can be calculated.

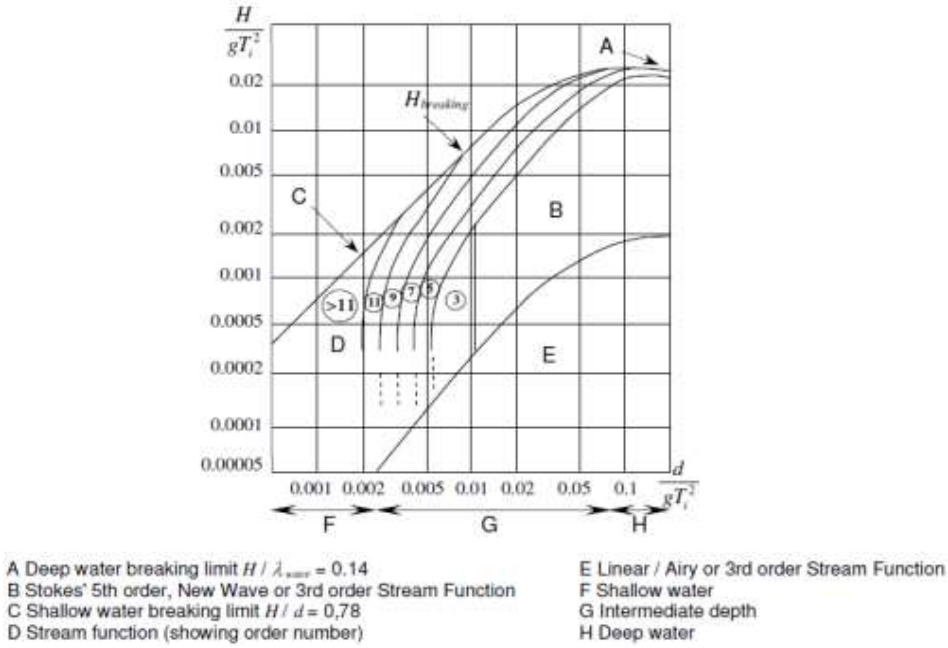

Figure 4.9 Regions of application of different wave theories (ISO 19901-1, 2005)

In deep water ($d > \frac{1}{2}\lambda$), waves break when $\frac{H}{\lambda}$ exceeds about 0,14. In shallow water ($d < \frac{1}{20}\lambda$), waves break when $\frac{H}{d}$ or, more accurate, when $\frac{H}{H_d}$ exceeds about 0,78 (DNV, 2014). For the chosen location, the value for shallow water should be taken.

It appears that for this location with a return period of 50 years, the ratio of the wave height over the breaking wave height ($\frac{H}{H_b}$) is larger than 0,78, see Table 2. This means that the waves will break. A breaking wave will exert a larger force on the structure, therefore the Morison formula cannot be used anymore. The accelerations of the water particles will be subordinate to the velocity of the water, and consequently the inertia force is negligible relative to the drag force.

The following formula should be used, where the drag coefficient is multiplied by 2,5 (DNV, 2014):

$$F_{breaking\ wave} = C_D{}^* K_D {H_b}^2 \frac{1}{2} \rho_{water} g D \tag{4.13}$$

Where:

$C_D{}^*$	drag coefficient in breaking waves $= 2{,}5 \cdot C_D$	[-]
K_D	correction for extent of drag force	[-]
H_b	breaking wave height	[m]
D	pile diameter	[m]

The coefficients belonging to the selected location are calculated with aid of several graphs, see Appendix D. The values are shown in Table 4.10.

Table 4.10 Coefficients needed for the wave formula

Return period	$d/(gT^2)$	H_b	H/H_b	C_D	K_D	S_D
50 yr	0,017	17,8	0,84	3*	0,50	1,00
5 yr	0,020	16,7	0,76	1,2	0,44	0,94

The breaking wave force acts on the tower at water level and has a value of:

$$F_{breaking\ wave,d} = \gamma_f \cdot C_D{}^* K_D H^2 \frac{1}{2} \rho_{water} g D = 1{,}35 \cdot 3 \cdot 0{,}50 \cdot 14{,}9^2 \cdot \frac{1}{2} \cdot 1025 \cdot 9{,}81 \cdot 6 = 13561{,}6kN$$

The occurring moment at the bottom of the structure is:

$$M_{wave} = F_{breaking\ wave,d} \cdot d \cdot S_d = 13561{,}6 \cdot 20 \cdot 1{,}0 = 271232Nm$$

Where:

$F_{breaking\ wave,d}$	breaking wave force	[kN]
d	water depth	[m]
S_d	correction factor for the position of the breaking wave force	[-]

4.3.6 Permanent load

The total dead load of the structure is also a very important load that has to be taken into consideration. The weight of the rotor blades has an influence on the calculation of the total moment on the wind turbine. It provides a counter moment as can be seen in Figure 4.7. The dead load of the blades is 1000,62kN, so the counter moment will have a value of:

$$M_{top} = \gamma_f \cdot F_{blades} \cdot r = 1{,}00 \cdot 1000{,}62 \cdot 2{,}4 = 2401kNm$$

Where:

γ_f	load factor permanent loads	[-]
F_{blades}	dead load blades	[kN]
r	lever to the tower	[m]

The weight of the tower is:

$$F_{tower} = V_{tower} \cdot \rho_{aluminium} = 100{,}28 \cdot 27 = 2707{,}6kN$$

Weight of the tower and nacelle, hub, rotor unit (consisting of the rotor hub and blades):

$$F_{tower} + F_{nacelle,hub,rotor} = 2707{,}6 + 4826{,}52 = 7534{,}1kN$$

The volume is calculated with the aid of the spreadsheet.

4.4 Stress checks

4.4.1. Ultimate Limit State

In this paragraph the unity checks for the ultimate limit state will be checked with the loads as calculated in the previous paragraph. Only the calculations for the bottom part will be given, since the largest loads can be found here.

4.4.1.1 Compression

The design value of the axial compression for N_{Ed} shall satisfy (EN 1999-1-1, 2007):

$$\frac{N_{Ed}}{N_{C,Rd}} \leq 1{,}0gD \tag{4.14}$$

The design resistance for uniform compression $N_{C,Rd}$ is:

$$N_{C,Rd} = \frac{A_{eff} \cdot f_0}{\gamma_{M1}} gD \tag{4.15}$$

Where:

A_{eff} effective section area based on reduced thickness allowing for local buckling and HAZ softening but ignoring unfilled holes.

$$A_{eff,bottom} = A_{gross} - A_{weld} + \left(N_{weld} * 2 * b_{haz} * \rho_{o,haz} * t_w\right) = 1{,}675 - (30 * 2 * 0{,}040 * 0{,}060) + (30 * 2 * 0{,}040 * 0{,}605 * 0{,}060) = 1{,}62m^2$$

$$N_{Ed,bottom} = F_{tower} + F_{nacelle,hub,rotor} = 2707{,}55 \cdot 10^3 + 4826{,}52 \cdot 10^3 = 7534070N$$

$$N_{C,Rd,bottom} = \frac{A_{eff,bottom} \cdot f_0}{\gamma_{M1}} = \frac{1{,}62 \cdot 10^6 \cdot 275}{1{,}1} = 405004000N$$

$$\frac{N_{Ed,bottom}}{N_{C,Rd,bottom}} = \frac{7534070}{405004000} = 0{,}019 < 1{,}0$$

4.4.1.2 Shear

The design value of the shear force V_{Ed} at each cross-section shall satisfy (EN 1999-1-1, 2007):

$$\frac{V_{Ed}}{V_{Rd}} \leq 1{,}0 \tag{4.16}$$

Where $V_{Rd}$is the design shear resistance of the cross-section.

For non-slender sections:

$$V_{Rd} = A_V \frac{f_0}{\sqrt{3}\gamma_{M1}} \tag{4.17}$$

Where A_V is the shear area, for solid bars and round tubes taken as:

$A_V = \eta_V \cdot A_e$

Where:

$\eta_V = 0{,}6$ for a round tube

A_e is the full section area of an unwelded section, and the effective section area obtained by taking a reduced thickness $\rho_{o,haz}t$ for the HAZ material of a welded section.

$V_{Ed} = q_{hor,mast} \cdot l_{tower} + F_{rotor} = 2{,}28 \cdot 120 + 1881 = 2154kN$

$$A_V = \eta_V \cdot A_c = 0{,}6 \cdot \left(\pi \cdot \left({r_{1,0}}^2 - \left(r_{1,i} \cdot 0{,}87225 + \left(r_{1,o} - 2 \cdot t \cdot \rho_{o,haz}\right) \cdot 0{,}12755\right)^2\right) + \pi \cdot \left({r_{2,0}}^2 - r_{2,1}^2\right)\right) = 0{,}6((\pi \cdot (3^2 - (2{,}965 \cdot 0{,}87225 + (3 - 2 \cdot 0{,}035 \cdot 0{,}605) \cdot 0{,}12755)^2) + \pi \cdot (2{,}835^2 - 2{,}8^2)) \cdot 10^6) = 0{,}6 \cdot 1486927 = 892156mm^2$$

$$V_{Rd} = A_V \frac{f_0}{\sqrt{3}\gamma_{M1}} = 892156 \frac{275}{\sqrt{3} \cdot 1{,}10} = 128771614N$$

$$\frac{V_{Ed}}{V_{Rd}} = \frac{2154 \cdot 10^3}{128771614} = 0{,}017 \leq 1{,}0$$

4.4.1.3 Bending moment

The design value of the bending moment M_{Ed} at each cross-section shall satisfy (EN 1999-1-1, 2007):

$$\frac{M_{Ed}}{M_{Rd}} \leq 1{,}0 \tag{4.18}$$

The design resistance for bending about one principal axis of a cross-section M_{Rd} is determined as the lesser of $M_{u,Rd}$ and $M_{o,Rd}$ where:

$M_{u,Rd} = \frac{W_{net} \cdot f_u}{\gamma_{M2}}$ in a net section

$M_{o,Rd} = \frac{a \cdot W_{el} \cdot f_0}{\gamma_{M1}}$ at each cross-section

Where:

W_{net} the elastic modulus of the net section allowing for holes and HAZ softening. The latter deduction is based on the reduced thickness $\rho_{o,haz}t$

W_{el} the elastic modulus of the gross section

α shape factor. For cross-section 3 with longitudinal welds: $\alpha_{3,w} = \frac{W_{el,haz}}{W_{el}}$

Where:

$W_{el,haz}$ effective elastic modulus of the gross-section, obtained using a reduced thickness $\rho_{o,haz}t$ for the HAZ material,

$$W_{el,haz} = \frac{\pi\left({D_{1,0}}^4 - (D_{1,i} \cdot 0{,}87225 + (D_{1,o} - 2 \cdot t \cdot \rho_{o,haz}) \cdot 0{,}12755)^4\right)}{32 \cdot D_{1,0}} + \frac{\pi\left({D_{2,0}}^4 - {D_{2,i}}^4\right)}{32 \cdot D_{2,0}}$$
$$= \frac{\pi(6^4 - (5{,}93 \cdot 0{,}87225 + (6 - 2 \cdot 0{,}035 \cdot 0{,}605) \cdot 0{,}12775)^4)}{32 \cdot 6}$$
$$+ \frac{\pi(5{,}67^4 - 5{,}6^4)}{32 \cdot 5{,}67} = 1{,}79m^3$$

The percentage HAZ of the total perimeter is 12,775%. Thus in the calculation for the $W_{y,pl,haz}$ 0,12775 part of the diameter is decreased with $\rho_{o,haz}$.

$$W_{el} = \frac{\pi\left({D_{1,0}}^4 - {D_{1,i}}^4\right)}{32 \cdot D_{1,0}} + \frac{\pi\left({D_{2,0}}^4 - {D_{2,i}}^4\right)}{32 \cdot D_{2,0}} = \frac{\pi(6^4 - 5{,}93^4)}{32 \cdot 6} + \frac{\pi(5{,}67^4 - 5{,}6^4)}{32 \cdot 5{,}67} = 1{,}88m^3$$

$$\alpha = \frac{W_{eff,haz}}{W_{el}} = \frac{1{,}79}{1{,}88} = 0{,}97$$

$$M_{Ed} = M_{wind,tower} + M_{wind,rotor} - M_{top} = 16407 + 225722 - 2401{,}5kNm = 239728kNm$$
$$= 2{,}40 \cdot 10^{11}Nmm$$

$$M_{u,Rd} = \frac{W_{net} \cdot f_u}{\gamma_{M2}} = \frac{1{,}79 \cdot 10^9 \cdot 350}{1{,}25} = 5{,}02 \cdot 10^{11}Nmm$$

$$M_{o,Rd} = \frac{a \cdot W_{el} \cdot f_0}{\gamma_{M1}} = \frac{0{,}97 \cdot 1{,}88 \cdot 10^9 \cdot 275}{1{,}10} = 4{,}49 \cdot 10^{11}Nmm$$

$$\frac{M_{Ed}}{M_{o,Rd}} = \frac{2{,}40 \cdot 10^{11}}{4{,}49 \cdot 10^{11}} = 0{,}54 < 1{,}0$$

4.4.1.4 Bending and axial force

Hollow sections should satisfy the following criterion (EN 1999-1-1, 2007):

$$\left(\frac{N_{Ed}}{\omega_o N_{Rd}}\right)^{1,3} + \left[\left(\frac{M_{y,Ed}}{\omega_0 M_{y,Rd}}\right)^{1,7} + \left(\frac{M_{z,Ed}}{\omega_0 M_{z,Rd}}\right)^{1,7}\right]^{0,6} \leq 1{,}00 \qquad (4.19)$$

Where:

N_{Ed} design values of the axial compression or tension force

$M_{y,Ed}$ bending moment about the y-y axis

$M_{z,Ed}$ bending moment about the z-z axis

$N_{Rd} = \frac{A_{eff} \cdot f_0}{\gamma_{M1}}$

$$M_{y,Rd} = \frac{W_{y,pl,haz} \cdot f_0}{\gamma_{M1}}$$

ω_o If a section is affected by HAZ softening with a specified location along the length and if the softening does not extend longitudinally a distance greater than the least width of the member, then the limiting stress should be taken as the design ultimate strength $\rho_{u,haz} \cdot f_u/\gamma_{M2}$ of the reduced strength material:

$$\rho_{u,haz} = \frac{f_u}{f_{u,haz}} = \frac{350}{224} = 0{,}640$$

$$\omega_o = \frac{\rho_{u,haz} \cdot f_u/\gamma_{M2}}{f_0/\gamma_{M1}} = \frac{0{,}640 \cdot 350/1{,}25}{275/1{,}1} = 0{,}7168$$

$N_{Ed} = 7534070N$

$N_{C,Rd} = 405004000N$

$M_{y,Ed} = 2{,}40 \cdot 10^{11} Nmm$

$$W_{y,pl,haz} = \frac{\left({D_{1,o}}^3 - (D_{1,i} \cdot 0{,}87225 + (D_{1,o} - 2 \cdot t \cdot \rho_{o,haz}) \cdot 0{,}12755)^3\right)}{6} + \frac{\left({D_{2,o}}^3 - {D_{2,i}}^3\right)}{6} = \frac{6^3 - (5{,}93 \cdot 0{,}87225 + (6 - 2 \cdot 0{,}035 \cdot 0{,}605) \cdot 0{,}12775)^3}{6} + \frac{5{,}67^3 - 5{,}6^3}{6} = 2{,}295m^3$$

$$M_{y,Rd} = \frac{W_{y,pl,haz} \cdot f_0}{\gamma_{M1}} = \frac{2{,}295 \cdot 275}{1{,}1} = 5{,}737 \cdot 10^{11} Nmm$$

$$\left(\frac{N_{Ed}}{\omega_o N_{Rd}}\right)^{1,3} + \left[\left(\frac{M_{y,Ed}}{\omega_0 M_{y,Rd}}\right)^{1,7} + \left(\frac{M_{z,Ed}}{\omega_0 M_{z,Rd}}\right)^{1,7}\right]^{0,6} = \left(\frac{7534070}{0{,}7168 \cdot 405004000}\right)^{1,3} + \left[\left(\frac{2{,}295 \cdot 10^{11}}{0{,}7168 \cdot 5{,}737 \cdot 10^{11}}\right)^{1,7} + \left(\frac{0}{0{,}7168 \cdot 5{,}737 \cdot 10^{11}}\right)^{1,7}\right]^{0,6} = 0{,}59 < 1{,}00$$

4.4.1.5 Flexural buckling

Members in bending and axial compression that are not susceptible to torsional deformations, such as circular hollow sections, need to be checked on flexural buckling only.

Hollow cross-sections and tubes should satisfy the following criterion (EN 1999-1-1, 2007):

$$\left(\frac{N_{Ed}}{\chi_{min}\omega_x N_{Rd}}\right)^{0,8} + \frac{1}{\omega_0}\left[\left(\frac{M_{y,Ed}}{M_{y,Rd}}\right)^{1,7} + \left(\frac{M_{z,Ed}}{M_{z,Rd}}\right)^{1,7}\right]^{0,6} \leq 1{,}00 \qquad (4.20)$$

Where:

N_{Ed} design value of the axial compressive force

$M_{y,Ed}$ design values of bending moment about the y-y axis

$M_{z,Ed}$ design values of bending moment about the z-z axis

$N_{Rd} = \dfrac{\kappa \cdot A_{eff} \cdot f_0}{\gamma_{M1}}$

$M_{y,Rd} = \dfrac{\alpha_y \cdot W_y \cdot f_0}{\gamma_{M1}}$

$M_{z,Rd} = \dfrac{\alpha_z W_z \cdot f_0}{\gamma_{M1}}$

$\chi_{min} = \min(\chi_y, \chi_z)$

χ_y and χ_z are the reduction factors for buckling in the z-x plane and the y-x plane, respectively. It depends on the type of aluminium alloy and the slenderness parameter λ_c. The determination of this factor is given below.

κ factor to allow for the weakening effects of welding.

$\kappa = 1 - \left(1 - \frac{A_I}{A}\right) 10^{-\lambda_c} - \left(0{,}05 + 0{,}1 \frac{A_I}{A}\right) {\lambda_c}^{1{,}3(1-\lambda_c)}$

$A_I = A - A_{haz}(1 - \rho_{0,haz})$

A_{haz}: area of HAZ

ω_o for a member subject to HAZ softening, ω_o should generally be based on the ultimate strength of the HAZ softened material. If such softening occurs only locally along the length, then $\omega_o = \frac{\rho_{u,haz} \cdot f_u / \gamma_{M2}}{f_0 / \gamma_{M1}}$ but $\leq 1{,}00$

Where $\rho_{u,haz}$ is the reduction factor for the heat affected material.

α_y, α_z shape factors, for cross-section 1 with longitudinal welds: $\alpha = \frac{W_{pl,haz}}{W_{el}}$. Should not be taken larger than 1,25.

The reduction factor χ is calculated from:

$$\chi = \frac{1}{\phi + \sqrt{\phi^2 \cdot {\lambda_c}^2}} \quad \text{but } \chi \leq 1{,}0$$

Where:

$\phi = 0{,}5\,(1 + \alpha(\lambda_c - \lambda_0) + {\lambda_c}^2)$

$\lambda_c = \sqrt{\frac{f_0}{E}}$

L_{cr} buckling length $L_{cr} = kL$ where L is the length between points of lateral support; for a cantilever, k=1

i radius of gyration about the relevant axis, determined using the properties of gross cross-section $i = \sqrt{\frac{I}{A}}$

α imperfection factor, $\alpha = 0{,}20$ for buckling class A

λ_0 limit of the horizontal plateau, $\lambda_0 = 0{,}10$ for buckling class A

N_{cr} elastic critical force for the relevant buckling mode based on the gross cross-sectional properties

For slenderness $\lambda_c \leq \lambda_0$or for $N_{Ed} \leq \lambda_0 N_{cr}$ the buckling effect may be ignored and only cross-sectional check apply.

$A_{haz} = N_{weld} \cdot 2 \cdot b_{haz} \cdot t_w = 30 \cdot 2 \cdot 0{,}04 \cdot 2 \cdot 0{,}035 = 0{,}0812 m^2$

$A_I = A - A_{haz}(1 - \rho_{0,haz}) = 1{,}675 - 0{,}0812(1 - 0{,}605) = 1{,}643 m^2$

$$I = \left(\frac{1}{4}\pi\left(r_{1,0}^4 - r_{1,i}^4\right)\right) + \left(\frac{1}{4}\pi\left(r_{2.0}^4 - r_{2,i}^4\right)\right) = \left(\frac{1}{4}\pi(3^4 - 2{,}965^4)\right) + \left(\frac{1}{4}\pi(2{,}835^4 - 2{,}8^4)\right) = 5{,}38m^4$$

$$i = \sqrt{\frac{I}{A}} = \sqrt{\frac{5{,}38}{1{,}675}} = 1792mm$$

$$\lambda_c = \frac{L_{cr}}{\pi i}\sqrt{\frac{f_0}{E}} = \frac{120 \cdot 10^3}{\pi \cdot 1792}\sqrt{\frac{275}{70000}} = 1{,}34$$

$$\phi = 0{,}5\left(1 + \alpha(\lambda_c - \lambda_0) + {\lambda_c}^2\right) = 0{,}5(1 + 0{,}2(1{,}34 - 0{,}1) + 1{,}34^2) = 1{,}516$$

$$\chi = \frac{1}{\phi + \sqrt{\phi^2 \cdot {\lambda_c}^2}} = \frac{1}{1{,}516 + \sqrt{1{,}516^2 \cdot 1{,}34^2}} = 0{,}283$$

$$\kappa = 1 - \left(1 - \frac{A_I}{A}\right)10^{-\lambda_c} - \left(0{,}05 + 0{,}1\frac{A_I}{A}\right){\lambda_c}^{1{,}3(1-\lambda_c)}$$
$$= 1 - \left(1 - \frac{1{,}643}{1{,}675}\right)10^{-1{,}34} - \left(0{,}05 + 0{,}1\frac{1{,}643}{1{,}675}\right)1{,}34^{1{,}3(1-1{,}34)} = 0{,}869$$

$$N_{Ed} = 7534070N$$

$$N_{Rd} = \frac{\kappa \cdot A_{eff} \cdot f_0}{\gamma_{M1}} = \frac{0{,}869 \cdot 1{,}487 \cdot 10^6 \cdot 275}{1{,}10} = 322904117N$$

$$M_{y,Ed} = 2{,}40 \cdot 10^{11}Nmm$$

$$M_{y,Rd} = \frac{\alpha \cdot \mathrm{W}_y \cdot f_0}{\gamma_{M1}} = \frac{0{,}97 \cdot 1{,}84 \cdot 10^9 \cdot 275}{1{,}10} = 4{,}48 \cdot 10^{11}Nmm$$

$$\left(\frac{N_{Ed}}{\chi_{min}\omega_x N_{Rd}}\right)^{0{,}8} + \frac{1}{\omega_0}\left[\left(\frac{M_{y,Ed}}{M_{y,Rd}}\right)^{1{,}7} + \left(\frac{M_{z,Ed}}{M_{z,Rd}}\right)^{1{,}7}\right]^{0{,}6}$$
$$= \left(\frac{7014953{,}44}{0{,}339 \cdot 0{,}7168 \cdot 265951876{,}5}\right)^{0{,}8} + \frac{1}{0{,}7168}\left[\left(\frac{2{,}40 \cdot 10^{11}}{4{,}48 \cdot 10^{11}}\right)^{1{,}7} + \left(\frac{0}{4{,}48 \cdot 10^{11}}\right)^{1{,}7}\right]^{0{,}6}$$
$$= 0{,}92 < 1{,}00$$

4.4.2. Resonance check

The support structure is likely to fail due to the large sinusoidal deformations resulting in fatigue. To avoid resonance, the structure should be designed in such a way that its natural frequency does not coincide with either 1P or 3P frequencies. As discussed in the *Paragraph 2.3.4* this creates three possible intervals and therefore three possible structures; a very stiff structure with a high natural frequency greater than 3P (stiff-stiff), a natural frequency between 1P and 3P (soft-stiff) and a very soft structure less than 1P (soft-soft) (Kühn, 2001). In literature, the term soft is commonly used for flexible turbine systems. In the first interval, the dynamic load occurs mostly due to waves with an eigenfrequency of 0,04Hz (25s) to 0,5 à 1,0Hz (2s à 1s). In the middle range, the dynamic load is mainly caused by wind. The excitation frequencies are calculated in *Paragraph 2.3.2*.

An onshore wind turbine can be schematized as a mass-on-pole system. The main force with a harmonic character is the wind load which is applied at the mass on top of the pole. An offshore wind turbine has to deal with wave loads besides wind loads, which are applied on a second mass. Thus, an offshore wind turbine can be schematized as a two mass-on-pole system, see Figure 4.10.

It consists of a laterally loaded uniform beam with two masses, which is embedded in the soil. The two main forces with a harmonic character are the wave and wind forces. The upper mass m_2 represents the nacelle, hub and rotor mass, which is located at hub height. This mass will be loaded with a harmonic force due to the wind (F_2). The lower mass m_1 represents the mass of the support structure above the fixed support. In reality, the pile continues below the schematized support. This mass is not taken into account since it will not take part in the dynamic vibrations. The mass of the support structure is concentrated at mean sea level (MSL), since the harmonic wave load (F_1) is applied here. Figure 4.12 shows the reduction of the mass-on-pole system to an equivalent 2-mass-spring-damper system.

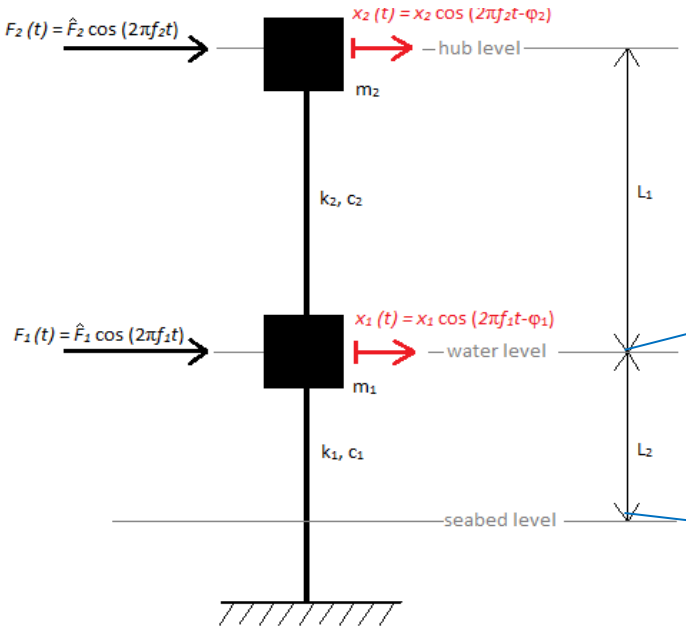

Figure 4.10 Mass-on-pole system (Wijngaarden M., 2013 -

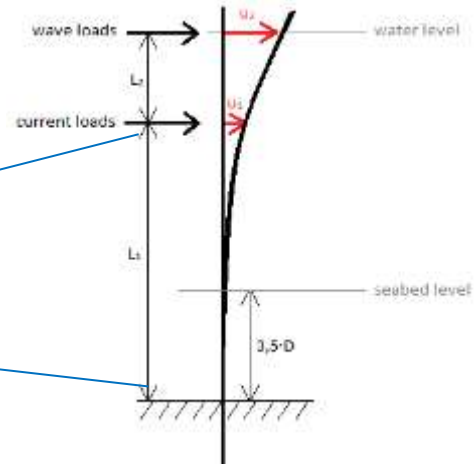

Figure 4.11 Lateral displacements of the support structure due to waves and current (Wijngaarden, M., 2013)

The equation of motion belonging to this model is the following (Tempel J. van der, 2006):

$$[M]\frac{d^2u}{dt^2} + [C]\frac{du}{dt} + [K]u = [F]\cos(\omega t - \theta) \qquad (4.21)$$

Where:

M	=	mass matrix	[kg]
C	=	damping matrix	[Ns/m]

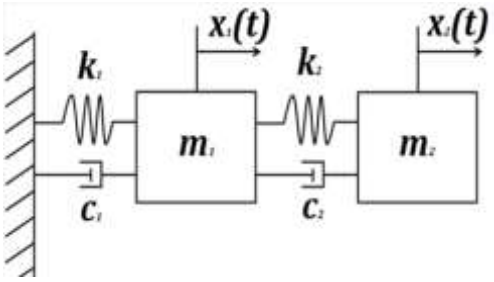

Figure 4.12 2-mass-spring-damper system

K	=	stiffness matrix	[N/m]
$\frac{d^2u}{dt^2}$	=	acceleration vector	[m/s²]
$\frac{du}{dt}$	=	velocity vector	[m/s]
U	=	displacement vector	[m]

From the equation of motion, the following equation can be obtained:

$$m_1 m_2 \omega^4 - \big(m_1 k_2 + m_2(k_1 + k_2)\big)\omega^2 + k_1 k_2 = 0 \tag{4.22}$$

The derivation of this equation can be found in Appendix A of the *Literature Suvey*. From this equation four angular frequencies can be obtained, however two will be of a negative sign and do not have any physical meaning. The two remaining angular frequencies ω_1 and ω_2 [rad/s] result into two natural frequencies with $f = \frac{\omega}{2\pi}$. The lower natural frequency f_1 is mainly determined by the turbine characteristics (m_2 and k_2 in Figure 4.10). The upper natural frequency f_2 is mainly determined by the support structure characteristics (m_1 and k_1 in Figure 4.10).

The masses and stiffness parameters will be explained now. The mass of the tower is divided over the two schematized masses, however not all structural mass will be equally excited. Depicted in Figure 4.11, the upper mass m_2, represents the top mass and a part of the tower structure. In the case of a uniform beam this mass is:

$$m_2 = m_{top} + 0{,}23 m_{tower}$$

which is obtained from the formula for the angular frequency of a cantilevered beam in Figure 4.13. However, in this case the mass of the tower is not uniformly distributed. The upper 0,23 part of the tower represents 15% of the total tower mass. So in this case, m_2 should be calculated with:

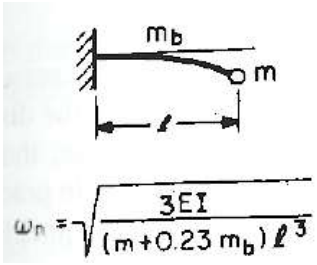

Figure 4.13. Baumeister's equation (Avallone E.A. and Baumeister T., 1996)

$$m_2 = m_{top} + 0{,}15 m_{tower}$$

The lower mass m_1 represents the remaining mass of the tower and the mass of the support structure:

$$m_1 = m_{ss} + 0{,}85 m_{tower}$$

In the schematization, the two masses are connected through linear springs. The horizontal wave and current forces result in a static displacement u_2 of the support structure, see Figure 4.12.

The displacement at water level can be calculated with the following two formulas:

$$u_1 = \frac{F_{current} {l_1}^3}{3EI} \tag{4.23}$$

$$u_2 = u_1 + \frac{F_{current} {l_1}^2}{2EI} + \frac{F_{wave} {l_2}^3}{3EI} \tag{4.24}$$

Filling in the values in formulas (4.23) and (4.24) gives:

$$u_1 = \frac{F_{current} {l_1}^3}{3EI} = \frac{53{,}81 \cdot 34{,}33^3}{3 \cdot 70 \cdot 10^6 \cdot 18{,}9} = 0{,}182mm$$

$$u_2 = u_1 + \frac{F_{current} {l_1}^2}{2EI} + \frac{F_{wave} {l_2}^3}{3EI} = 0{,}182 + \frac{53{,}81 \cdot 34{,}33^2}{2 \cdot 70 \cdot 10^6 \cdot 18{,}9} + \frac{10046 \cdot 6{,}67^3}{3 \cdot 70 \cdot 10^6 \cdot 18{,}9} = 183mm$$

Assumed is a mono pile with a diameter of 6m.

The stiffness k_1 can be calculated with:

$$k_1 = \frac{F_{wave} + F_{current}}{U_2} \tag{4.25}$$

The stiffness k_2 can be calculated with simple deformation formulas for a one-sided fixed beam:

$$k_2 = \frac{3EI}{{l_2}^2} \tag{4.26}$$

Where:

$$I = \left(\frac{1}{4}\pi\left(r_{1,0}^4 - r_{1,i}^4\right)\right) + \left(\frac{1}{4}\pi\left(r_{2.0}^4 - r_{2,i}^4\right)\right) \tag{4.27}$$

This is the moment of inertia calculated by hand for the double walled tower without the triangular connection in between. With the aid of AutoCAD this moment of inertia was compared with the actual value, which corresponded. The results of the calculations are shown in Table 4.9.

Now the masses and stiffness parameters can be calculated, the two angular frequencies ω_1 and ω_2 can now be determined, followed by the two natural frequencies with:

$$f_{1,2} = \frac{\omega_{1,2}}{2\pi} \tag{4.28}$$

Table 4.11 shows the obtained values. The results found when inserting these values in the fourth order polynomial equation are displayed in Table 4.12. These are obtained with the aid of the website Wolframalpha.com. Table 4.13 shows the excitation frequency ranges as calculated in *Paragraph 2.3.2*.

Table 4.11 Parameters for the dynamic calculations

k_1	55261998	[N/m]
k_2	336696	[N/m]
m_1	1484472	[kg]
m_2	533400	[kg]

Table 4.12 Natural frequency

ω_1	0,7921	[rad/s]
ω_2	6,1202	[rad/s]
f_1	0,1261	[Hz]
f_2	0,9741	[Hz]

Table 4.13 Excitation frequency ranges for the 8.0MW wind turbine

	min	max	
1P	0,080	0,203	[Hz]
3P	0,240	0,609	[Hz]

The natural frequencies are indicated with the black vertical lines in Figure 4.14. It appears that the first natural frequency f_1 is located in the 1P frequency range. Although the most common wind velocity 10,61m/s causes an excitation frequency of 0,165Hz (indicated with the blue vertical line), still

resonance will occur. The design could be changed to make sure no resonance will occur, although this would have large consequences. For example, a larger stiffness can be obtained by increasing tower wall thickness, although this will also increase the mass of the tower, which cancels the profit of the increase in stiffness; the natural frequency will remain the same Another solution for increasing the stiffness is by increasing the diameter of the tower, this should be more effective. However, Table 4.2 shows that a tower with a bottom diameter of 8m still has a natural frequency which is located in the 1P range.

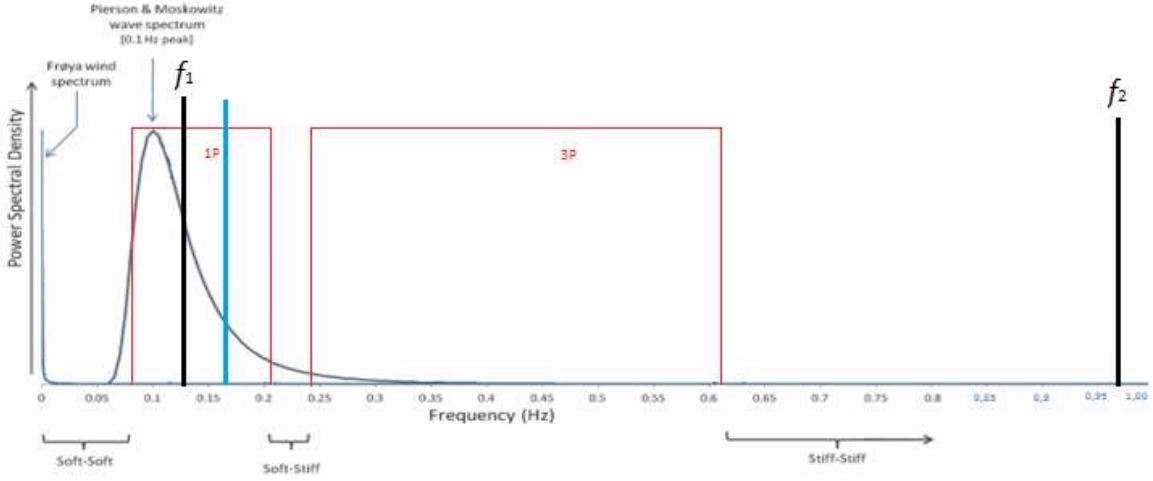

A solution that requires no changes to the design is using a tuned mass damper system (TMD). A TMD is a device consisting of a mass, a spring, and a damper that is attached to a structure in order to reduce the dynamic response of the structure. The frequency of the damper is tuned to a particular structural frequency so that when that frequency is excited, the damper will resonate out of phase with the structural motion. It appears that increasing the mass ratio $m_{ratio} = \frac{m_{damper}}{m_{structure}}$ magnifies the damping. However, since the added mass also increases, there is a practical limit on m_{ratio} (Connor, J.J., 2002).

The majority of applications have been for mechanical systems, but TMDs have also been used to improve the response of building structures under wind excitation. Besides, research has been done to applying TMD systems to wind turbines via finite element method by the University of Brasilia. In this research, the vibration of the tower was controlled using a pendulum damper, see Figure 4.15. It concerned a steel onshore wind turbine with a height of 60m, a diameter of 3m and a wall thickness of 15mm. The mass of the pendulum was equal to 8% of the structural total mass of 34899kg and had a length of 1,75m. The maximum nodal displacement decreased from approximately $2{,}5 \cdot 10^{-3}$m to $3{,}2 \cdot 10^{-10}$m with a shift of the maximum frequency from 0,8Hz to 0,5Hz and 0,75Hz (Avila, S and De Morais, M.V.G., 2013)

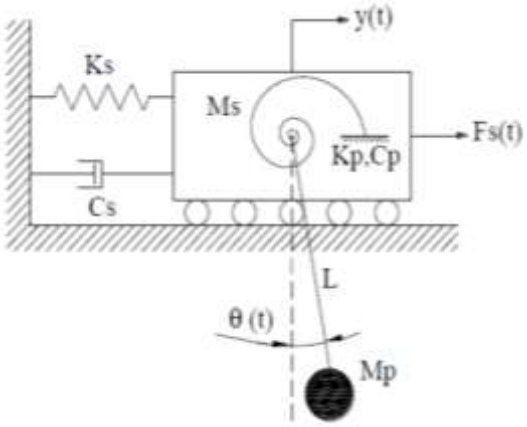

Figure 4.15 Wind tower depicted as a SDOF system with pendulum (Avila, S and De Morais, M.V.G., 2013)

In another research, Stewart and Lackner (2014) analyzed the use of structural control to mitigate loading in offshore wind turbines due to wind and waves. Passive TMDs were used to absorb and dissipate structural vibrations. In particular, the study investigated the load mitigation potential of passive TMDs for a 5MW offshore wind turbine supported by a mono pile, and subjected to realistic external conditions that include wind-wave misalignment. This misalignment causes large loads on the tower in the side-side direction, which has very little structural damping compared to the fore-aft direction (wind and waves are aligned in the same direction). The study made clear that two optimally tuned passive TMDs of approximately 2% of the total system mass are capable of reducing the tower's fore-aft and side-side fatigue loads by approximately 4-6% and 40% respectively. One TMD oscillates in the fore-aft direction and the other in the side-side direction. The TMD can be placed in the nacelle or on the platform, see Figure 4.16. It also appeared that increasing the TMD mass from 10.000kg to 20.000kg does not lead to a great advantage and that the orientation of the TMDs does not affect the loads. This insensitivity to orientation, combined with the small displacement of the TMDs suggests that being located at the top of the tower rather than in the nacelle is just as effectively. This is even more convenient, since there will be no or little extra space available in the nacelle.

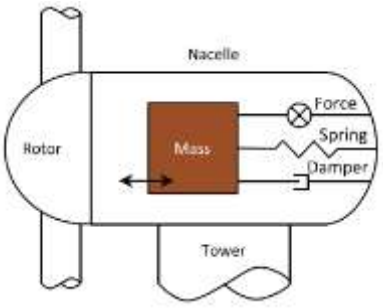

Figure 4.16 Schematization of a fore-aft TMD in the nacelle (Stewart, G.M. and Lackner, M.A., 2014)

From a practical perspective, TMDs are a relatively cheap and robust solution to suppress tower vibrations in the offshore environment, resulting in lower fatigue loads. The extra mass added to the structure can be 'dumb' mass constituted by concrete or even water (Stewart, G.M. and Lackner, M.A., 2014).

4.4.3. Serviceability limit state

Concerning the serviceability limit states for offshore structures, the DNV (2014) only gives limiting values for vertical deflections of the deck beams. In dissertations of Nicholson, J.C. (2011) and Jamil F (2012), a limiting value can be found for the horizontal deflection of the tower as a percentage of the tower height of 1,25% and 1% respectively. Also, to avoid interference between the turbine blades and the tower, a maximum rotation at the top of the tower should be set. Both Nicholson, J.C. (2011) and Jamil F (2012) apply a limit of 5°.

4.4.3.1. Tower top deflection

The tower can be assumed to behave as a cantilevered beam. The tower top deflection can then be determined by applying a uniform lateral load q along the height l of the tower. For I the average over the tower height is taken. So, the maximum deflection δ at the free end is obtained by:

$$\delta = \frac{qL^4}{8EI} \tag{4.29}$$

$$\delta < 0{,}01l \tag{4.30}$$

$$\delta = \frac{qL^4}{8EI} = \frac{1{,}82 \cdot 120^4}{8 \cdot 70 \cdot 10^6 \cdot 2{,}77} = 0{,}24m < 0{,}01 \cdot 120 = 1{,}20m$$

4.4.3.2. Tower top rotation

The rotation is determined by:

$$\theta = \frac{qL^3}{6EI} \tag{4.31}$$

Inserting the values gives the following tower top rotation:

$$\theta = \frac{qL^3}{6EI} \quad = \frac{1{,}82 \cdot 120^3}{6 \cdot 70 \cdot 10^6 \cdot 2{,}77} = 0{,}0027 < 0{,}05$$

4.5. Joints

Connections are an important part of every structure not only from the point of view of structural behavior, but also in relation to the cost of production. In this paragraph two joints are featured, namely the vertical joints between the extruded parts and the horizontal joints between the tower parts.

4.5.1 Vertical joints

The extruded parts are connected with each other at two points, encircled in Figure 4.17. For both joints butt welds will be applied. The initial idea was to apply integrated features at the bottom joint. However, since the sides will be cut off, this is no longer an option. The consideration which was made for the type of joint can be found in *Paragraph 3.4* in the *Literature Survey*.

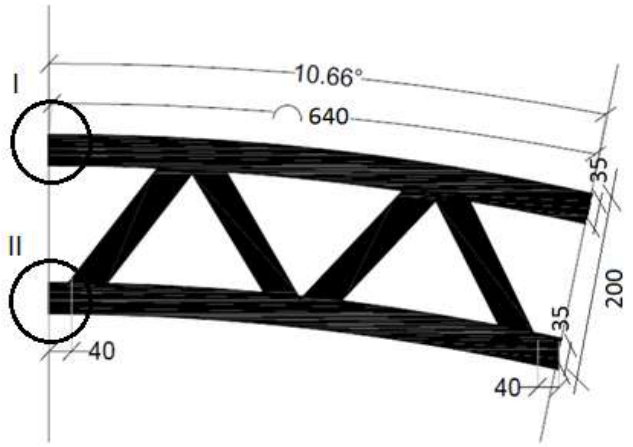

Figure 4.17 Vertical joints indicated in horizontal cross-section of an extruded part

4.5.1.1 Filler metal

Most of the wrought alloys in the 1xxx, 3xxx, 5xxx, 6xxx, and several in the 7xxx series are weldable with the MIG-welding technique. When the base material is a tempered alloy, the alloy for the welds should be different in order to prevent solidification cracks. The strength of the weld metal is usually lower than the strength of the parent material. The limiting strength of weld metal strongly depends on the filler metal used. Table 4.14 shows a selection of filler metals for each parent metal combination. A weld of two alloy 7020 parts can best be welded with filler metal of alloy 5556A, type 5 or type 4 (see Table 4.15). The first alloy has the maximum weld strength, type 5 has the maximum resistance to corrosion and type 4 avoids persistent weld cracking but should only be used in special cases due to the lower strength of the weld and elongation of the joint. In this case, corrosion is decisive, thus an

alloy of type 5 is preferred. 5556A also falls within type 5, so this filler metal is chosen. Table 4.16 shows the characteristic strength of filler metals. According to note 2, the value of filler metal 5356 can be applied for filler metal 5556A, which is $f_w = 260N/mm^2$.

Table 4.14 Selection of filler metals (EN 1999-1-1, 2007)

Parent metal combination [1]							
1st Part	2nd Part						
	Al-Si castings	Al-Mg castings	3xxx series alloys	5xxx- series alloys except 5083	5083	6xxx-series alloys	7020
7020	NR[2]	Type 5 Type 5 Type 5	Type 5 Type 5 Type 4	Type 5 Type 5 Type 5	5556A Type 5 5556A	Type 5 Type 5 Type 4	5556A Type 5 Type 4[4]

[1] In each box the filler metal for the maximum weld strength is shown in the top line; in the case of 6xxx series alloys and EN-AW 7020, this will be below the fully heat treated parent metal strength. The filler metal for maximum resistance to corrosion is shown in the middle line. The filler metal for avoidance of persistent weld cracking is shown on the bottom line.

[2] NR = Not recommended. The welding of alloys containing approximately 2% or more of Mg with Al-Si filler metal, or vice-versa is not recommended because sufficient Mg_2Si precipitate is formed at the fusion boundaries to embrittle the weld. Where unavoidable see prEN 1011-4.

[3] The corrosion behaviour of weld metal is likely to be better if its alloy content is close to that of the parent metal and not markedly higher. Thus for service in potentially corrosive environments it is preferable to weld EN-AW 5454 with 5454 filler metal. However, in some cases this may only be possible at the expense of weld soundness, so that a compromise will be necessary.

[4] Only in special cases due to the lower strength of the weld and elongation of the joint.

Table 4.15 Alloy grouping used in Table 4.16 (EN 1999-1-1, 2007)

Filler metal grouping	Alloys
Type 3	3103
Type 4	4043A, 4047A[1]
Type 5	5056A, 5356 / 5356A, 5556A / 5556B, 5183 / 5183A

[1] 4047A is specifically used to prevent weld metal cracking in joints. In most other cases, 4043A is preferable.

Table 4.16 Characteristic strength values of weld metal f_w (EN 1999-1-1, 2007)

Characteristic strength	Filler metal	Alloy								
		3103	5052	5083	5454	6060	6005A	6061	6082	7020
f_w [N/mm²]	5356	-	170	240	220	160	180	190	210	260
	4043A	95	-	-	-	150	160	170	190	210

1 For alloys EN AW-5754 and EN AW-5049 the values of alloy 5454 can be used;
for EN AW-6063, EN AW-3005 and EN AW-5005 the values of alloy 6060 can be used;
for EN AW-6106 the values of alloy 6005A can be used;
for EN AW-3004 the values of alloy 6082 can be used;
for EN AW-8011A a value of 100 N/mm² for filler metal Type 4 and Type 5 can be used.

2 If filler metals 5056,5356A, 5556A/5556B, 5183/5183A are used then the values for 5356 have to be applied.

3 If filler metals 4047A or 3103 are used then the values of 4043A have to be applied.

4 For combinations of different alloys the lowest characteristic strength of the weld metal has to be used.

4.5.1.2 Design strength weld

A full penetration butt weld will be applied. The effective thickness can be taken equal to the thickness of the connected members. The distribution of forces acting in the weld is similar to that in the connected members (TALAT 2302, 2007).

For a butt welded connection compromising a square butt weld, the forces shall be calculated at the weakest section adjacent to the weld, see Figure 4.18. If the strength of the filler metal is lower than that of the heat affected zone in the parent material $f_w \leq f_{u,haz}$, forces shall also be calculated at the weakest section through the weld (TALAT 2302, 2007).

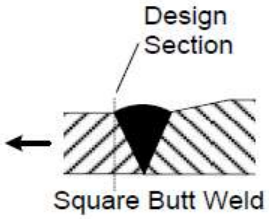

Figure 4.18 Design section for a square butt weld (TALAT 2302, 2007)

According to EN 1999-1-1 (2007) the check of butt welds is done in the following way (see Figure 4.19):

- For normal stress perpendicular to the weld axis

$$\sigma_{\perp Ed} \leq \frac{f_w}{\gamma_{mw}} \tag{4.32}$$

- For shear stress

$$\tau_{Ed} \leq 0{,}6\frac{f_w}{\gamma_{mw}} \tag{4.33}$$

- For combined normal and shear stress:

$$\sqrt{\sigma_{\perp Ed}^2 + 3\tau_{Ed}^2} \leq \frac{f_w}{\gamma_{mw}} \tag{4.34}$$

Where:

f_w limiting strength weld metal
$\sigma_\perp$ normal stress, perpendicular to the weld axis
τ shear stress, parallel to the weld axis
γ_{mw} partial safety factor for welded joints $\gamma_{mw} = 1{,}25$

Normal stresses parallel to the weld axis do not have to be considered.

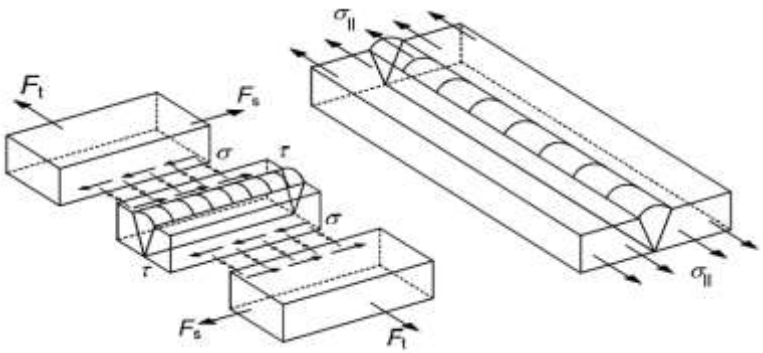

Figure 4.19 Definition of rupture section and stresses in a butt weld (TALAT 2302, 2007)

Only formula (4.32) applies here. The butt welds at the bottom of the tower will be checked, since here the stresses are largest. The following maximum compressive and tensile stresses at the extreme fibers are found in a horizontal cross-section:

$$\sigma_c = -\frac{M_{tot}}{W_{bottom}} - \frac{F_{tower} + F_{nacelle,hub,rotor}}{A_{bottom}} = -\frac{239728}{1{,}84} - \frac{7534}{1{,}675} = -134{,}8N/mm^2$$

$$\sigma_t = \frac{M_{tot}}{W_{bottom}} - \frac{F_{tower} + F_{nacelle,hub,rotor}}{A_{bottom}} = \frac{239728}{1{,}84} - \frac{7534}{1{,}675} = 125{,}8N/mm^2$$

Inserting the maximum stress in formula (4.32) gives:

$$134{,}8 \leq \frac{260}{1{,}25} = 208$$

So the welds meet the ULS check.

4.5.1.3 Design strength HAZ

The HAZ values are only valid for MIG welding and thickness up to 15mm. In *Paragraph 4.2* it was noted that for higher thickness the HAZ values and ρ-factors have to be further reduced by a factor of 0,8. The new values were given in Table 4.4, and repeated here:

Table 4.15 New HAZ values and ρ-factors

$f_{u,haz}$ [N/mm²]	$\rho_{u,haz}$
224	0,640

According to EN 1999-1-1 (2007), the HAZ is assumed to extend a distance b_{haz} in any direction from a weld, measured transversely from the center line of an in-line butt weld. For a MIG weld laid on unheated material, and with interpass cooling to 60°C or less when multi-pass welds are laid and with a thickness larger than 25mm, b_{haz} has a value of 40mm.

The value of the design strength of the HAZ according to EN 1999-1-1 (2007) is:

- For tensile force perpendicular to the failure plane

$$\sigma_{haz} \leq \frac{f_{u,haz}}{\gamma_{mw}} \tag{4.35}$$

- For shear force in the failure plane

$$\tau_{haz} \leq \frac{f_{v,haz}}{\gamma_{mw}} \tag{4.36}$$

- For combined tension and shear stress:

$$\sqrt{\sigma^2 + 3\tau^2} \leq \frac{f_{0,haz}}{\gamma_{mw}} \tag{4.37}$$

Where:

σ_{haz} design normal stress perpendicular to the weld axis
τ_{haz} design shear stress parallel to the weld axis
$f_{0,haz}$ limiting strength of HAZ
$f_{v,haz}$ limiting shear strength of HAZ
γ_{mw} partial safety factor for welded joints $\gamma_{mw} = 1{,}25$

Only formula (4.35) applies here. The same maximum stresses apply here as calculated for the weld. Inserting the value in formula (4.35) gives:

$$134{,}8 \leq \frac{224}{1{,}25} = 179{,}2$$

This check satisfies the requirements.

In this case the strength of the filler metal is higher than the strength of the heat affected zone in the parent material, thus no forces should be calculated at the weakest section through the weld.

4.5.2 Horizontal joints

The aluminium tower is divided into four sections of 30m each. Thus, the tower is installed in four pieces, each piece placed on top of the other using lattice cranes. The pieces for existing steel towers are welded or bolted together, forming a complete tower. In this case, the choice is made for bolting on site. This allows for an easy and fast fitting and obtains a reliable connection (DNV, 2005). Also, welding can only be done when the weather conditions permit; high wind and rain make it difficult to produce a high quality weld. For the flanges alloy 6082-T6 will be applied, since this alloy has good resistance to corrosion and dynamic loading. The flanges will be welded with t-butt welds to the ends of the tower parts, in the same way as can be seen Figure 4.20, which make it possible to bolt the parts together on site with preloaded stainless steel bolts. The concept of the connection can be seen in Figure 4.21, where the slope is illustrated very exaggerated.

Figure 4.20 A technician prepares equipment to weld a flange to a tower part (Lincoln Electric, 2010)

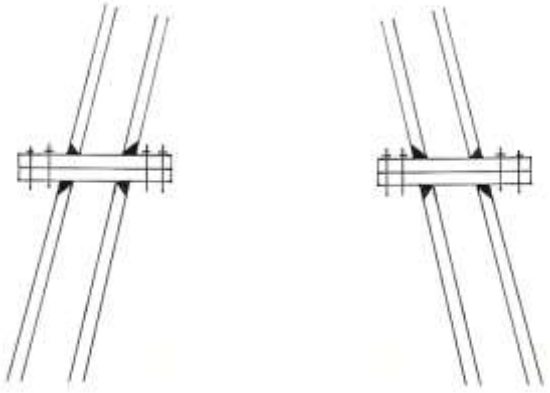

Figure 4.21 Concept horizontal joint

4.5.2.1 Joint between the tower parts and flanges

For the design of welds the throat section should be taken as the governing section (EN 1999-1-1, 2007). The stresses acting on the throat section of a fillet weld are defined in Figure 4.22. The normal stress $\sigma_{\parallel}$ parallel to the axis of a weld need not be included when checking the resistance of a weld. The design resistance of a fillet weld should fulfil:

$$\sqrt{\sigma_{\perp Ed}^2 + 3(\tau_{\perp Ed}^2 + \tau_{\parallel Ed}^2)} \leq \frac{f_w}{\gamma_{Mw}} \qquad (4.38)$$

Where:

$\sigma_{\perp}$	normal stress perpendicular to the throat section
$\tau_{\perp}$	shear stress acting on the throat section perpendicular to the weld axis
$\tau_{\parallel}$	shear stress acting on the throat section parallel to the weld axis
f_w	the characteristic strength of weld metal
γ_{Mw}	the partial safety factor for welded joints

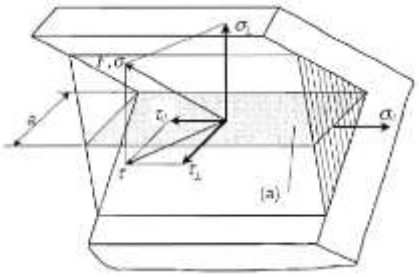

Figure 4.22 Stresses acting on the throat section of a fillet weld (EN 1999-1-1- (2007)

A single fillet welded joints does not fulfill the requirements. A single sided full penetration T-butt weld is a better choice, see Figure 2.24. Here, the weld throat has a full section thickness of 35mm.

First the perpendicular normal and shear stresses are calculated:

$$\sigma_{\perp} = \frac{\frac{1}{2}\sqrt{2} \cdot F}{a \cdot l} = \frac{\frac{1}{2}\sqrt{2} \cdot 125{,}8 \cdot 35 \cdot 640}{35 \cdot 640} = 89 N/mm^2$$

$$\tau_{\perp} = \frac{\frac{1}{2}\sqrt{2} \cdot F}{a \cdot l} = \frac{\frac{1}{2}\sqrt{2} \cdot 125{,}8 \cdot 35 \cdot 640}{35 \cdot 640} = 89 N/mm^2$$

Filling in the values into formula 4.38 gives:

$$\sqrt{89^2 + 3 \cdot 89^2} \leq \frac{260}{1{,}25}$$

$$178 < 208$$

The weld satisfies the requirements.

The following applies for the HAZ in the flange of the tower wall:

$$\sigma_{haz} \leq \frac{f_{u,haz}}{\gamma_{mw}} \qquad (4.39)$$

$$125{,}8 \leq \frac{224}{1{,}25} = 179{,}2$$

For the HAZ in the flange:

$$\tau_{haz} \leq \frac{f_{v,haz}}{\gamma_{mw}} \qquad (4.40)$$

$$125{,}8 \leq \frac{224}{1{,}25} = 179{,}2$$

4.5.2.2. Joint between the tower parts

The welded flanges at the ends of the tower sections are bolted on site. A stainless steel preloaded M27 bolt with a grade of 410-HT is assumed with an ultimate strength of 1240MPa. Preloaded bolts can be an advantage above using non preloaded bolts considering corrosion and fatigue resistance. A disadvantage is the fact that preloaded bolts creep over time, hereby losing part of the prestress. Stainless steel can very easily be tightened with the hydraulic tensioning. Tightening with a hydraulic bolt tensioner preserves the condition of the components, no matter how many successive tightening and untightening operations occur (SKF, 2001). Galvanic corrosion will be prevented by passivation of the bolts (see Paragraph 4.5.2.3).

The bolt has a tensile stress area of $459{,}41mm^2$. The diameter of the hole d_0 is 29mm. The spacing between the fasteners are calculated based on the M27 bolt. In this case a double row of fasteners is applied, of which the spacing symbols can be seen in Figure 4.23 on the right.

$e_1 = 2{,}0 \cdot d_0 = 2{,}0 \cdot 29 = 58mm$

$e_2 = 1{,}5 \cdot d_0 = 1{,}2 \cdot 29 = 43{,}5mm$

$p_1 = 2{,}5 \cdot d_0 = 2{,}2 \cdot 29 = 72{,}5mm$

$p_2 = 3{,}0 \cdot d_0 = 2{,}4 \cdot 29 = 87mm$

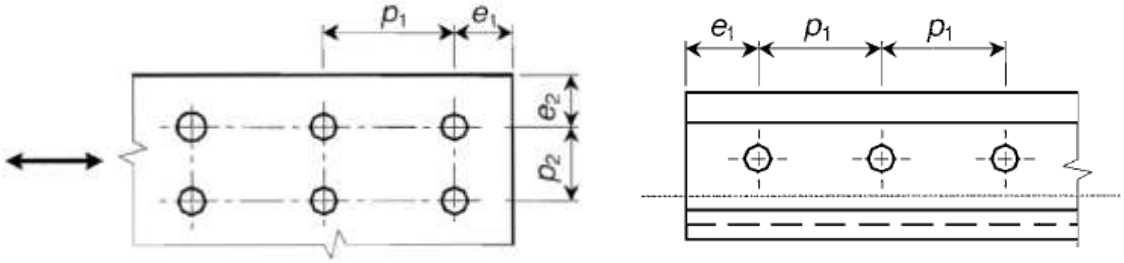

Figure 4.23 Symbols for spacing of fasteners (EN 1999-1-1, 2007)

Category E connections with preloaded high strength bolts are applicable here. In this category preloaded high strength bolts with controlled tightening should be used. Such preloading improves fatigue resistance. The following criteria apply here:

$$F_{t,Ed} \leq F_{t,Rd} \tag{4.41}$$

$$F_{t,Ed} \leq B_{p,Rd} \tag{4.42}$$

Where:

$F_{t,Ed}$ design tensile force per bolt at the ultimate limit state
$F_{t,Rd}$ desgin tension resistance per bolt
$B_{p,Rd}$ design resistance for punching shear resistance

The design tension resistance $F_{t,Rd}$ is according to:

$$F_{t,Rd} = \frac{k_2 f_{ub} A_s}{\gamma_{M2}} \tag{4.43}$$

Where:

$k_2 = 0{,}9$	for steel bolts
A_s	tensile stress area of the bolt

Now the design tension force on one bolt will be calculated. The distance between the bolts is 45mm, the thickness of the tower wall is 35mm. This gives an F_t as schematized in Figure 4.24 of:

$$F_t = \sigma_t \cdot A = 125{,}8 \cdot 72{,}5 \cdot 35 = 319217{,}5N$$

According to EN 1999-1-1 (2007), where fasteners are required to carry an applied tensile force, they should be proportioned to also resist the additional force due to prying action, where this can occur, see Figure 4.24. These prying forces F_p must be added to the tensile forces due to the external load, which has a value of:

$$F_p = \frac{M}{n} = \frac{F_t b}{n} = \frac{319217{,}5 \cdot (0{,}5 \cdot 87 + 43{,}5 + 15 + 17{,}5)}{43{,}5 + 0{,}5 \cdot 87} = 438465N$$

Where:

b	distance from bolt to weld toe
n	end distance

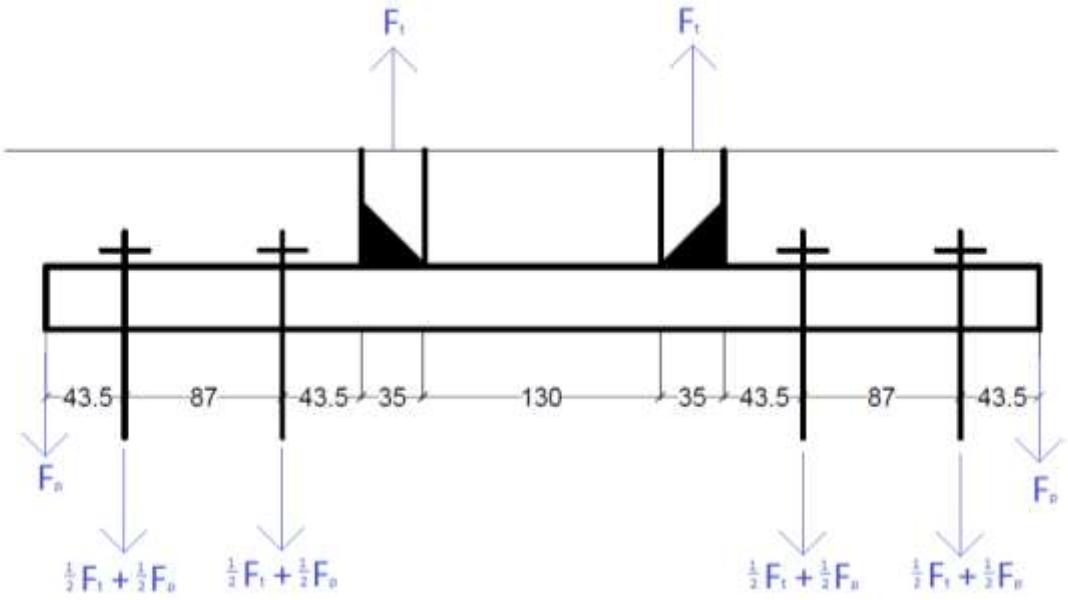

Figure 4.24 Forces in the flange joint

This gives a design tensile force per bolt of:

$$F_{t,Ed} = \frac{1}{2}F_t + \frac{1}{2}F_p = \frac{1}{2}\cdot 319217{,}5 + \frac{1}{2}\cdot 438465 = 378841{,}5N$$

$$F_{t,Rd} = \frac{k_2 f_{ub} A_s}{\gamma_{M2}} = \frac{0{,}9\cdot 1240\cdot 459{,}41}{1{,}25} = 410161N$$

$$F_{t,Ed} < F_{t,Rd}$$

$$378841{,}5N < 410161N$$

It satisfies the requirements.

The design resistance for punching shear resistance is:

$$B_{p,Rd} = \frac{0{,}6\pi\cdot d_m\cdot t_p\cdot f_u}{\gamma_{M2}} \tag{4.44}$$

Where:

d_m the mean of the across points and across flats dimensions of the bolt head or the nut or if washers are used the outer diameter of the washer, whichever is smaller

t_p the thickness of the plate under the bolt head or the nut

f_u the characteristic ultimate strength of the member material

Filling in the values gives:

$$B_{p,Rd} = \frac{0{,}6\pi\cdot d_m\cdot t_p\cdot f_u}{\gamma_{M2}} = \frac{0{,}6\pi\cdot 1{,}5\cdot 27\cdot 35\cdot 310}{1{,}25} = 662637N$$

$$F_{t,Ed} < B_{p,Rd}$$

$$378841{,}5N < 662637N$$

This also satisfies the requirements.

Now the flanges will be checked. The minimal thickness of the flange should be:

$$t_{min} = \sqrt{\frac{1{,}10\cdot 4\cdot M}{f_y\cdot w}} = \sqrt{\frac{1{,}10\cdot 4\cdot 198135\cdot 111{,}5}{310\cdot 488}} = 27mm$$

Assumed is a thickness of 35mm, equal to the tower wall thicknesses.

In the cases where prying forces develop, the tension resistance of a flange $F_{u,Rd}$should be taken as the smallest value for the four possible failure modes (see Figure 4.25) and has to be determined as follows:

- Mode 1: Flange failure by developing four hardening plastic hinges, two of which are at the web-to-flange connection and two at the bolt location:

$$F_{u,Rd} = \frac{2(M_{u,1})_w + 2(M_{u,1})_b}{m} \tag{4.45}$$

In the formula, $(M_{u,1})_w$ should be evaluated according to (4.49) with $\rho_{u,haz} < 1$, while $(M_{u,1})_b$ with $\rho_{u,haz} = 1$ and considering the net area.

- Mode 2a: Flange failure by developing two hardening plastic hinges with bolt forces at the elastic limit:

$$F_{u,Rd} = \frac{2M_{u,2} + n\sum B_o}{m+n} \tag{4.46}$$

- Mode 2b: Bolt failure with yielding of the flange at the elastic limit:

$$F_{u,Rd} = \frac{2M_{o,2} + n\sum B_u}{m+n} \tag{4.47}$$

- Mode 3: Bolt failure:

$$F_{u,Rd} = \sum B_u \tag{4.48}$$

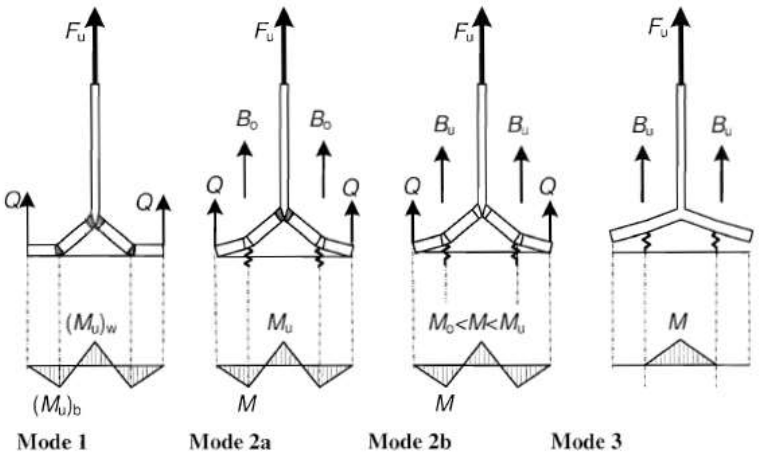

Figure 4.25 Failure modes of an equivalent T-stub (EN 1999-1-1, 2007)

With:

$$M_{u,1} = 0{,}25 \cdot t_f^2 \cdot \sum (l_{eff,1}\rho_{u,haz} f_u) \cdot \frac{1}{k} \cdot \frac{1}{\gamma_{M1}} \tag{4.49}$$

$$M_{u,2} = 0{,}25 \cdot t_f^2 \cdot \sum (l_{eff,2}\rho_{u,haz} f_u) \cdot \frac{1}{k} \cdot \frac{1}{\gamma_{M1}} \tag{4.50}$$

$$M_{o,2} = 0{,}25 \cdot t_f^2 \cdot \sum (l_{eff,1}\rho_{o,haz} f_u) \cdot \frac{1}{\gamma_{M1}} \tag{4.51}$$

$n = e_{min}$ but $n \leq 12{,}5m$

$$\frac{1}{k} = \frac{f_0}{f_u}\left(1 + \psi\frac{f_u - f_o}{f_o}\right) \tag{4.52}$$

$$\psi = \frac{\varepsilon_u - 1{,}5 \cdot \varepsilon_o}{1{,}5 \cdot (\varepsilon_u - \varepsilon_o)} \tag{4.53}$$

$$\varepsilon_o = \frac{f_o}{E} \tag{4.54}$$

Where:

ε_u the ultimate strain of the flange material

B_u the tension resistance $B_{t,Rd}$ of a bolt-plate assembly

B_o the conventional bolt strength at elastis limit, for steel bolts:

$$= \frac{0{,}9 \cdot f_y \cdot A_s}{\gamma_{M2}}$$

Where:

A_s the stress area of bolt

$\sum B_u$ the total value of B_u for all the bolts

$l_{eff,1}$ the value of l_{eff} for mode 1

$l_{eff,2}$ the value of l_{eff} for mode 2

e_{min} and m are as indicated in Figure 4.26.

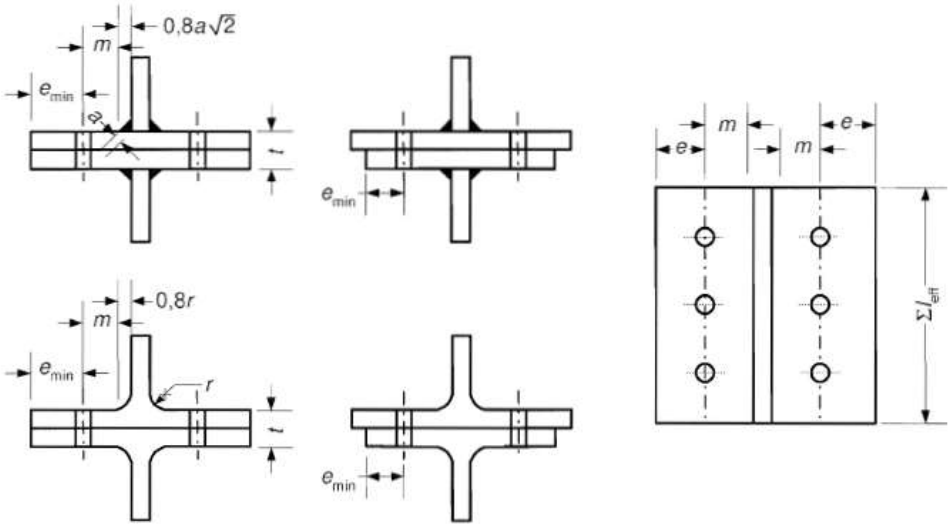

Figure 4.26 Dimensions of an equivalent T-stub (EN 1999-1-1, 2007)

For mode 1, the following applies:

$$m = 43{,}5mm \; ; \; e = 43{,}5mm \; ; \; e_1 = 58mm \; ; \; t_f = 35mm$$

$$l_{eff,1} = l_{eff,nc} = \begin{cases} 4m + 1{,}25e = 4 \cdot 43{,}5 + 1{,}25 \cdot 43{,}5 = 228mm \\ 2m + 0{,}625e + e_1 = 2 \cdot 43{,}5 + 0{,}625 \cdot 43{,}5 + 58 = \mathbf{172mm} \end{cases}$$

$$\frac{1}{k} = \frac{f_0}{f_u}\left(1 + \psi\frac{f_u - f_0}{f_0}\right) = \frac{260}{310}\left(1 + 0666 \cdot \frac{310 - 260}{260}\right) = 0{,}95$$

$$\psi = \frac{\varepsilon_u - 1{,}5 \cdot \varepsilon_o}{1{,}5 \cdot (\varepsilon_u - \varepsilon_o)} = \frac{0{,}443 - 1{,}5 \cdot 0{,}0037}{1{,}5 \cdot (0{,}443 - 0{,}0037)} = 0{,}666$$

$$\varepsilon_o = \frac{f_0}{E} = \frac{260}{70000} = 0{,}0037$$

$$\varepsilon_u = 0{,}30 - 0{,}22\frac{f_0}{400} = 0{,}30 - 0{,}22 \cdot \frac{260}{400} = 0{,}443$$

Filling in the values gives:

$$\left(M_{u,1}\right)_w = 0{,}25 \cdot t_f^2 \cdot \sum\left(l_{eff,1}\rho_{u,haz}f_u\right) \cdot \frac{1}{k} \cdot \frac{1}{\gamma_{M1}} = 0{,}25 \cdot 35^2 \cdot 172 \cdot 0{,}839 \cdot 310 \cdot 0{,}95 \cdot \frac{1}{1{,}1}$$
$$= 11{,}8 \cdot 10^6 Nmm$$

$$\left(M_{u,1}\right)_b = 0{,}25 \cdot t_f^2 \cdot \sum\left(l_{eff,1}\rho_{u,haz}f_u\right) \cdot \frac{1}{k} \cdot \frac{1}{\gamma_{M1}} = 0{,}25 \cdot 35^2 \cdot 172 \cdot 1{,}0 \cdot 310 \cdot 0{,}95 \cdot \frac{1}{1{,}1}$$

$$= 14{,}1 \cdot 10^6 Nmm$$

$$F_{u,Rd} = \frac{2(M_{u,1})_w + 2(M_{u,1})_b}{m} = \frac{2 \cdot 11{,}8 + 2 \cdot 14{,}1}{0{,}0435} = 1191kN$$

For mode 2a, the following applies:

$$l_{eff,2} = l_{eff,nc} = \begin{cases} 4m + 1{,}25e = 4 \cdot 43{,}5 + 1{,}25 \cdot 43{,}5 = 228mm \\ 2m + 0{,}625e + e_1 = 2 \cdot 43{,}5 + 0{,}625 \cdot 43{,}5 + 58 = \mathbf{172mm} \end{cases}$$

This gives a similar value for $M_{u,2}$as for $M_{u,1}$:

$$B_o = \frac{0{,}9 \cdot f_y \cdot A_s}{\gamma_{M2}} = \frac{0{,}9 \cdot 930 \cdot 459{,}41}{1{,}25} = 307621N$$

$$F_{u,Rd} = \frac{2M_{u,2} + n\sum B_o}{m + n} = \frac{2 \cdot 11{,}8 + 0{,}0435 \cdot 307{,}6}{0{,}0435 + 0{,}0435} = 425kN$$

For mode 2b, the following applies:

$$M_{o,2} = 0{,}25 \cdot t_f^2 \cdot \sum\left(l_{eff,1}\rho_{u,haz}f_u\right) \cdot \frac{1}{\gamma_{M1}} = 0{,}25 \cdot 35^2 \cdot 172 \cdot 0{,}839 \cdot 310 \cdot \frac{1}{1{,}1} = 12{,}5 \cdot 10^6 Nmm$$

$$B_u = B_{t,Rd} = lowest\ value\ of \begin{cases} F_{t,Rd} \\ B_{p,Rd} \end{cases}$$

$$F_{t,Rd} = \frac{k_2 \cdot f_{ub} \cdot A_s}{\gamma_{M2}} = \frac{0{,}9 \cdot 1240 \cdot 459{,}42}{1{,}25} = 410161N$$

$$B_{p,Rd} = \frac{0{,}6\pi \cdot d_m \cdot t_p \cdot f_u}{\gamma_{M2}} = \frac{0{,}6\pi \cdot 1{,}5 \cdot 27 \cdot 35 \cdot 310}{1{,}25} = 662637N$$

$$B_u = F_{t,Rd} = 410161N$$

$$F_{u,Rd} = \frac{2M_{o,2} + n\sum B_u}{m+n} = \frac{2 \cdot 12{,}5 + 0{,}0435 \cdot 410}{0{,}0435 + 0{,}0435} = 492{,}4kN$$

For mode 3, the following applies:

$$F_{u,Rd} = \sum B_u = 410kN$$

In this case, mode 3 is decisive. Bolt failure will occur first. As calculated before, this requirement is satisfied. Thus, the assumed stainless steel M27 bolt satisfies the requirements.

4.5.2.3. Joint between tower and transition piece

The transition piece which supports the tower of the turbine is located at a height of 13,23+MSL. It is a steel tubular element containing a platform on top, a boat lander on the outside and electrical components on the inside, see Figure 4.24. It has a somewhat larger diameter to cover the head of the mono pile, which is always damaged by the ramming procedure. Normally, on top of the transition piece, a flange secures the connection with the steel tower using nuts and bolts (Karimirad, 2014). In this case, the aluminium tower and steel transition piece have to be connected. Since the wind tower is located in an offshore environment, there is a risk of galvanic corrosion. This type of corrosion may occur when there is both metallic contact and an electrolytic bridge between different metals. Three possible solutions for avoiding galvanic corrosion are:

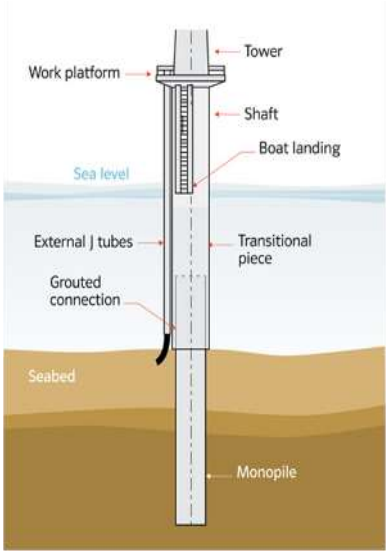

Figure 4.24 Mono pile foundation (4C Offshore, 2015)

- Breaking the connection by electrically insulating the two materials from each other. This might not be the most optimal solution in combination with preloaded bolts since plastics creep.
- Stalgard coating: a proprietary coating process providing protection against atmospheric corrosion and galvanic corrosion protection (Barrett, 2016). A disadvantage of a coating is that it can be damaged.
- Passivation and preoxidation: when stainless steel fasteners are passivated or preoxidated prior to assembly, no galvanic corrosion will occur. Passivation is the formation of a protective oxide coating on the steel by treating it briefly with an acid. By doing this the presence of metallic (free) iron from the surface will be removed. The oxide coating is almost inert. Preoxidation is the formation of an oxide coating by exposing the fasteners to a temperature of approximately 700°C in an air furnace. The surface formed is inert enough to prevent galling due to galvanic corrosion (Barrett, 2016). Also in this case, the corrosion-

resistant surface can be damaged through mechanical means, heat or chemical damage. In contrast to the Stalgard coating, the passive layer can heal itself naturally.

Thus, the best solution to prevent galvanic corrosion in this case is passivation of the stainless steel bolts. The design of the joint will be similar as the joint between the tower sections, as is elaborated in the previous paragraph. For the area where the aluminium flange and steel flange are in contact, elextrically insulation may be applied.

4.5.2.4 Joint between tower and nacelle

The connection between the tower and nacelle is schematized in Figure 4.26. At a factory, the (fiberglass) nacelle is bolted around the equipment. The yaw-system is located at the bottom of the nacelle. At the site, the nacelle is lifted onto the completed tower and bolted into place (Miceli, F., 2012).

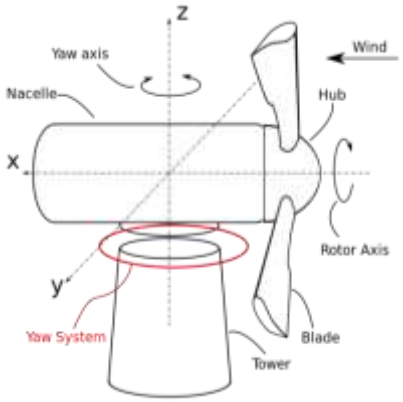

Figure 4.26 Schematic representation of the main nacelle components (Wikipedia, 2015)

5 Conclusion and discussion

The problem as stated in *Paragraph 1.2* will be answered in this chapter.

How will a support structure from aluminium extruded sections be designed and is this a more optimal solution for offshore wind turbines than the existing steel ones?

5.1 Brief summary

The goal of this thesis is to develop a conceptual design for a support structure of an aluminium offshore wind turbine. This was done first by exploring some design limits. The conceptual design was reduced to the design of the tower of the wind turbine. Besides, applying extrusion technique leads to a limit on the dimensions of the extruded parts. Moreover, the wind and wave loads cause excitation frequencies which should be taken into account while designing the tower.

After determining the design limits and starting points, a design concept and its final dimensions are obtained; see Table 5.1 and Figures 5.1, 5.2, 5.3 and 5.4. Figure 5.3 and 5.4 show enlargements of the tower wall at the top and bottom respectively of part D as shown in Figure 5.2. The vertical lines indicate the boundaries of the extrusion parts. To realize a conical shape of the tower, small parts are cut off diagonally of either side of the extruded parts. This is the reason why the extruded parts fit well together in Figure 5.3, in contrast to Figure 5.4. A distance of 40mm has to be removed of both sides of an extrusion part at the top, as indicated in Figure 5.4.

Subsequently, the cross-sections are classified. The cross-section of the tower can be classified in class 3 and the cross-section of an extruded part is classified in class 1.

Table 5.1 Tower dimensions and important characteristics of the design

D,bottom	**6**	[m]
t,w	**35**	[mm]
t,towerwall	**200**	[mm]
F.B check	**0,9**	[-]
Frequency f_1	**0,126**	[Hz]
Volume tower	**100,28**	[m3]
Number of welds	**30**	[-]
Welded area	**0,0812**	[m2]

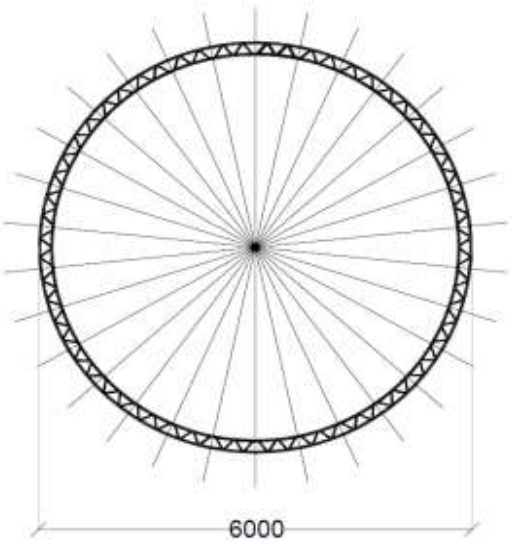

Figure 5.1Horizontal cross-section of the 8MW wind turbine tower

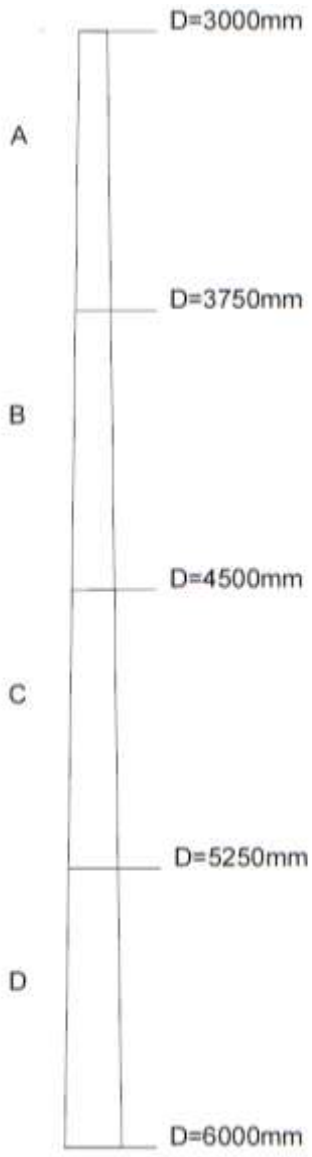

Figure 5.2 Tower view with indicated the top and bottom diameters of the four extruded parts

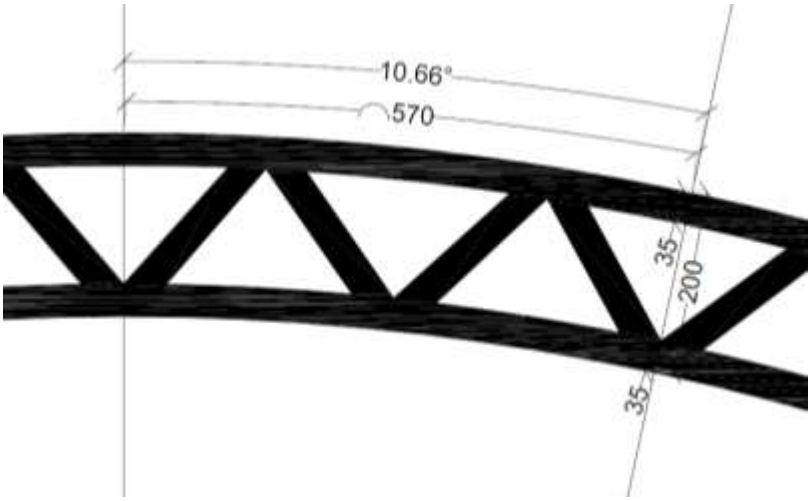

Figure 5.3 Close-up of one extruded part in a horizontal cross-section at the top of part D

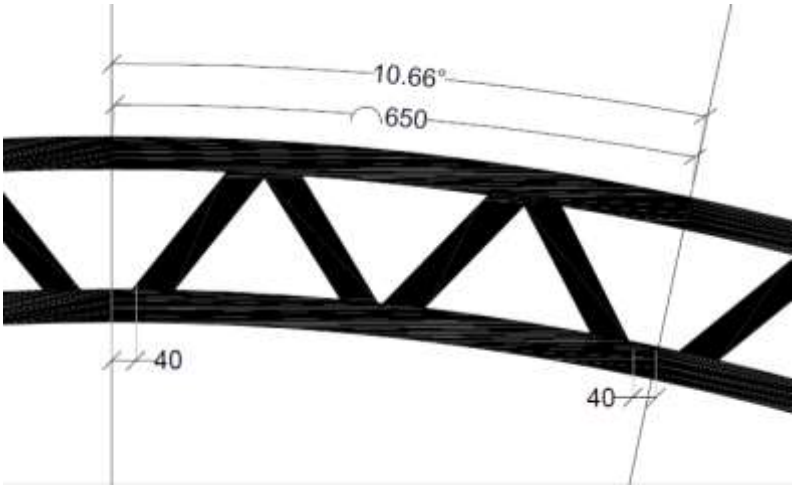

Figure 5.4 Close-up of one extruded part in a horizontal cross-section at the bottom of part D

Then the loads are calculated, which are summarized in Table 5.2 and indicated in Figure 5.5.

Table 5.2Loads overview

$F_{wind,rotor}$	1881	kN
$q_{wind,tower}$	2,46	kN/m
$F_{current}$	72,65	kN
F_{wave}	13561,6	kN
F_{tower}	2707,6	kN
F_{blades}	1000,62	kN
$F_{nacelle,hub,rotor}$	4826,52	kN

Next, the checks were performed, which are summarized in Table 5.3.

Table 5.3 Checks overview

Compression	0,019
Shear	0,017
Bending moment	0,54
Bending and axial force	0,59
Flexural buckling	0,92
Deflection δ	0,24m<1,20m
Rotation θ	0,84°<5°

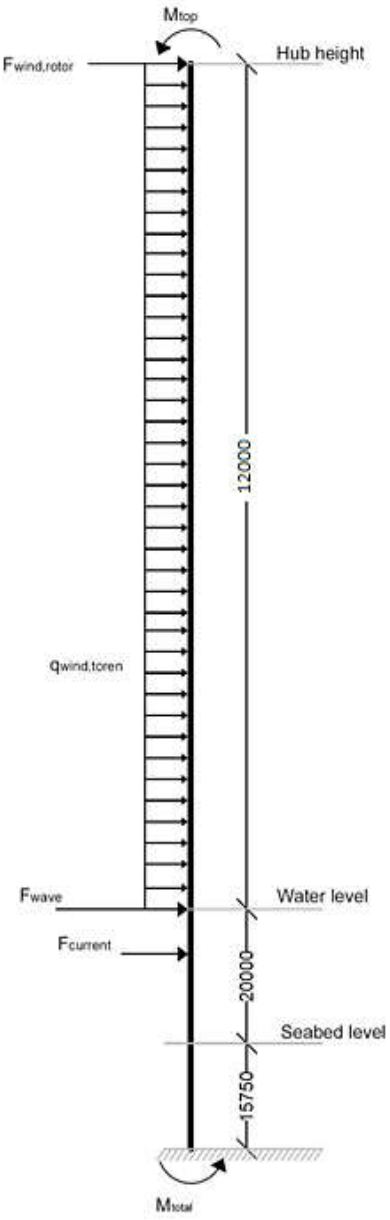

Figure 5.5 Forces acting on the support structure

Figure 5.6 shows the values of the following frequencies: the rotor frequency 1P, the blade passing frequency 3P, the main excitation frequency caused by the wind (blue vertical line) and the natural frequencies $f_1$and f_2 (black vertical lines). They are also summarized in Tables 5.4 and 5.5.

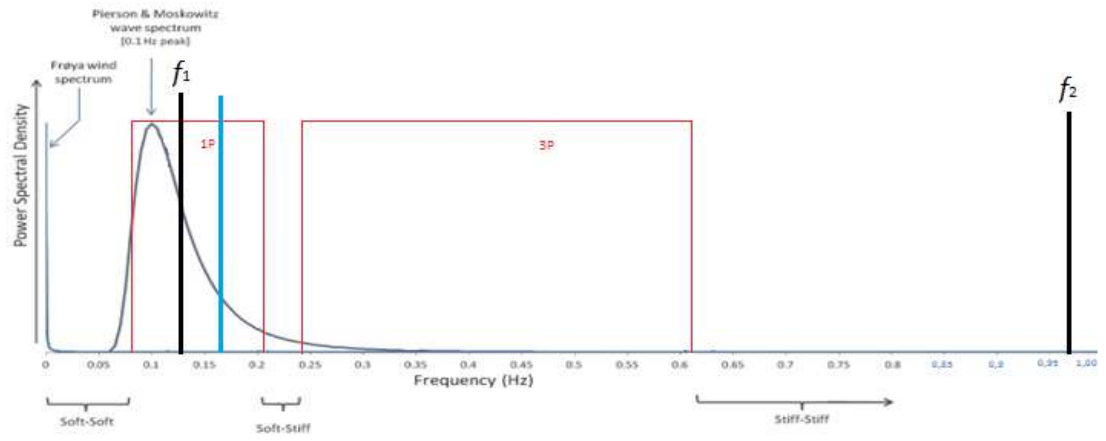

Figure 5.6 Frequency overview (Bhattacharya, S., 2014 - edited)

Table 5.4Natural frequencies

f_1	0,1261	[Hz]
f_2	0,9741	[Hz]

Table 5.5 Excitation frequency ranges for the 8.0MW wind turbine

	min	max	
1P	0,080	0,203	[Hz]
3P	0,240	0,609	[Hz]

It appears that the first natural frequency f_1 is located in the 1P frequency range. Resonance will occur, which likely will lead to failure of the tower due to the large deformations resulting in fatigue. Although the most common wind velocity 10,61m/s causes an excitation frequency of 0,165Hz (indicated with the blue vertical line), still resonance will occur. There are two solutions: changing the design to make sure no resonance will occur or using a tuned mass damper system (TMD). The lower natural frequency f_1 is mainly determined by the turbine characteristics (mass m_2 and stiffness k_2 in Figure 5.7). It is difficult to influence the turbine characteristics, since this is already designed by the manufacturer. Major adjustments should be made to the design in order to influence the first natural frequency. Therefore, using a TMD could be more beneficial. From a practical perspective, TMDs are a relatively cheap and robust solution to suppress tower vibrations in the offshore environment, resulting in lower fatigue loads. The extra mass added to the structure can be 'dumb' mass constituted by concrete or even water (Stewart, G.M. and Lackner, M.A., 2014).

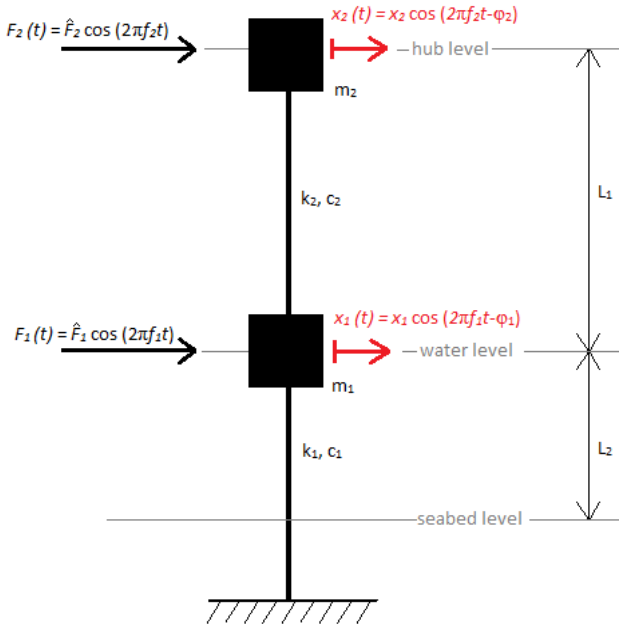

Figure 5.7 Mass-on-pole system (Wijngaarden M., 2013 - edited)

5.2 General conclusions

An aluminium design for an 8MW offshore wind turbine is obtained based on satisfying the checks with about the same loads applied as on the steel design. The two designs are now be compared with each other, see Table 5.6. Especially the characteristics which are represented in bold are important in the comparison. The dimensions are roughly the same. The only significant difference is the tower mass.

Table 5.6 Comparison of the steel and aluminium design characteristics

	Steel	Aluminium	
Rated power	8.0	8.0	[MW]
Rpm range	4,8-12,2	4,8-12,2	[-]
Rotor diameter	164	164	[m]
Swept area	21124	21124	[m^2]
Hub height	**125**	**120**	**[m]**
Rotor, hub and nacelle mass	492	492	[ton]
Tower mass	**480**	**276**	**[ton]**
Diameter tower top	**4,7**	**3,0**	**[m]**
Diameter tower bottom	**6,0**	**6,0**	**[m]**
Thickness t_w	**75**	**2x35 (200)**	**[mm]**
Rated wind speed	11	11	[m/s]
Cut out wind speed	25	25	[m/s]

The steel and aluminium design are compared by means of several criteria:

- **Structural weight**

  It can be concluded that the weight of an aluminium design is less than a steel one, which makes sense since the dimensions are comparable as is clear from Table 5.6. A lightweight structure is eases the installation and requires a smaller foundation, making it less expensive. In earthquake prone areas this would also contribute to smaller seismic loads.

- **Manufacturing process**

  The fabrication of a steel wind turbine exists of the following steps:

  - Steel plates are formed in the conical shape with large rollers.
  - The rolled sheets are submerged arc welded into the four tower sections, each made up of around 15 rings, depending on the required height for transportation and installation. This leads to 48 longitudinal welds.
  - Welding of flanges
  - The sections are welded or mostly bolted to the ends of other sections at the site

  The fabrication of an aluminium wind turbine exists of the following steps:

  - Extrusion of 30x4 parts with a length of 30m.
  - Cutting off parts of the extruded parts which are necessary to create the conical shape.
  - Assembly of the 30 components per part (120 in total) by welding.
  - Welding of the flanges
  - Mechanical fastening of the four tower parts at the site

  The aluminium wind turbine exists of many more parts than the steel design, which requires more labor. Besides, the process will take longer.

- **Weld volume**

  The two aluminium walls combined (2x35mm) have approximately the same thickness as the steel tower wall (75mm). With 120 longitudinal welds (of 30m in length) the aluminium design needs more weld material than the steel tower with a total of 48 longitudinal welds (of 2m in length). More welds mean more vulnerabilities.

- **Material usage (sustainability)**

  An advantage of the aluminium design is the fact that with extrusion technique, the wall does not have to be solid. The steel design has a wall thickness of 75mm, while that of aluminium has a thickness of 2x35mm. Adding material to the outer sides of the cross-section increases the moment of inertia. In combination with the lower modulus of elasticity, this can lead to an equal stiffness. However, although the design has a higher average moment of inertia than the steel design (see Table 5.7), it can still not compensate for the low modulus of elasticity. This leads to a lower stiffness of the aluminium tower than the steel one.

- **Resonance**

  The first natural frequency of the aluminium structure is located in the rotor frequency, causing resonance. This will lead to large deformations resulting in fatigue. Aluminium has lower fatigue strength than steel, making this an important aspect in the comparison. Besides the occurrence of major consequences, for example striking of the tower by the rotor blades, a shorter lifetime of the structure will be reached. Adequate damping control is necessary, or a tuned mass damper system could be applied.

  The reason for the low value of the first natural frequency can be found when comparing the masses and stiffness parameters of the steel and aluminium designs. The parameters $k_2$and $m_2$determine the first natural frequency. The mass m_2 is equal to the steel one, while the stiffness k_2 is 3 times lower. This can be explained with formula (4.26), which was:

$$k_2 = \frac{3EI}{{l_2}^2} \tag{5.1}$$

  The low modulus of elasticity E causes the low k_2.

Table 5.7 Comparison steel and aluminium parameters

	Steel	Aluminium		factor
k_1	164000000	55261998	[N/m]	3
k_2	1080000	336696	[N/m]	3,2
m_1	6500	1484	[tons]	4,4
m_2	530	533	[tons]	1
E	210000000	70000000	[kN/m²]	3
I	2,03	3,0	[m⁴]	0,7

It should be noted that alloy 7020 T6 was chosen when 6082 T6 did not satisfy the requirements. However, in hindsight this might not be the best choice, since this alloy is less extrudable It also less suitable for marine conditions than alloy 6082 and is susceptible to stress corrosion cracking. It would be better to apply alloy 6082 T6 and if needed increase the thicknesses of the tower wall at the welds.

A conclusion can be drawn that an aluminium tower does not lead to a more optimal solution for offshore wind turbines. In this thesis two different materials were compared based on somewhat similar designs. It appears that the aluminium design does satisfy the bearing capacity, but falls short in terms of stiffness. In order to do so, an entirely different design is necessary, probably leading to a less optimal solution.

6 Recommendations

Now the conclusions are drawn, some recommendations can be given for future research.

- The main limiting factor in this thesis is the extrusion press. The maximum dimensions of one extruded part are small compared to the tower dimensions. Perhaps it is worth to invest in a larger extrusion press. In the long term the investments will be recovered since aluminium has a high end-of-life value and is easy to recycle due to the homogeneous composition and the low melting temperature.

- Since this 8MW wind turbine tower design did not satisfy the resonance requirements without applying a TMD, the possibilities for smaller wind turbines should be examined. A wind turbine with a smaller height and lower top mass could be carried out relatively stiffer.

- In this thesis, only analytical calculations were done. For future research, when a proper design is made, a numerical analysis should be performed and thus a time series analysis can be carried out on the model. This is actually necessary according to the DNV (2014) when the natural period is greater than 2,5s to determine the Dynamic Amplification Factor, see *Paragraph 4.3.2*. By means of a time domain analysis, an accurate calculation of the fatigue damage can easily be performed.

- Only the tower of the wind turbine was examined, the foundation was left out of account. When a correct design is made for the foundation, it could be interesting how this influences the design tower of the wind turbine. In this thesis, a diameter of 7m was assumed.

7 References

4C OFFSHORE (2015) *Monopiles Support Structures*
http://www.4coffshore.com/windfarms/monopiles-support-structures-aid269.html

AALST, W. VAN (1984) *The Closure of Tidal Basins: Closing of Estuaries, Tidal Inlets and Dike Breaches*, Delft University Press

ANCONA D. AND MCVEIGH J. (2001) *Wind turbine – Materials and Manufacturing Fact Sheet*, Princeton Energy Resources International LLC

AVILA, S AND DE MORAIS, M.V.G. (2013) *Structural Control of a Wind Turbine Tower using a Tuned Mass Damper via Finite Element Method*, conference paper, University de Brasilia

BARRET (2016) *Fastener Design Manuel, Part One*
http://www.designnotes.com/companion/manual-1.html

BHATTACHARYA, S. (2014) *Challenges in Design of Foundations for Offshore Wind Turbines*, The Institution of Engineering and Technology, May 2014

BOEM (2016) *Offshore Wind Energy*, Bureau of Ocean Energy Management
http://www.boem.gov/Renewable-Energy-Program/Renewable-Energy-Guide/Offshore-Wind-Energy.aspx

CONNOR, J.J. (2002) *Introduction to Structural Motion Control*, Lebanon, Indiana, U.S.A.: Prentice Hall, 2002

DNV (2005) *Technical Rapport; Joining Methods – Technological Summaries*, Petroleum Safety Authority Norway (PSA) Det Norske Veritas

DNV (2014) *Design Of offshore Wind Turbine Structures*, Det Norske Veritas Offshore Standard, Mei 2014

EN 1999-1-4 (2005) *Eurocode 1: Actions on Structures- Part 1-4: General actions – wind actions*

EN 1999-1-1 (2007) *Eurocode 9: Design of aluminium structures - Part 1-1: General Structural rules*

EN 1999-1-3 (2007) *Eurocode 9: Design of aluminium structures - Part 1-1: Structures susceptible to fatigue*

GINHOVEN, J. VAN (2006) *Het effect van erosie en grondeigenschappen op het dynamische gedrag van offshore windturbines, betreffende stalen en betonnen mono paal funderingen*, M.Sc. rapport offshore windturbines, Delft University of Technology, Faculty of Civil Engineering & Geosciences

HÖGLUND T. ET AL. (2014) *AluMATTER*
www.aluminium.matter.org.uk/

ISO 19901-1 (2005) *Petroleum and natural gas industries— Specific requirements for offshore structures — Part 1: Metocean design and operating considerations*, International Organization for Standardization, Geneva, Switzerland

JAMIL, F. (2012) *To Study of Wind Resistant Stability of Tubular Wind Turbine Tower*, Mechanical Engineering, Ned University Of Engineering & Technology, December 2012

JONKMAN J.M. (2007) *Dynamics Modeling and Loads Analysis of an Offshore Floating Wind Turbine*, Technical rapport, National Renewable Energy Laboratory, pp 1-2

JONKMAN B. AND JONKMAN J. (2015), *FAST v8.12.00.a-bjj*, National Renewable Energy Laboratory

KARIMIRAD, M. (2014) *Offshore Energy Structures; For Wind Power, Wave Energy and Hybrid Marine Platforms*, Springer Cham Heidelberg New York Dordrecht London

KÜHN (1997) *Soft Stiff; A Fundamental Question for Designers of Offshore Wind Energy Converters*, EWEC '97

KÜHN (2001) *Dynamics and Design Optimisation of Offshore Wind Energy Conversion Systems*

KULUNK, E. (2011) *Aerodynamics of Wind Turbines, Fundamental and Advanced Topics in Wind Power*, Rupp Carriveau (Ed.), InTech

LINCOLN ELECTRIC (2010) *Fastening and Joining; Welding Challenges in the Fabrication of Offshore Wind Towers*, The Lincoln Electric Company Euclid, Ohio

MICELI, F. (2012) *Towers and Foundations, Concrete towers for onshore wind farm: an overview* http://www.windfarmbop.com/tag/concrete-tower/

NICHOLSON J.C. (2011) *Design of wind turbine tower and foundation systems- optimization approach*, MS thesis, University of Iowa

SAPA (2013) *Meeting design challenges of turbines*, SAPA Group www.sapagroup.com/en/sapa-profiler-ab/news/2013/meeting-desing-challenges-of-turbines/

SKF (2001) *Bolt-tightening Handbook, Linear motion & Precision Technologies*, The SKF Group, 2001

SOETENS F. ET AL. (2014) *Aluminium Structural Design; Lecture handbook 'Aluminium Structures'* Eindhoven University of Technology, Department Architecture, Building and Planning, Unit Structural Design, Chair Aluminium Structures

STEWART, G.M. AND LACKNER, M.A. (2014) *The Impact of Passive Tuned Mass Dampers and Wind-Wave Misalignment on Offshore Wind Turbine Loads*, Department of Mechanical and Industrial Engineering, University of Massachusetts Amherst, USA http://www.sciencedirect.com/science/article/pii/S0141029614002673

TALAT 2301 (2009) *Design of Members*, TALAT lecture 2301, European Aluminium Association

TALAT 2302 (2007) *Design of Joints*, TALAT lecture 2302, European Aluminium Association

TEMPEL J. VAN DER (2006) *Design of Support Structures for Offshore Wind Turbines;* Proefschrift april 2006

TEMPEL J. VAN DER AND MOLENAAR D. (2002) *Wind Turbine Structural Dynamcis – A Review of the Principles for Modern Power Generation, Onshore and Offshore*, Wind Engineering Volume 26, No. 4, 2002

UPWIND (2010) *Upwind Design Basis; WP4: Offshore Foundations and Support Structures*, Endowed Chair of Wind Energy (SWE) at the Institute of Aircraft Design Universität Stuttgart

WIJNGAARDEN M. VAN (2013) *Concept Design of Steel Bottom Founded Support Structures for Offshore Wind Turbines*, Bachelor Thesis, Delft University of Technology, Faculty of Civil Engineering and Geosciences

WIKIPEDIA (2015) *Yaw Bearing*
https://en.wikipedia.org/wiki/Yaw_system

Appendix A

Elaboration telescopic design

The telescopic design for the 8.0MW wind turbine is divided into four parts, see Figure A1. Each part will have a profile with different optimized dimensions, see Table A1. This leads to four different moment of inertia and section moduli. For each part, the loads and the moments at the transitions (A, B, C and D) have to be calculated. Only the wind loads will be calculated here. In this design, the tower (120m) will be designed separately from the submerged part of the structure. In between the two parts, a transition piece is positioned. The current and wave loads only act on the submerged part, these loads will be needed when calculating the fatigue damage in the final conceptual design.

Table A1 Dimensions of the four parts

	Outer diameter [m]	Thickness outer wall [mm]	Inner diameter [m]	Thickness inner wall [mm]	Tower wall thickness [mm]
Part A	2,2	40	1,9	40	150
Part B	3,0	50	2,7	50	150
Part C	3,3	60	3,0	60	150
Part D	3,8	50	3,5	50	150

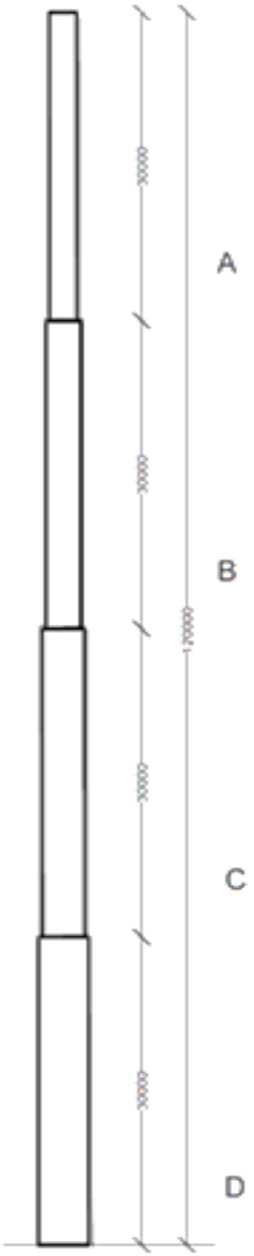

Figure A1 Telescopic tower design

A visual overview of the loads can be seen in Figure A1.

The horizontal load on the tower as a result of the wind force can be calculated as follows:

$$q_{wind,tower,A,d} = \gamma \cdot \frac{1}{2} \cdot C_{w,tower} \cdot \rho_{air} \cdot A_{tower,A} \cdot {v_c}^2 = 1{,}35 \cdot \frac{1}{2} \cdot 1 \cdot 1{,}225 \cdot 2{,}2 \cdot 25^2 = 1{,}14 kN/m$$

This load acts on the upper 30m of the tower. The corresponding moment at transition A will thus be:

$$M_{wind,tower,A} = q_{wind,tower} \cdot l_u \cdot \frac{1}{2} l_u = 1{,}14 \cdot 30 \cdot 15 = 511{,}6 kNm$$

The value for the horizontal load exerted by the rotor blades is:

$$F_{wind,rotor,A,d} = \gamma \cdot \frac{1}{2} \cdot C_T \cdot \rho_{air} \cdot A_{rotor} \cdot {v_r}^2 = 1{,}35 \cdot \frac{1}{2} \cdot 0{,}89 \cdot 1{,}225 \cdot 21124 \cdot 14^2 = 1881 kN$$

This causes a moment at transition A with a value of:

$$M_{wind,rotor,A} = F_{wind,rotor} \cdot l_A = 1881 \cdot 30 = 56430 kNm$$

The weight of the rotor blades causes a counter moment:

$$M_{top} = F_{blades} \cdot r = 1000{,}62 \cdot 2{,}4 = 2401{,}5kNm$$

The total moment at transition A is:

$$M_{total,A} = M_{wind,tower,A} + M_{wind,rotor,A} - M_{top} = 511{,}5 + 56430 - 2401{,}5 = 54540{,}7kNm$$

In the same way, the moments will be calculated at the other three transitions. Table A2 shows the results, which are also depicted in Figure A2.

Table A2 Moment calculations for transition A to D

Transition A 30m from top					
$q_{wind,\ towerA}$	1,14	[kN/m]	$M_{wind,\ tower\ A}$	1,14·30·15 = 511,5	[kNm]
$F_{wind,\ rotor}$	1881	[kN]	$M_{wind,\ rotor}$	1881·30 = 56430	[kNm]
$F_{rotorblades}$	1001	[kN]	M_{top}	-1001·2,4 = -2401,5	[kNm]
			$M_{total,A}$	**54540,7**	**[kNm]**
Transition B 60m from top					
$q_{wind,\ tower\ A}$	1,14	[kN/m]	$M_{wind,\ tower\ A}$	1,14·30·45 = 1534,9	[kNm]
$q_{wind,\ tower\ B}$	1,55	[kN/m]	$M_{wind,\ tower\ B}$	1,55·30·15 = 697,7	[kNm]
$F_{wind,\ rotor}$	1881	[kN]	$M_{wind,\ rotor}$	1881·60 = 112861	[kNm]
$F_{rotorblades}$	1001	[kN]	M_{top}	-1001·2,4 = -2401,5	[kNm]
			$M_{total,B}$	**112692,1**	**[kNm]**
Transition C 90m from top					
$q_{wind,\ tower\ A}$	1,14	[kN/m]	$M_{wind,\ tower\ A}$	1,14·30·75 = 2558,1	[kNm]
$q_{wind,\ tower\ B}$	1,55	[kN/m]	$M_{wind,\ tower\ B}$	1,55·30·45 = 2093	[kNm]
$q_{wind,\ tower\ C}$	1,71	[kN/m]	$M_{wind,\ tower\ C}$	1,71·30·15 = 767,4	[kNm]
$F_{wind,\ rotor}$	1881	[kN]	$M_{wind,\ rotor}$	1881·90 = 169291,6	[kNm]
$F_{rotorblades}$	1001	[kN]	M_{top}	-1001·2,4 = -2401,5	[kNm]
			$M_{total,C}$	**172308,7**	**[kNm]**
Transition D 120m from top					
$q_{wind,\ tower\ A}$	1,14	[kN/m]	$M_{wind,\ tower\ A}$	1,14·30·105 = 3581,4	[kNm]
$q_{wind,\ tower\ B}$	1,55	[kN/m]	$M_{wind,\ tower\ B}$	1,55·30·75 = 3488,4	[kNm]
$q_{wind,\ tower\ C}$	1,71	[kN/m]	$M_{wind,\ tower\ C}$	1,71·30·45 = 2302,3	[kNm]
$q_{wind,\ tower\ D}$	1,96	[kN/m]	$M_{wind,\ tower\ D}$	1,96·30·15 = 883,7	[kNm]
$F_{wind,\ rotor}$	1881	[kN]	$M_{wind,\ rotor}$	1881·120 = 225722,1	[kNm]
$F_{rotorblades}$	1001	[kN]	M_{top}	-1001·2,4 = -2401,52401,5	[kNm]
			$M_{total,D}$	**233576,4**	**[kNm]**

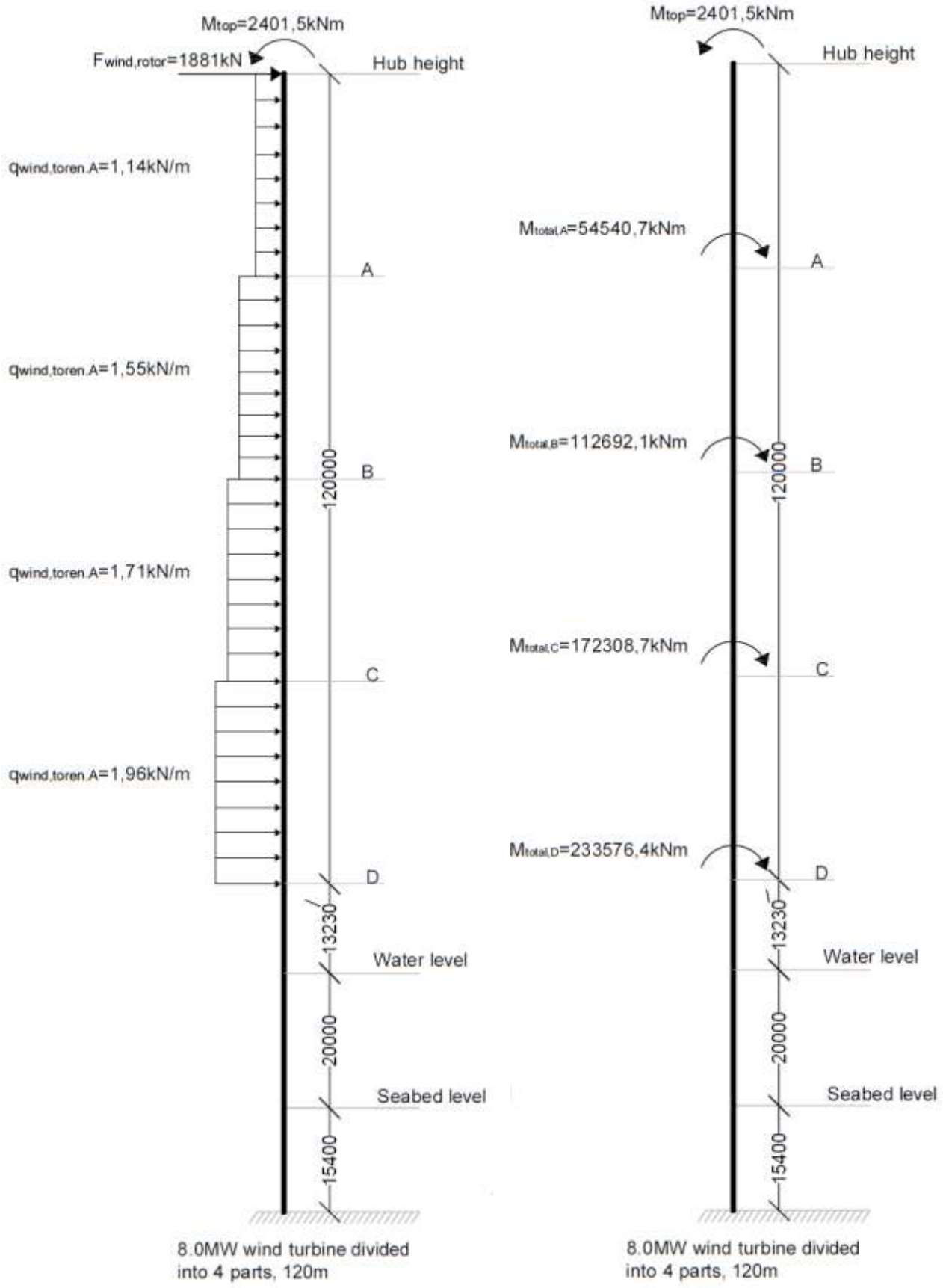

Figure A2 Schematic overview of the forces on the different parts of the tower

Stress checks

Part A

Top

$$\sigma = -\frac{M_{top}}{W_A} - \frac{F_{nacelle}}{A_A} = -\frac{2401,5}{0,25} - \frac{4826,5}{0,52} = -19041kN/m^2 = -19,04N/mm^2 < 260N/mm^2$$

Bottom

$$\sigma = -\frac{M_{total\ A}}{W_A} - \frac{F_{tower+nacelle}}{A_A} = -\frac{54540,7}{0,25} - \frac{5584,8}{0,52} = -230525,8kN/m^2 = -230,5N/mm^2 < 260N/mm^2$$

Part B

Top

$$\sigma = -\frac{M_{total\ A}}{W_B} - \frac{F_{tower+nacelle}}{A_B} = -\frac{54540,7}{0,61} - \frac{5584,8}{0,90} = -95874kN/m^2 = -95,87N/mm^2 < 260N/mm^2$$

Bottom

$$\sigma = -\frac{M_{total\ B}}{W_B} - \frac{F_{tower+nacelle}}{A_B} = -\frac{112692,1}{0,61} - \frac{6343,2}{0,90} = -192291kN/m^2 = -192,3N/mm^2 < 260N/mm^2$$

Part C

Top

$$\sigma = -\frac{M_{total\ B}}{W_C} - \frac{F_{tower+nacelle}}{A_C} = -\frac{112692,1}{0,90} - \frac{6343,2}{1,19} = -131230kN/m^2 = -131,2N/mm^2 < 260N/mm^2$$

Bottom

$$\sigma = -\frac{M_{total\ C}}{W_C} - \frac{F_{tower+nacelle}}{A_C} = -\frac{172308,7}{0,90} - \frac{7101,5}{1,19} = -198466kN/m^2 = -198,5N/mm^2 < 260N/mm^2$$

Part D

Top

$$\sigma = -\frac{M_{total\,C}}{W_D} - \frac{F_{tower+nacelle}}{A_D} = -\frac{172308,7}{1,01} - \frac{7101,5}{1,15} = -177220kN/m^2 = -177,22N/mm^2$$
$$< 260N/mm^2$$

Bottom

$$\sigma = -\frac{M_{total\,D}}{W_D} - \frac{F_{tower+nacelle}}{A_D} = -\frac{233576,4}{1,01} - \frac{7859,8}{1,15} = -238693kN/m^2 = -238,7N/mm^2$$
$$< 260N/mm^2$$

Resonance check

In this case, the natural frequency is calculated differently since the section of the tower is not homogeneous, see Figure A2. The larger section at the bottom of the structure has a positive influence on the natural frequency of soft structures. This is due to the fact of a reduction in mass and a change in the moment of inertia over the height. To take this into account in the calculation of the natural frequency, a different method will be used (Ginhoven, J. van, 2006):

$$\omega^2 = \frac{\pi}{16} \cdot \frac{EI_{eq}}{(M_{top} + m_{eq}L)L^3}$$

Where:

$$I_{eq} = \frac{\sum_{j=1}^{n} I_j l_j cos^2\left(\frac{\pi x_j}{2L}\right)}{L} \quad [m^4]$$

$$m_{eq} = \frac{\sum_{j=1}^{n} m_j l_j \left(1 - cos\left(\frac{\pi x_j}{2L}\right)\right)^2}{L} \quad [kg/m]$$

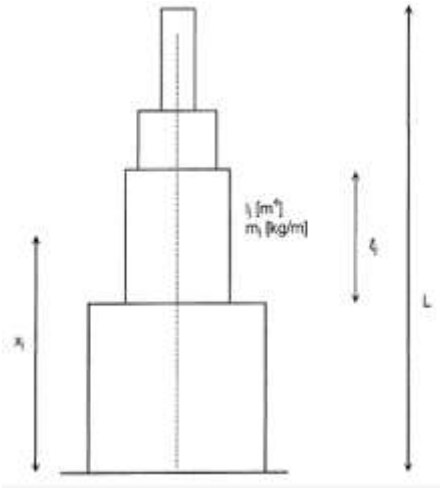

Figure A2 Structure divided into four parts (Ginhoven, J. van, 2006)

Where:

ω	angular frequency	[rad/s]
m_{eq}	equivalent mass	[kg/m]
I_{eq}	equivalent moment of inertia	[m⁴]
l_i	length of element j	[m]
X_j	distance to center of gravity of element j	[m]
L	total length	[m]
E	Young's modulus	[N/m²]
M_{top}	nacelle and rotor mass	[kg]

Table A3 shows the values for the equivalent moment of inertia, equivalent mass, the obtained angular frequency and then finally the natural frequency of the 8.0MW wind turbine.

Table A3 Data for the calculation of the natural frequency for the 8.0MW wind turbine

I_{eq}	0,789	[m⁴]
m_{eq}	110,32	[kg]
ω	0,620	[rad/s]
f	0,0988	[Hz]

Table A4 shows the ranges of the 1P and 3P frequencies.

Table A4 Excitation frequency ranges for the 8.0MW wind turbine

	min	max	
1P	0,080	0,202	[Hz]
3P	0,240	0,605	[Hz]

In this case the natural frequency of 0,0988Hz is located in the 1P frequency range. This will cause resonance of the structure. The stiffness should increase slightly, this can be done by increasing the towers diameters or wall thicknesses. This design has not been optimized; focus is placed on the final design.

Appendix B

Elaboration 3.6MW Wind Turbine

A design was made for a 3.6MW wind turbine to explore the possibilities in aluminium. First, a steel 3.6 MW wind turbine was analyzed, see Table B1. The same height of the steel tower and rotor dimensions were appointed to the aluminium variant. As a starting point, a tubular design is assumed consisting of a double walled cylinder, the two walls connected by a triangular part, see Figure B1. In the *Literature Survey* was decided to apply the 6082-T6 alloy. With assumed initial dimensions, the loads can be calculated with the aid of a spreadsheet. When the global order of magnitude of the loads is known, the assumed dimensions can be optimized to fulfil the checks regarding stiffness and strength; the tower was not optimized regarding the natural frequency and therefore the degree of resonance. Also, no dynamic factor was taken into account, only static calculations are done. The resulting dimensions are illustrated in Figure B1. The calculations related to this profile section are discussed in this appendix. The complete description of the loads, including the origin of the formulas and factors can be found in *Paragraph 4.4* of this Master's thesis.

Table B1 Data offshore wind turbine (Ginhoven, J. van, 2006)

Rated power	3.6	[MW]
Rpm range	8.0-13.0	[-]
Rotor diameter	100	[m]
Swept area	7854	[m^2]
Hub height	70	[m]
Rotor, hub and nacelle mass	227	[ton]
Tower mass	335	[ton]
Diameter tower top	2.8	[m]
Diameter tower bottom	4.6	[m]
Thickness t_w	54	[mm]
Rated wind speed	14	[m/s]
Cut out wind speed	30	[m/s]

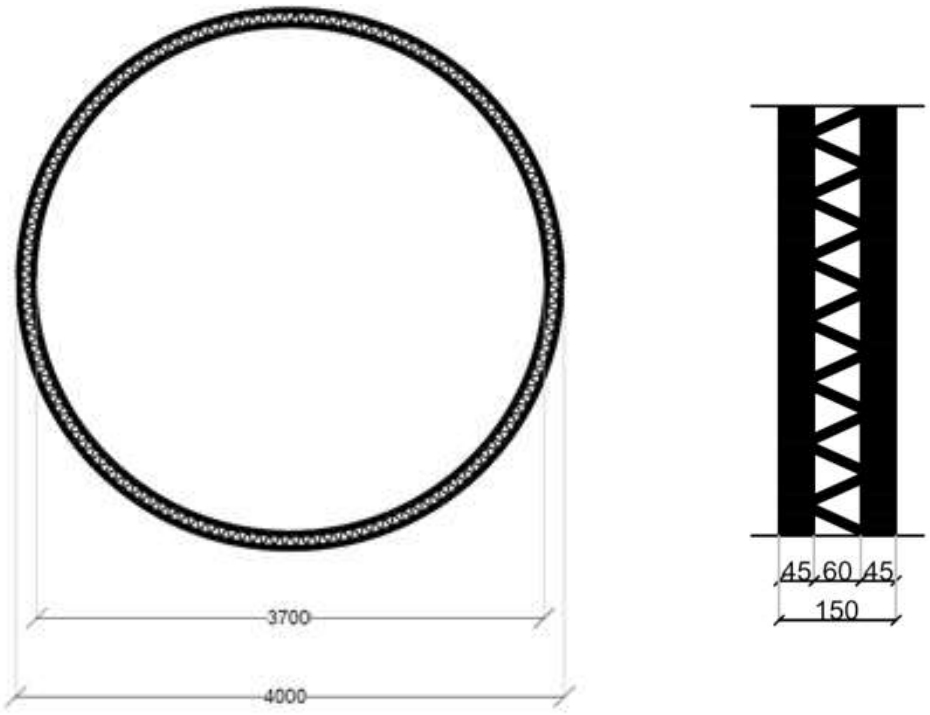

Figure B1 Profile sections with optimized dimensions for the 3.6MW wind turbine

Wind loads

The value for the horizontal load exerted by the rotor blades can be calculated with the following formula (DNV, 2014):

$$F_{wind,rotor,d} = \gamma_f \cdot \frac{1}{2} \cdot C_T \cdot \rho_{air} \cdot A_{rotor} \cdot {v_r}^2$$

Where:

C_T	thrust coefficient of the rotor	[-]
ρ_{air}	density air	[kg/m³]
A_{rotor}	swept area	[m²]
v_r	rated wind speed	[m/s]

Filling in the values gives a horizontal load of:

$$F_{wind,rotor,d} = 1{,}35 \cdot \frac{1}{2} \cdot 0{,}89 \cdot 1{,}225 \cdot 7854 \cdot 14^2 = 1132{,}9kN$$

The corresponding moment will be:

$$M_{wind,rotor} = F_{wind,rotor,d} \cdot \left(\frac{1}{2} l_w + l_s + l_e\right) = 1132{,}9 \cdot (70 + 20 + 15{,}75) = 117818kNm$$

The horizontal line load on the tower as a result of the wind can be determined with the following formula (DNV, 2014):

$$q_{wind,tower,d} = \gamma_f \cdot \frac{1}{2} \cdot C_{w,tower} \cdot \rho_{air} \cdot A_{tower} \cdot {v_c}^2$$

Where:

$C_{w,tower}$	shape drag coefficient	[-]
ρ_{air}	density air	[kg/m³]
A_{tower}	area facing wind flow	[m²]
v_c	cut-out wind speed	[m/s]

Filling in the values gives a line load on the tower of:

$$q_{wind,tower,d} = 1{,}35 \cdot \frac{1}{2} \cdot 0{,}85 \cdot 1{,}225 \cdot 4 \cdot 30^2 = 2{,}52 kN/m$$

This load acts on the upper 70m of the tower. The corresponding moment at the bottom of the support structure will thus be:

$$M_{wind,tower} = q_{wind,tower,d} \cdot l_u \cdot \left(\frac{1}{2} l_u + l_s + l_e\right) = 1{,}87 \cdot 70 \cdot (35 + 20 + 15{,}75) = 9282{,}2 kNm$$

Where:

$q_{wind,tower}$	horizontal line load on the tower	[N/m]
l_u	upper part of the tower above water	[m]
l_s	submerged part of the tower	[m]
l_e	embedded part of the tower	[m]

Current load

The current load can be derived using a formula for flow around slender structures, which consists of a static and a dynamic part of the drag force (Ginhoven, J. van, 2006):

$$F_{current,d} = \gamma_f \cdot \frac{1}{2} \cdot \rho_{water} \cdot u^2 \cdot (C_D + C'_D) \cdot A_{water}$$

Where:

ρ_{water}	density water	[kg/m³]
u	extreme current velocity	[m/s]
C_D	static drag coefficient	[-]
C'_D	dynamic drag coefficient	[-]
A_{water}	area facing water flow	[m²]

Filling in the values give a current load of:

$$F_{current,d} = 1{,}35 \cdot \frac{1}{2} \cdot 1025 \cdot 1^2 \cdot (0{,}7 + 0{,}175) \cdot (20 \cdot 4) = 48{,}4 kN$$

This load is applied on the support structure at a height of 2/3 of the water depth viewed from the bottom. The occurring moment will be:

$$M_{current} = F_{current,d} \cdot \left(\frac{2}{3} \cdot l_s + l_e\right) = 48{,}4 \cdot \left(\frac{2}{3} \cdot 20 + 15{,}75\right) = 1043{,}4 kNm$$

Wave load

The following formula should be used (DNV, 2014):

$$F_{breaking\ wave,d} = \gamma_f \cdot {C_D}^* \cdot K_D \cdot {H_b}^2 \cdot \frac{1}{2} \cdot \rho_{water} \cdot g \cdot D$$

Where:

C_D^*	drag coefficient in breaking waves = 2,5·C_D	[-]
K_D	correction for extent of drag force	[-]
H_b	breaking height of the wave	[m]
D	pile diameter	[m]

The coefficients belonging to the selected location are calculated with aid of several graphs, see Appendix D. The values are shown in Table B2.

Table B2 Coefficients needed for the wave formula

Return period	$d/(gT^2)$	H_b	H/H_b	C_D	K_D	S_D
50 yr	0,017	17,8	0,84	3*	0,50	1,00
5 yr	0,020	16,7	0,76	1,2	0,44	0,94

Thus, the breaking wave force will have a value of:

$$F_{breaking\ wave,d} = 1{,}35 \cdot 3 \cdot 0{,}50 \cdot 14{,}9^2 \cdot \frac{1}{2} \cdot 1025 \cdot 9{,}81 \cdot 4 = 9041kN$$

The occurring moment at the bottom of the structure is:

$$M_{wave} = F_{breaking\ wave,d} \cdot d \cdot S_d = 6697 \cdot 20 \cdot 1{,}0 = 180819kNm$$

Where:

d	water depth
S_d	correction factor for the position of the breaking wave force

Permanent load

The total dead load of the structure is also a very important load that has to be taken into consideration. The weight of the rotor blades has an influence on the calculation of the total moment on the wind turbine. It provides a counter moment as can be seen in Figure 3.7. The load caused by the blades is 720kN and the arm to the tower is 2,4m, so the counter moment will have a value of:

$$M_{top} = F_{blades} \cdot r = 720 \cdot 2{,}4 = 1728kNm$$

The weight of the tower is:

$$F_{tower} = V_{tower} \cdot \rho_{aluminium} = 125{,}8 \cdot 27 = 3396kN$$

Weight of the total wind turbine which includes the weight of the tower, nacelle, hub, rotor unit:

$$F_{turbine} = F_{tower} + F_{nacelle,hub,rotor} = 3396 + 2220 = 5616kN$$

The volume is calculated with the aid of the spreadsheet.

Moment

The total moment at the bottom of the support structure will now be determined:

$$M_{total} = M_{wind,rotor} + M_{wind,tower} + M_{current} + M_{wave} - M_{top}$$
$$= 117818 + 12531 + 1324 + 180819 - 1728kNm$$
$$= 310764kNm$$

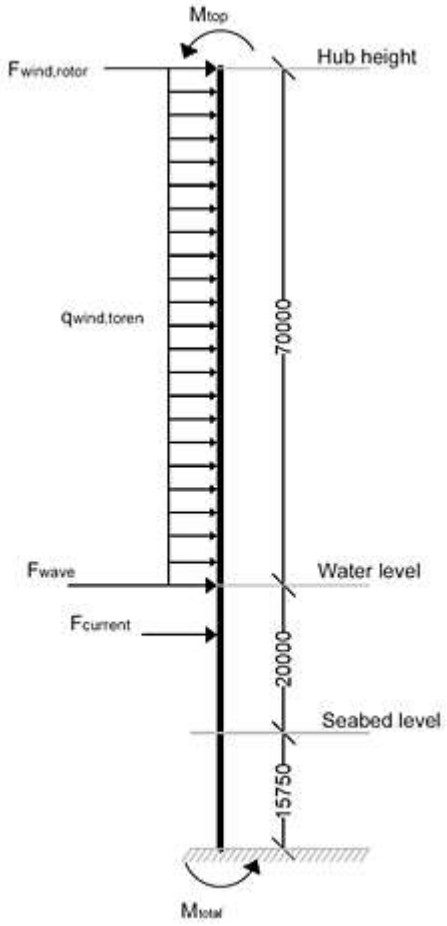

Figure 3.7 Location of the loads and moments on the 3.6MW wind turbine

Stress checks

The stresses at the top and bottom of the structure will be checked. In the *Literature Survey* was decided to apply the 6082-T6 alloy. This alloy has a proof stress of 250MPa.

Top

$$\sigma = -\frac{M_{top}}{W} - \frac{F_{nacelle}}{A_b} = -\frac{1728}{1,12} - \frac{2220}{1,21} = -3374kN/m^2 = 3,37N/mm^2$$
$$< 260N/mm^2$$

Bottom

$$\sigma = -\frac{M_{total}}{W} - \frac{F_{turbine}}{A_b} = -\frac{310764}{1,12} - \frac{5616}{1,21} = -231105kN/m^2$$
$$= -231N/mm^2 < 260N/mm^2$$

It meets the requirements adequately.

Resonance check

The support structure is likely to fail due to the large sinusoidal deformations resulting in fatigue. To avoid resonance, the structure should be designed in such a way that its natural frequency does not coincide with either 1P or 3P frequencies.

The excitation frequencies can be calculated as described in *Paragraph 2.3.2*. Currently, most wind turbines have a variable rotor speed and therefore a 1P and 3P frequency range. The 3.6MW wind turbine has a rpm range of 8.0-13.0. Now the 1P and 3P frequencies can be calculated:

$$f_{1P,min} = \frac{rpm}{60} = \frac{8}{60} = 0,133Hz$$

$$f_{1P,max} = \frac{rpm}{60} = \frac{13}{60} = 0,217Hz$$

$$f_{3P,min} = 3 \cdot f_{1P} = 3 \cdot 0{,}133 = 0{,}400Hz$$

$$f_{3P,max} = 3 \cdot f_{1P} = 3 \cdot 0{,}217 = 0{,}650Hz$$

An overview is given in Table B3.

Table B3 Excitation frequency ranges for the 3.6MW wind turbine

	min	max	
1P	0,133	0,217	[Hz]
3P	0,400	0,650	[Hz]

From the equation of motion, the following equation can be obtained:

$$m_1 m_2 \omega^4 - \big(m_1 k_2 + m_2(k_1 + k_2)\big)\omega^2 + k_1 k_2 = 0$$

This equation is elaborated in the *Literature Survey*. From this equation two angular frequencies can be obtained ω_1 and ω_2 (rad/s) which result into two natural frequencies with:

$$f_{1,2} = \frac{\omega_{1,2}}{2\pi}$$

For this structure, Table B4 shows the obtained values. The results found when inserting these values in the fourth order polynomial equation are displayed in Table B5.

Table B4 Parameters for the dynamic calculations

k_1	694062949	[N/m]
k_2	1292361	[N/m]
m_1	680000	[kg]
m_2	270000	[kg]

Table B5 Natural frequency

ω_1	2,1727	[rad/s]
ω_2	30,936	[rad/s]
f_1	0,3458	[Hz]
f_2	4,924	[Hz]

The first natural frequency is larger than the maximum value of the 1P frequency range: $f_1 > 1P_{max}$ and smaller than the lowest value of the 3P frequency range $f_1 < 3P_{min}$. The structure meets the requirements adequately. However, the second natural frequency is extremely high. The calculations done by Van Wijngaarden for the steel wind turbines have been repeated with his input to verify the fourth order equation, see Table B6.

Table B6 Verification natural frequencies

		Van Wijngaarden	Validation	
3.6MW	f_1	0,3639	0,3627	[Hz]
	f_2	1,0101	1,0786	[Hz]
8.0 MW	f_1	0,2254	0,2478	[Hz]
	f_2	0,8038	0,8150	[Hz]

It seems that the fourth order equation is valid.
The parameters for the calculation of the natural frequency from the steel and aluminium designs are compared, see Table B7. The last column shows with which factor the values differ.

Table B7 Comparison steel and aluminium parameters

	Steel	Aluminium		factor
k_1	164000000	648938365,4	[N/m]	0,25
k_2	1080000	1292360,90	[N/m]	0,84
m_1	6500	680	[tons]	9,6
m_2	530	270	[tons]	2
E	210000000	70000000	[kN/m^2]	3
I	2,03	2,02	[m^4]	5

Parameter k_1 is approximately four times larger for the aluminium design. This can be explained by the lower Young's modulus. Also, the masses are much lower.
This means that the high second natural frequency is not unusual, considering that the natural frequency for a single degree of freedom system can be calculated with: $\omega = \sqrt{\frac{k}{m}}$. The mass of the aluminium mono pile is almost 10 times lower than the steel mono pile. This leads to a ω which is 3 times larger. The factor of difference between the second natural frequency of the steel and aluminium mono pile is 6. An explanation for the dissimilar values could be the fact that it actually is a two degree of freedom system.

Appendix C

Elaboration 8.0MW Wind Turbine

Now, the possibilities for larger wind turbines will be looked into, namely by examining a wind turbine with a rated power of 8.0MW. Data for this wind turbine is obtained from existing offshore steel wind turbines, manufactured by Vestas, see Table C1.

Table C1 Data offshore wind turbine (Ginhoven, J. van, 2006)

Rated power	8.0	[MW]
Rpm range	4.8-12.2	[-]
Rotor diameter	164	[m]
Swept area	21124	[m^2]
Hub height	125	[m]
Rotor, hub and nacelle mass	492	[ton]
Tower mass	480	[ton]
Diameter tower top	4.7	[m]
Diameter tower bottom	6.0	[m]
Thickness t_w	75	[mm]
Rated wind speed	11	[m/s]
Cut out wind speed	25	[m/s]

Assigning the dimensions from the 3,6MW wind turbine to the 8MW turbine will obviously not fulfil the stress checks. Eventually, the dimensions illustrated in Figure C1 were obtained.

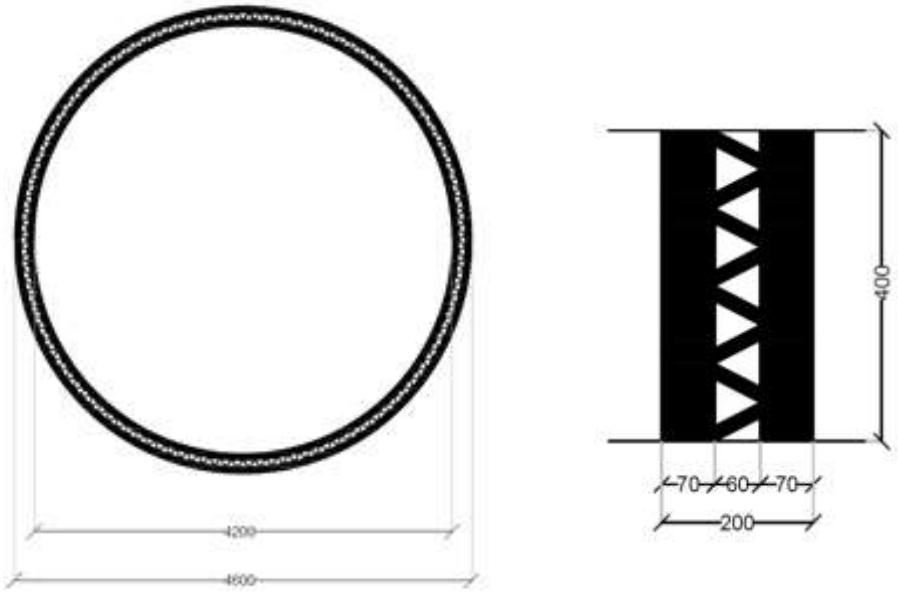

Figure C1Profile sections with optimized dimensions for the 8MW wind turbine

Wind loads

The horizontal load on the tower as a result of the wind force is:

$$q_{wind,tower,d} = \gamma \cdot \frac{1}{2} \cdot C_{w,tower} \cdot \rho_{air} \cdot A_{tower} \cdot {v_c}^2 = 1{,}35 \cdot \frac{1}{2} \cdot 1 \cdot 1{,}225 \cdot 4{,}6 \cdot 25^2 = 2{,}38 kN/m$$

This load acts on the upper 120m of the tower. The corresponding moment at the bottom of the support structure will thus be:

$$M_{wind,tower} = q_{wind,tower,d} \cdot l_u \cdot \left(\frac{1}{2} l_u + l_s + l_e\right) = 2{,}38 \cdot 120 \cdot (60 + 20 + 16{,}1) = 27414{,}6 kNm$$

The value for the horizontal load exerted by the rotor blades is:

$$F_{wind,rotor,d} = \gamma \cdot \frac{1}{2} \cdot C_T \cdot \rho_{air} \cdot A_{rotor} \cdot {v_r}^2 = 1{,}35 \cdot \frac{1}{2} \cdot 0{,}89 \cdot 1{,}225 \cdot 21124 \cdot 11^2 = 1881 kN$$

The corresponding moment will be:

$$M_{wind,rotor} = F_{wind,rotor,d} \cdot (l_u + l_s + l_e) = 1881 \cdot (120 + 20 + 16{,}1) = 293624{,}1 kNm$$

Current load

Also in this case, a value of 0,7 can be obtained for the coefficient C_D with the aid of the Reynolds number. The maximum dynamic drag coefficient C'_D is assumed to be 0,25·C_D. The current load can now be calculated:

$$F_{current,d} = \gamma \cdot \frac{1}{2} \cdot \rho_{water} \cdot u^2 \cdot (C_D + C'_D) \cdot A_{water} = 1{,}35 \cdot \frac{1}{2} \cdot 1025 \cdot 1^2 \cdot (1 + 0{,}25) \cdot (20 \cdot 4{,}6) = 55{,}7 kN$$

This load acts on $\frac{2}{3}$ of the water depth viewed from the fixed support on the structure. The occurring moment will be:

$$M_{current} = F_{current,d} \cdot \left(\frac{2}{3} \cdot l_s + l_e\right) = 55{,}7 \cdot \left(\frac{2}{3} \cdot 20 + 16{,}1\right) = 1639{,}3 kNm$$

Wave load

The breaking wave force will have a value of:

$$F_{breaking\ wave,d} = \gamma \cdot {C_D}^* \cdot K_D \cdot H^2 \cdot \frac{1}{2} \cdot \rho_{water} \cdot g \cdot D = 1{,}35 \cdot 3{,}0 \cdot 0{,}5 \cdot 14{,}9^2 \cdot \frac{1}{2} \cdot 1025 \cdot 9{,}81 \cdot 4{,}6 = 6065{,}1 kN$$

The occurring moment at the bottom of the structure is:

$$M_{wave} = F_{breaking\ wave,d} \cdot d \cdot S_d = 6065{,}1 \cdot 20 \cdot 1{,}0 = 121301{,}2 kNm$$

Permanent load

The weight of the rotor blades provides a counter moment. The load caused by the blades is 1000,62kN and the arm to the tower is 2,4m, so the counter moment will have a value of:

$$M_{top} = F_{blades} \cdot r = 1000{,}62 \cdot 2{,}4 = 2401{,}5kNm$$

The weight of the tower is:

$$F_{tower} = V_{tower} \cdot \rho_{aluminium} = 337{,}4 \cdot 27 = 9108{,}5kN$$

Weight of the total wind turbine which includes the weight of the tower, nacelle, hub, rotor unit:

$$F_{turbine} = F_{tower} + F_{nacelle,hub,rotor} = 9108{,}5 + 4826{,}5 = 13935kN$$

The volume is calculated with the aid of the spreadsheet.

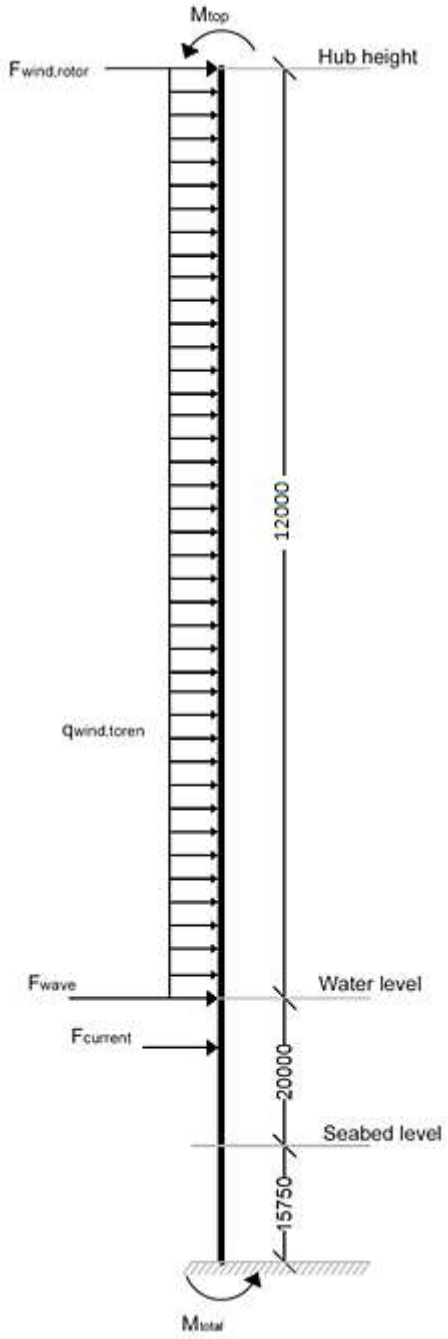

Figure C2 Location of the loads and moments on the 3.6MW wind turbine

Total moment

The total moment at the bottom of the support structure can now be determined, see Figure C2:

$$M_{total} = M_{wind,tower} + M_{wind,rotor} + M_{current} + M_{wave} - M_{top}$$
$$= 27414{,}6 + 293624{,}1 + 1639{,}3 + 121301{,}2 - 2401{,}5kNm$$
$$= 441577{,}7kNm$$

Stress checks

Top

$$\sigma = -\frac{M_{top}}{W} - \frac{F_{nacelle}}{A} = -\frac{2401{,}5}{2{,}04} - \frac{4826{,}5}{1{,}94} = -3670kN/m^2$$
$$= -3{,}67N/mm^2 < 260N/mm^2$$

Bottom

$$\sigma = -\frac{M_{total}}{W} - \frac{F_{turbine}}{A} = -\frac{441577{,}7}{2{,}04} - \frac{13935}{1{,}94}$$
$$= -223642{,}6kN/m^2 = -223{,}6N/mm^2$$
$$< 260N/mm^2$$

Resonance check

As mentioned before, it is important to stay outside the 1P and 3P excitation frequencies of the rotor. The 8.0MW wind turbine has a rpm range of 4,8-12,.1. Now the 1P and 3P frequencies can be calculated:

$$f_{1P,min} = \frac{rpm}{60} = \frac{4,8}{60} = 0,08Hz$$

$$f_{1P,max} = \frac{rpm}{60} = \frac{12,2}{60} = 0,203Hz$$

$$f_{3P,min} = 3 \cdot f_{1P} = 3 \cdot 0,08 = 0,240Hz$$

$$f_{3P,max} = 3 \cdot f_{1P} = 3 \cdot 2,03 = 0,609Hz$$

An overview is given in Table B3.

Table C2 Excitation frequency ranges for the 8.0MW wind turbine

	min	max	
1P	0,080	0,203	[Hz]
3P	0,240	0,609	[Hz]

The natural frequency of the 8.0MW aluminium wind turbine is determined again with the fourth order equation. For this structure, Table C3 shows the obtained values. The results found when inserting these values in the fourth order polynomial equation are displayed in Table C4.

Table C3 Parameters for the dynamic calculations

k_1	1631700000	[N/m]
k_2	505000	[N/m]
m_1	1230000	[kg]
m_2	643000	[kg]

Table C4 Natural frequency

ω_1	0,885	[rad/s]
ω_2	24,742	[rad/s]
f_1	0,141	[Hz]
f_2	3,938	[Hz]

The first natural frequency is located in the $1P_{range}$ frequency range: $1P_{min} < f_1 < 1P_{max}$. Large deformations due to resonance will occur. The stiffness should increase slightly; this can be done by increasing the towers diameters or wall thicknesses. This design has not been optimized; focus is placed on the final design.

Appendix D

Determination of drag coefficient and correction factors

Graph for the determination of drag coefficient C_D

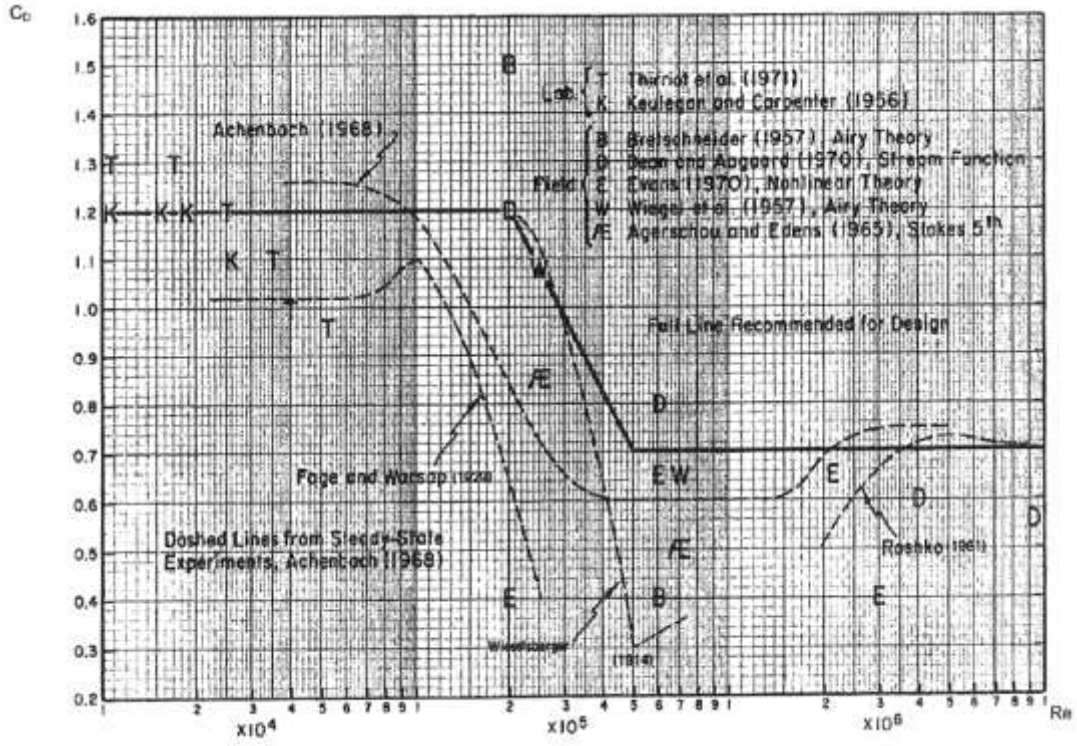

Graph for the determination of correction factor K_D

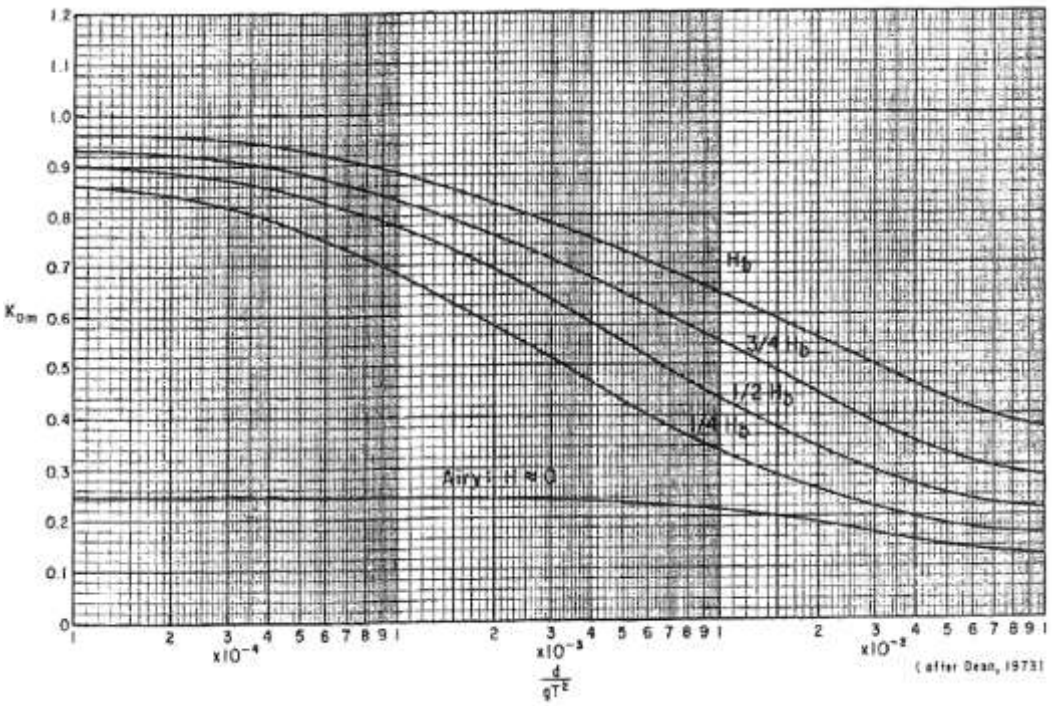

Graph for the determination of correction factor S_D

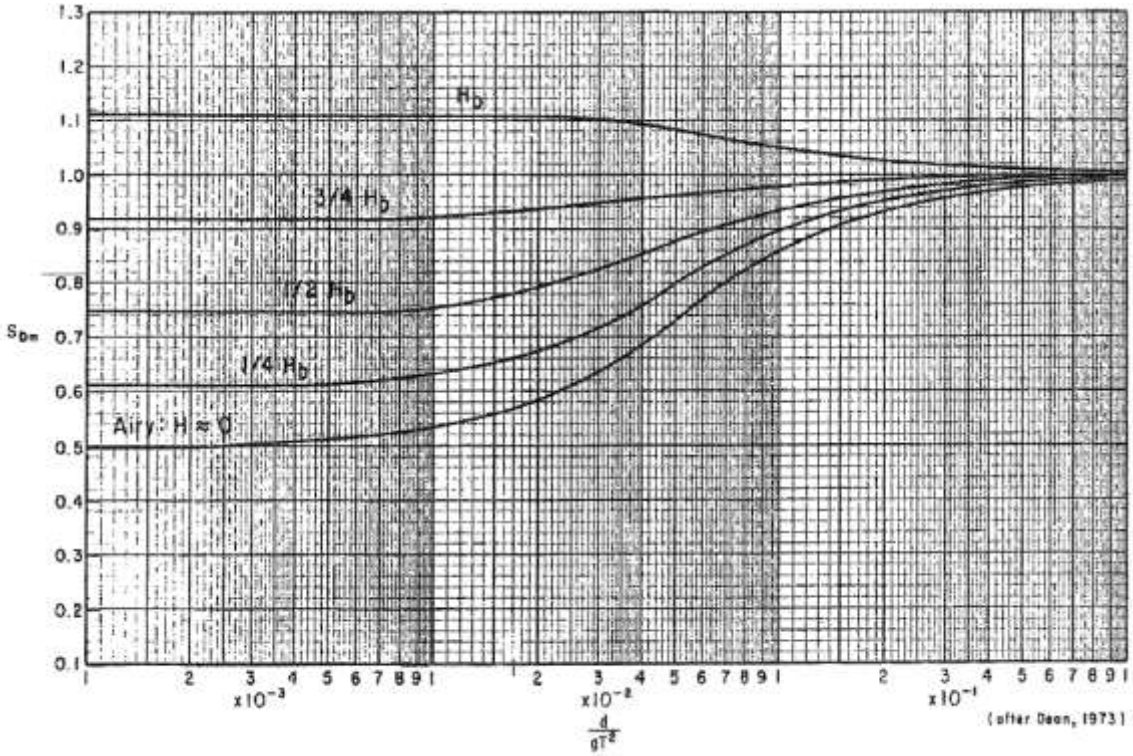

Literature Survey

Table of contents

1. Introduction

The subject of the final graduation project is the development of a conceptual design for a support structure of an aluminium offshore wind turbine. As an introduction to this research, a fundamental study should be done into certain topics. This will be documented in this literature survey.

First, general information concerning wind turbines will be provided, namely the components of a wind turbine, differences between offshore and onshore wind turbines and the manufacturing and installation processes.

Secondly, the advantages and disadvantages about the material aluminium will be given, an appropriate alloy will be chosen and possibilities with extrusion technique will be described.

After this, a literature study on dynamics is done, containing a schematization of the tower, excitation frequencies and the stiffness of the support structure.

Then, the limit states and relevant loads acting on the structure will be described.

Lastly, a literature study on fatigue is conducted, consisting of fatigue in general and its design methods and fatigue for wind turbines specific.

2. Literature study on wind turbines

First general information concerning wind turbines will be provided to comprehend this thesis better. A description of the different components of the wind turbines will be given. Next the differences between onshore and offshore wind turbines will be highlighted. Then the manufacturing and installing process will be explained.

All wind turbines use wind power to produce electric energy. However, the way this is done may differ. There are two types of wind turbines, namely turbines with blades rotating about a horizontal axis and turbines with blades that rotate about a vertical axis, see Figure 2.1. The horizontal axis wind turbine (HAWT) is most commonly used. In this graduation thesis, only this type of wind turbine will be considered.

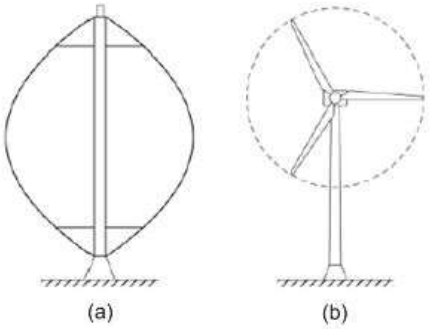

Figure 2.1. Vertical axis (a) and horizontal axis (b) wind turbine (Chen B., 2012)

2.1 Wind turbine components

The five main components of the horizontal axis wind turbine are shown in Figure 2.2, which are the rotor, the nacelle, the tower, transition piece and mono pile. The tower, substructure and foundation together form the support structure. In this thesis, emphasis is placed in the tower. The dimensions for the mono pile are assumed, based on the tower dimensions.

- **Rotor**

The rotor consists of the rotor hub and the blades. The hub is the connection between the rotor blades and the rotating bar that goes into the nacelle. The particular design of the blades, which is similar to that of an airplane wing, causes the rotating motion. The rotor is placed upwind of the tower on most wind turbines, which means it is facing the wind. This is primarily done because the air current behind the tower is very turbulent. The rotor converts the energy in the wind into rotary mechanical movement. The rotor blades are mainly made of glass-fibre or carbon fibre reinforced plastic (GRP, CFRP).

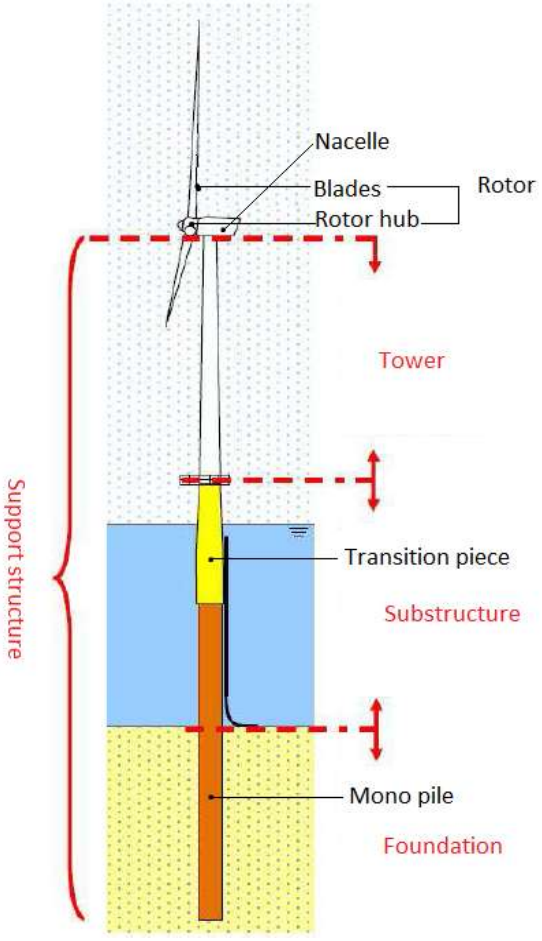

Figure 2.2. Components wind turbine

- **Nacelle**

The nacelle holds all the turbine machinery, see Figure 2.3. It must be able to rotate to follow the wind direction; it is therefore connected to the tower via bearings. It consists out of the gearbox that converts the rotor motion of 18-50 rpm into the desirable 1500 rpm, a generator that converts mechanical energy into electrical energy and a brake system which can force the rotation to stop in case of too strong winds or if failure occurs.

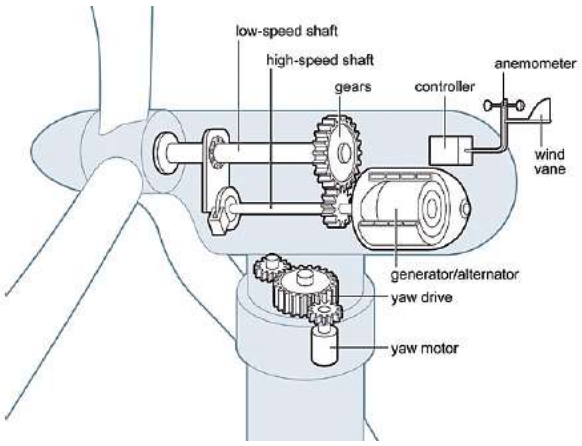

Figure 2.3. Cross-section nacelle (World Steel, 2012)

- **Tower**

The tower of wind turbine must absorb the huge static loads caused by the varying power of the wind. A typical modern 1000kW turbine will have a tower of 50 to 80 meters. The higher the tower is, the greater the wind speed is. It is common practice to design a wind turbine tower as a conical tubular column, since this provides more stability against wind loads and saves material. The thickness of the cross-section varies from 8mm at the top to 65mm at the base, and is often made of high quality steel. The following types of onshore towers are available (WWEA, 2014):

- **Tubular steel**, most commonly used. They are manufactured in sections of 20-30m with flanges at either end and bolted together on the site.
- **Concrete towers with climbing formwork** are constructed on site and make transport and fitting easier (called in-situ concrete.) Great care must be taken at significant heights and in winter.
- **Pre-cast concrete towers.** Here the segments are placed on top of one another on site and braced with steel cables in the wall.
- **Steel lattice towers** are manufactured using welded steel profiles. They require half as much material as a tubular column with a similar stiffness.
- **Hybrid towers** consist of components of the above-mentioned types of tower.
- **Guyed poles** are very common in small wind generators, as on the one hand they are light and on the other hand can be set up without a crane.

- **Transition piece**

The transition piece connects the tower with the mono pile. It is a steel prefabricated tubular element which contains a platform on top and a boat lander. The transition piece is connected to the mono pile by a grout connection. Rubber profiles at the bottom of the transition piece close the gap between the transition piece and the mono pile, after which the upper gap can be filled with grout when the transition piece is lowered over the (outside) mono pile. Other possible connections are a bolted flange of slip joints (Wijngaarden M., 2013).

- **Mono pile**

The mono pile supports the nacelle and transfers all the loads to the seabed. Other type of foundation structures are shown in figure 2.4. The mono pile is the most common type, which is well suited for sites with water depth ranging from 0 to 25 meters. A mono pile is a steel pipe pile of up to six meters in diameter with a wall thickness up to 150mm. The vertical loads are transferred to the seabed by shaft friction and tip resistance. The vertical bearing capacity is therefore mainly determined by the diameter of the mono pile, which influences the horizontal loads due to wind, waves and current. These horizontal loads will be transferred to the soil by bending moments, so the passive soil resistance should be large enough.

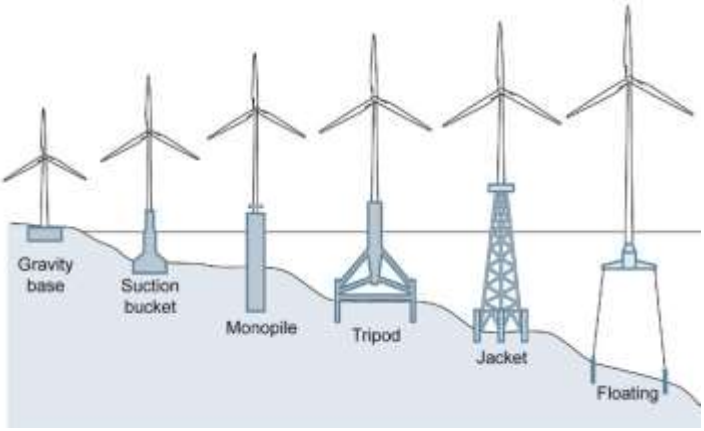

Figure 2.4. Types of foundation structures (World Steel, 2012)

In shallower environments with firm seabed substrates, gravity-based systems can be used which avoids the need to use a large pile-driving hammer.

Tripods and jackets foundations have been deployed in areas where the water depth starts to exceed the practical limit for mono piles. A tripod foundation consists of a mono pile divided at its bottom into a frame of steel rods. This is attached to the seabed with piles of smaller diameters. The jacket foundation is similar to a lattice tower. It is a squared network of steel rods, anchored at four anchorage points. The whole structure can be mounted in one piece (Clausen A.V., 2012). In this graduation thesis, only the frequently occurring mono pile will be considered.

The bottom part of the mono pile ensures the stability for the wind turbine by transferring and spreading the loads acting on the foundation to the ground. Besides the dead load from the tower, the nacelle and the rotor blades, the wind also contributes to the vertical force acting on the foundation. As a result of the large height of the tower, a horizontal wind force is giving a considerably great bending moment at the foundation.

2.2 Offshore wind turbines

Wind turbines can be installed offshore. If the tower is subject to hydrodynamic loading, a wind turbine shall be considered as an offshore wind turbine. In Europe, where vacant land is scarce and vast shallow-water wind resources are available, offshore wind turbines are ideal. Installing wind energy offshore has the following advantages (Jonkman J.M., 2007):

- The wind tends to blow more strongly and consistently, with lower turbulence and gust factors along with a smoother wind shear and more stable wind directionality.
- The restrictions on dimensions for onshore towers caused by the cost of transportation are not relevant offshore if they can be manufactured near the coastline.

- The visual and noise annoyances of wind turbines can be avoided if the turbines are installed a sufficient distance from shore.
- Larger areas are available that allows implementing larger projects and the installation will not occupy land, interfering with other land uses.

Of course, placing wind turbines offshore also has several disadvantages (Jonkman J.M., 2007):

- Offshore wind farms are more costly than the onshore applications, due to the high costs of electrical grid connections and foundations and the challenges in offshore installations such as weather and wind.
- Offshore installations are less accessible than onshore installations, which raises the operations and maintenance costs and possibly increases the downtime of the machines.
- Not only do offshore wind turbines experience higher extreme mean wind speeds, but they must also withstand other conditions, such as hydrodynamic loading from waves and sea currents. As a result, the complexity of the design increases.

When the wind turbines are used in offshore environments some modifications are integrated. The first important one is protection against corrosion. This includes a qualified coating system (Clausen A.V., 2012). Other modifications for wind turbines in offshore environments consist of strengthening the tower to manage loading forces from waves or ice flows and adding brightly colored access platforms for navigation safety and maintenance access. To reduce the cost for everyday servicing, offshore turbines may have automatic greasing systems to oil bearings and blades, as well as heating and cooling systems to maintain gear oil temperature within a specified range. Lightning protection systems minimize the risk of damage from lightning strikes that occur frequently in some offshore locations. A last difference is that offshore turbines are larger than onshore turbines to take advantage of the steadier winds and have an increased generation capacity; offshore turbines have tower heights greater than 60 meters and rotor diameters of 75 to 130 meters, while the capacity varies between 2MW and 5MW (MMS, 2006).

2.3 Manufacturing process

The cylinders forming the wind turbine tower are made from steel plates with flanges that are flame cut and primed. The manufacturing process of a steel wind turbine tower will be described in four steps, see Figure 2.5 (Gamesa, 2010):

1. **Shaping**
   The fan-shaped plate segments which are cut from rectangular parent steel plates are inserted in a machine with three large rollers. In this step, the conical shape is formed.

2. **Welding rings**

The rolled sheets are submerged arc welded into tower sections. Depending on the required height for transportation and installation, each section may be made up of between 4 and 12 rings. A section's thickness may vary from 8mm at the top to 65mm at the base, depending on the loads and steel grades used. Offshore installations usually use thicker or stronger plates. Due to transportation limits, the maximum tower diameter is roughly 4,3m.

3. Welding tower sections

The tower sections with the steel flanges are welded to the ends of other tower sections

4. Surface treatment and assembly of the auxiliary equipment

The structure is placed inside the painting and drying tunnel. Once the tower plating is finished, it is then given a surface treatment. This provides a C-5 level protection, which is required for offshore areas. Once the tower is dry, all the service elements (such as platforms and ladders) are mounted on it.

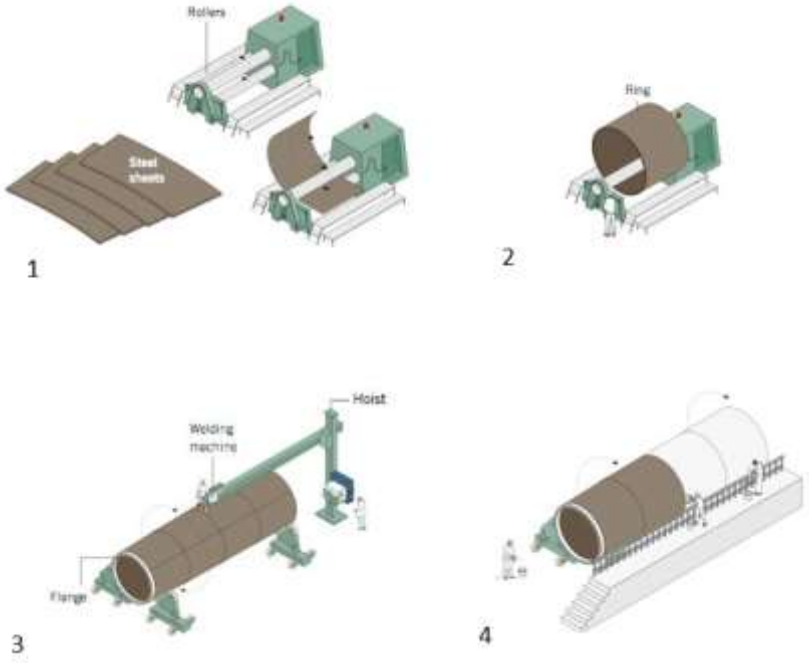

Figure 2.5. Steps manufacturing process (Gamesa, 2010)

2.4 Installation process

The installation of a complete offshore wind turbine is carried out as follows:

1. **Pile-driving mono piles**

   The installation of the pile starts with lifting it into position by a large crane or heavy lift vessel. The pile will be lifted from a floating position, afterwards the bulk heads will be removed and then the open ended pile can be aligned into position. This will be done by an alignment tool at a certain distance above sea level. The pile will penetrate into the seabed due to its own weight, depending on the soil conditions. To drive the pile into the ground, a hydraulic hammer is lifted onto the pile, or the pile can be drilled in case of very hard soil. The drilling procedure should be done from a stable platform. It starts with the drilling of a hole where the pile can be inserted. An alternative is inserting the drilling tool into the pile, then the drilling can take place while the pile is slowly lowered down. The last step is the grouting of the space between the soil and the steel pile (Wijngaarden M., 2013).

2. **Installing transition piece**

   The prefabricated transition piece is connected to the mono pile by a grout connection. Rubber profiles at the bottom of the transition piece close the gap between the transition piece and the mono pile, after which the upper gap can be filled with grout when the transition piece is lowered over the (outside) mono pile. Other possible connections are a bolted flange of slip joints (Wijngaarden M., 2013).

3. **Installing turbine tower**

   The tower sections are placed one on top of the other using lattice cranes. The tower is installed in either one piece or two pieces, which are welded or bolted to form a complete tower (Gamesa, 2010).

4. **Installing nacelle and rotor**

   Once the tower is assembled, the next step is to install the nacelle, hub and rotor blades. Here, there are three possibilities (Uraz E. 2011):

   - The nacelle, hub and two of the blades are assembled together, the third blade is placed separately.
   - First the nacelle is placed, and then the hub and three blades are assembled to shape the complete rotor, which is then connected on the nacelle.
   - The hub and nacelle are assembled and installed, then the blades are placed separately.

   The electrical connection is established to all components, parallel to the wind turbine assembly.

3. Literature study on aluminium

Lower weight and longer lifecycles have seen aluminium become the established material for helidecks and helideck support structures on offshore oil and gas rigs. The same reasons have resulted in the widespread use of aluminium in oil rig stair towers and telescopic personnel bridges (Aalco, 2015). The support structures of wind turbines are nowadays mostly made of steel. However, also in this field there is a trend toward lighter weight systems. So far, only research has been done to lightweight rotors and nacelle, since the top mass dictates the necessary support structure and thus a reduction in this mass will have a direct impact on the total turbine cost. However, the weight of the support structure is also significant because it is 60% of the weight of the wind turbine (Ancona D. and McVeigh J., 2001). Moreover, support structure costs account roughly for a quarter to a third of the capital cost of an offshore wind farm. Among that cost share, weight has a moderate direct contribution since also manufacturing and especially transportation and installation is of importance (Kühn, 1997).

So, a steel support structure may not be the most optimal solution; an alternative should be considered, for example a structure assembled from aluminium extruded sections.

The problem that will be looked into this thesis is as follows:

How will a support structure (including the tower of Figure 2) from aluminium extruded sections be designed and is this a more optimal solution for offshore wind turbines than one made of steel?

Regarding this problem statement, a study should be conducted concerning aluminium, in particular its properties and the possible alloys for offshore purposes.

3.1 Advantages and disadvantages

An aluminium alternative may have the following advantages:

- Aluminium is less sensitive to corrosion than steel. Due to its natural oxide layer, an aluminium surface does not corrode and does not need to be painted for surface protection.
- High end-of-life value and easy to recycle due to the homogeneous composition, the low melting temperature and lack of paint, thus compensating for the relatively high initial energy cost (SAPA, 2013).
- Ease of inspection, since it is rust-free and does not need to be painted.
- The low self-weight of the structure eases installation.
- It may enhance the possibility of floating structures in deep see (this will not be researched in this thesis).
- Aluminium provides design flexibility by making use of extrusions through (SAPA, 2013):

- Complex profile cross-section: allowing different parts and features to be integrated into the same profile.
- Fewer parts and fewer production steps in assembly.

Of course, an offshore support structure made from aluminium extruded sections also has disadvantages:

- In case of cyclic loading, the low Young's modulus is responsible for the lower fatigue strength of aluminium, circa half that of steel. This means that fatigue design should be considered more carefully than with steel structures (Höglund T. et al., 2014).
- The low Young's modulus and low density make aluminium structures susceptible to vibrations and in these cases the dynamic behavior for the structure has to be considered (Höglund T. et al., 2014).
- The low Young's modulus *E* also causes a higher sensitivity to stability problems (Höglund T. et al., 2014).
- Creating a structure which is conical by means of extruded sections could be challenging. A good method to assemble this type of structure from aluminium extruded sections ought to be developed.

Table 3.1. Material properties aluminium and steel (Höglund T. Et Al., 2014)

		Aluminium	Steel
Density, ρ	kg m^{-3}	2,700	7,800
Young modulus, E	N mm^{-2}	70,000	210,000
Shear modulus, G	N mm^{-2}	27,000	81,000
Poisson ratio, ν		0.33	0.3
Coefficient of linear thermal expansion, α	K^{-1}	23×10^{-6}	12×10^{-6}

3.2 Aluminium alloys

Pure aluminium is relatively soft and is only used when low strength or hardness is required. However, aluminium is very convenient for alloying with other materials, which make it possible to use aluminium for structural applications. A small addition (0,5 to 3%) of one or more other metals is sufficient to improve mechanical properties, hardness or chemical resistance. Other properties that can be improved by adding other materials are electrical conductivity and machining properties. The latter one can also be improves by certain treatments (Soetens, F. et al., 2014).

For some alloys, the strength can be improved by a heat treatment called precipitation hardening, also sometimes referred to as heat treatment. The amount of alloying element(s) that can dissolve in aluminium at elevated temperature is higher than at ambient temperature. This property is used in precipitation hardening. The heat treatability of an alloy depends on the alloying elements: a substantial solubility at high temperatures and a very low solubility at low temperatures of the alloying elements is needed in order to perform the heat treatment. The heat treatment sequence is as follows (see also Figure 3.1):

- Solution annealing (dissolving, homogenizing);
- Rapid cooling (quenching);
- Ageing (precipitation, at room or elevated temperature).

(Soetens, F. et al., 2014).

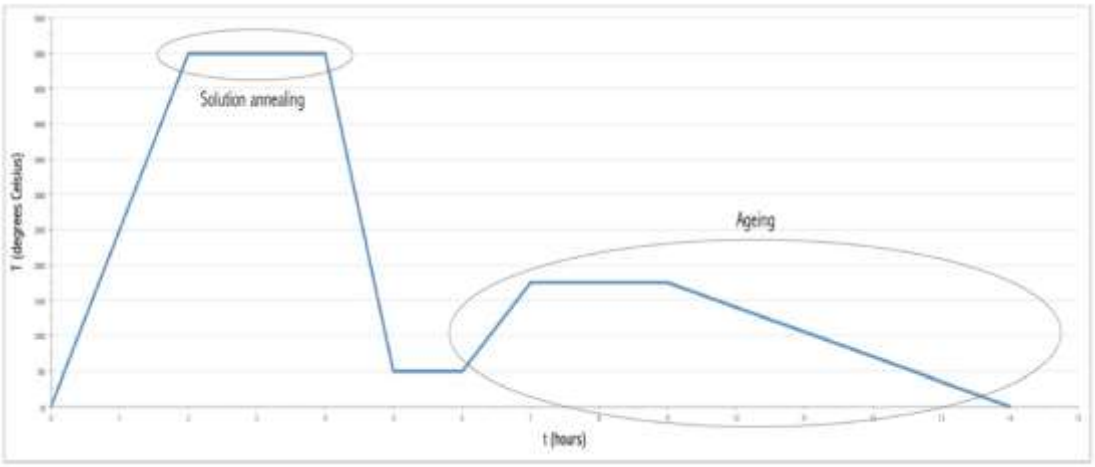

Figure 3.1. Principle of heat treatment (Soetens, F. et al., 2014)

Some alloys are suited for precipitation hardening (see Figure 3.2). They gain their strength by ageing. Ten different tempers exist (Matweb, 2015):

T1 - Cooled from an elevated temperature shaping process and naturally aged to a substantially stable condition.
T2 - Cooled from an elevated temperature shaping process, cold worked, and naturally aged to a substantially stable condition.
T3 - Solution heat treated, cold worked, and naturally aged to a substantially stable condition.
T4 - Solution heat treated, and naturally aged to a substantially stable condition.
T5 - Cooled from an elevated temperature shaping process then artificially aged.
T6 - Solution heat treated then artificially aged.
T7 - Solution heat treated then overaged/stabilized.
T8 - Solution heat treated, cold worked, then artificially aged.
T9 - Solution heat treated, artificially aged, then cold worked.
T10 -Cooled from an elevated temperature shaping process, cold worked, then artificially aged.

Non-heat treatable wrought alloys (see Figure 3.2) are strengthened by strain hardening (cold-work). This is indicated with a temper starting with Hxy or Hxyz.Hxy or Hxyz. The number x indicates the treatment after hardening – if any – which is usually done to recover part of the toughness (Matweb, 2015):

x=1: Strain hardened only
x=2: Strain hardened and partially annealed
x=3: Strain hardened and stabilized
x=4: Strain hardened and lacquered or painted. This assumes that thermal affects from the coating process affect the strain hardening; seldom encountered.

The number y indicates the level of strain hardening and is based on the minimum ultimate tensile strength obtained (Soetens, F. et al., 2014).

y = 1: quarter hard
y = 2: semi hard
y = 3: three quarters hard
y = 4: fully hard

The number z indicates a variation of the two digit temper.
Fully annealed alloys - alloys without any treatment - are indicated with temper O.

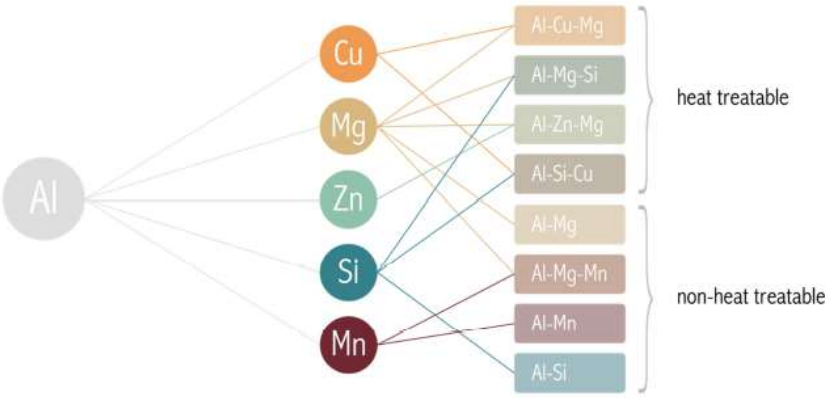

Figure 3.2. Heat treatable and non-heat treatable alloys (Soetens, F. et al., 2014)

Alloying elements

The most important alloying elements are: Copper (Cu), Magnesium (Mg), Manganese (Mn), Silicon (Si) and Zinc (Zn). These elements are added to increase the mechanical properties and the hardness of the aluminium. Magnesium and Manganese also improve the chemical resistance.

Wrought alloys contain smaller quantities of other elements (in most cases less than 3% but usually much less) compared to cast alloys (up to 12%). They are used for the production of semi-fabricates such as extruded profiles and tubes, or rolled plates.

A total of eight series of wrought alloys is distinguished, based on the most important alloying element. A four-digit registration system introduced by the Aluminum Association has been adopted internationally; four digits, sometimes combined with a letter, represent each registered alloy (Soetens, F. et al., 2014):

- The first (thousands) digit relates to the alloy series as follows:
  - 1xxx - pure aluminium (99% or higher);
  - 2xxx - copper alloy (Cu);
  - 3xxx - manganese alloy (Mn);
  - 4xxx - silicon alloy (Si);
  - 5xxx - magnesium alloy (Mg);
  - 6xxx - magnesium/silicon alloy (Mg/Si);
  - 7xxx - zinc alloy (Zn);
  - 8xxx - alloys with other elements (such as Li and Fe).
- The second digit indicates a modification of the original series. The digit 0 is for the original alloy while digits 1 to 9 indicate modifications;
- The third and fourth digits indicate the exact purity of the 1xxx series or identify a specific alloy for the other series of alloys;
- A letter preceding the four digits indicates an alloy that is not yet registered;
- A letter after the four digits indicates a local or national variation.

In order to select an appropriate alloy for aluminium offshore wind turbines, the following properties have to be considered (Soetens, F. et al., 2014):

- Strength, failure strain and hardness;
- Deformation capacity (sufficient elongation capacity before failure or stress release occurs);
- Toughness (sensitivity to instable fracture of a flawed component)
- Corrosion resistance;
- Weldability;
- Machinability;
- Suitability for anodizing.

Figure 3.3 provides an overview of several properties per alloy series. Since the 8XXX series is a collection of very different alloys, it is difficult to generalize this group. Also, the 4XXX series is almost exclusively used for welding rod and wire; the properties are not of importance for structural applications.

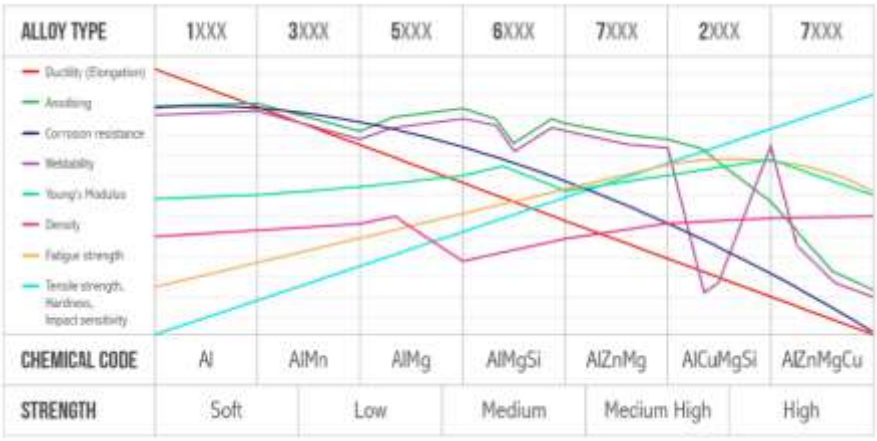

Figure 3.3. Overview of properties influenced by the alloying elements (TALAT 1501, 1994)

The eight aluminium series will be briefly explained below, after this several possibly appropriate alloys will be explained in detail.

Group 1XXX has low strength properties, and is therefore not used as a structural material (Soetens, F. et al., 2014).

The 2XXX series have a low corrosive resistance and a low weldability. The corrosive resistance can be increased by coating the material with pure aluminium or synthetic material, but this is not an optimal solution for an offshore application (Soetens, F. et al., 2014).

The 3XXX aluminium alloy series has overall good mechanical properties. However, only for moderately loaded applications can this series alloys to be efficiently applied as structural material (Soetens, F. et al., 2014).

The 4XXX series has a high weldability and is therefore almost exclusively used for welding rod and wire (Soetens, F. et al., 2014).

Group 5XXX also has overall good properties, namely:

- Increasing hardness for cold deformation and increasing magnesium content
- High strength
- Good corrosive resistance
- Decreasing ductility when increasing magnesium content
- High weldability

The ultimate tensile strength and strain are at a relatively high level. When the alloys are annealed they should not be applied as a structural material, because the ultimate strain is too low in this state. The 5XXX alloys are used in a wide range of applications amongst which are heavy loaded structures such as shipbuilding, panels, transport industry, storage tanks, sewage treatment but also welding wire. Most alloys in the 5XXX series have a relatively high corrosive resistance and are often applied in structures in sea-environments. The 5083 alloy is well known for its use at low temperatures, maintaining high strength and ductility. This alloy could be an appropriate one for the support structure (Soetens, F. et al., 2014).

The most important properties of the 6XXX series are:

- High strength (including heat treatment)
- Good formability
- High corrosive resistance
- Good fatigue properties

This combination of properties results in a wide application range similar to those of the 5XXX alloys: infrastructural projects, civil projects, shipbuilding and cranes are some of the applied areas (Soetens, F. et al., 2014). Moderately high levels of strength are obtained through heat treating, giving higher

strength levels than 5XXX series alloys (Alcoa, 2015). Complex cross-sectional areas can be realized by extrusion. Hence, 5XXX alloys are generally applied as sheets and plates and 6xxx alloys as extrusions. The 6XXX alloys are also applied for dynamically loaded structures and connections, making this alloy highly applicable for offshore wind turbines (Soetens, F. et al., 2014).

Most of the 7XXX aluminium alloy series are sensitive to stress-corrosion. This can be limited by adding small amounts of boron and zirconium in combination with a full heat treatment. The area of appliance is almost the same as the 6XXX series but for more heavily loaded structures. Thus, this alloy series should also be taken into consideration for the support structure (Soetens, F. et al., 2014).

Group 8XXX has a low self-weight and high strength, which make it vital for the aircraft industry. Riveting and gluing are the only possibilities to create connections of this type of alloy to be able to benefit from the favorable properties (Soetens, F. et al., 2014).

When comparing the alloys on the important properties mentioned before, the appropriate alloy is expected to be found in the 5XXX, 6XXX or 7XXX series. Therefore, the following aluminium alloys will be explained in detail:

- 5083
- 6061, 6082
- 7020

In the 5XXX aluminium alloy series, 5083 will be highlighted. As mentioned before, alloys in this series are generally applied as sheets and plates, but simple extruded hollow shapes are also possible. The 5083 alloy is known for exceptional performance in extreme environments. It is highly resistant to attack by both seawater and industrial chemical environments. 5083 has the highest strength of the non-heat treatable alloys which is retained also after welding. Alloy 5083 is typically used in:

- Shipbuilding
- Rail cars
- Vehicle bodies
- Tip truck bodies
- Mine skips and cages
- Pressure vessels

In the 6XXX aluminium alloy series, 6061 and 6082 will be highlighted.

Aluminium alloy 6061 is one of the most commonly used general-purpose aluminium alloy, typically supplied as extrusions. It is a medium to high strength heat-treatable alloy. It has very good corrosion resistance and weldability, although reduced strength in the weld zone. It has medium fatigue

strength. It has good cold formability in the temper T4 (heat treated and naturally aged), but limited in T6 (heat treated and artificially aged) temper, which is the most common temper for 6061. It is not suitable for very complex cross-sections. Alloy 6061 is typically used for heavy duty structures in (Aalco, 2015):

- Rail coaches
- Truck frames
- Ship building
- Bridges and military bridges
- Aerospace applications including helicopter rotor skins
- Tubes
- Pylons and towers
- Transport
- Motorboats

The second aluminium alloy in the 6XXX series that will be described is 6082. This is a medium strength alloy with excellent corrosion resistance. It has the highest strength of the 6000 series alloys. As a relatively new alloy, the higher strength of 6082 has seen it replace 6061 in many applications. The addition of a large amount of manganese controls the grain structure which in turn results in a stronger alloy and a good resistance to dynamic loading conditions. It is difficult to produce thin walled, complicated extrusion shapes in alloy 6082. Also, the high strength of 6086 T6 is not retained after welding. Besides, the extruded surface finish is not as smooth as other similar strength alloys in the 6000 series. In the T6 and T651 temper, alloy 6082 machines well. 6082 is typically used in:

- Highly stressed applications
- Trusses
- Bridges
- Cranes
- Transport applications
- Beer barrels
- Milk churns
- Offshore constructions

In the 7XXX aluminium alloy series, 7020 will be highlighted. It is a high strength alloy for highly loaded structural applications with a relatively low formability. It is available in sheet, plates, strips and bars. Typical applications are (Nedal, 2015):

- Rail transport,
- Aircraft storage containers
- Mobile cranes.
- Armored vehicles
- Military bridges
- Motor cycles and bicycle frames

It can be concluded that aluminium alloy 7020 and 6061 are not the most suitable alloys. Alloy 7020 has relatively low formability which limits the shapes that can be extruded, while alloy 6061 is not suitable for use in a wind turbine since it has medium fatigue strength. Since aluminium alloy 5083 is mostly applied in sheets and plates, and as extruded material only for simple shapes, this alloy is also not the best choice for the wind turbine. This remains the 6082 alloy, which appears most suitable since this alloy is extrudable and has good resistance to corrosion and dynamic loading. The most common T6 temper is chosen.

Table 3.2. Data alloy 6082 T6 (EN 1999-1-1, 2007)

Alloy EN-AW	Product form	Temper	Thick-ness t mm 1) 3)	f_o 1)	f_u 1)	A 5) 2)	$f_{o,haz}$ 4)	$f_{u,haz}$ 4)	HAZ-factor 4)		BC 6)	n_p 7)
				N/mm²		%	N/mm²		$\rho_{o,haz}$	$\rho_{u,haz}$		
6082	EP,ET,ER/B	T4	$t \le$ **25**	110	205	14	100	160	0,91	0,78	B	8
	EP	T5	$t \le 5$	230	270	8	125	185	0,54	0,69	B	28
	EP ET	T6	$t \le 5$	250	290	8	125	185	0,50	0,64	A	32
			5 < $t \le$ **15**	260	310	10			0,48	0,60	A	25
	ER/B	T6	$t \le 20$	250	295	8			0,50	0,63	A	27
			20< $t \le$150	260	310	8			0,48	0,60	A	25
	DT	T6	$t \le 5$	255	310	8			0,49	0,60	A	22
			5 < $t \le 20$	240	310	10			0,52	0,60	A	17

3.3 Extrusion process

An important difference between steel and aluminium structures will be the manufacturing process. As mentioned before, the aluminium wind turbine will be assembled from extruded sections. First, extrusion technique will be explained briefly.

The term extrusion is usually applied to both the process and the product obtained, when a hot cylindrical billet of aluminium is pushed through a shaped die (direct extrusion, see Figure 3.4 – left). The resulting section can be used in large lengths or cut into short parts. In order to produce extrusions with wide section sizes, it is also possible to use rectangular shaped billets. Other presses are designed to push the die into the billet. This is called indirect extrusion, see Figure 3.4 – right. Direct extrusion is the most common extrusion process. In this process, the ram pressure not only has to deform the metal but also overcome the friction between the billet and the container (green part in Figure 3.4). With the indirect process, the billet and container do not move relative to each other and thus all of the available press load is used for deformation. However, the cross-sectional area is limited by the maximum size of the stem.

The variation in available alloys and cross-sectional areas makes extrusion one of the most valued assets in helping the aluminium producer supply users with solutions to their design requirements

Figure 3.4. Direct (left) and indirect (right) extrusion process (TALAT 1302, 1994)

(TALAT 1302, 1994).

Extrusion of aluminium profiles is possible because aluminium gets soft at relatively low temperatures of around 450 to 500 °C. So, the first step is to heat the billets used for extrusion to preceding temperature range. Subsequently, the billets are placed into a press containing the die. Air is removed from the press using a vacuum to prevent it from getting into the extrusion. A hydraulic cylinder presses a ram against the billet, pushing the aluminium through the die. The required pressure for this varies between 500 and 20000 tonnes, although the majority ranges between 1000 and 3000 tonnes. On average about five to fifty meter aluminium profile can be produced per minute. If the temperature at which the section leaves the die is too high, cracking of the surface can occur. Therefore, directly after extrusion, the profiles are cooled with air and/or water. In order to obtain straight profiles and to eliminate residual stresses, the profiles are stretched between 1 and 2%, followed by artificial ageing to stabilize their properties.

Simple hollow sections such as rounds, squares and ovals can be produced from a hollow billet using a mandrel (Figure 3.5). Here the product has a uniform structure across the section. Profiles with a uniform wall thickness are the simplest to produce. However, where necessary, wall thickness within a profile can easily be varied. For example, a profile's bending strength can be increased by concentrating weight/thickness away from the center of gravity. More complex sections are made using bridge or port hole dies in which the metal flows around a shaped bridge and joins again by hot pressure welding in a mixing chamber (Figure 3.6).

To optimize cost-efficiency, a profile's design should always be as production-friendly as possible. To achieve this, the profile should:

- have a uniform wall thickness
- have simple, soft lines and curved corners
- be symmetrical
- have a small circumscribing circle
- not have deep, narrow channels
- should have solid profiles if possible or fewer cavities in hollow sections

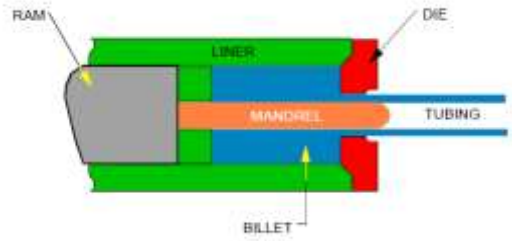

Figure 3.5. Extruding tubing with die and mandrel (TALAT 1302, 1994)

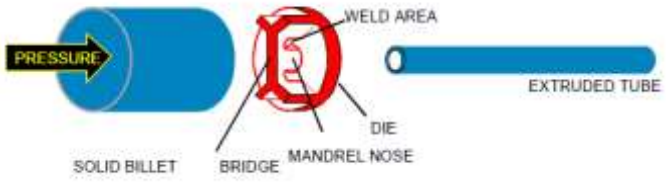

Figure 3.6. Extrusion of hollow section (TALAT 1302, 1994)

The key of this thesis is the development of a conceptual design for a support structure of an aluminium offshore wind turbine. Using extrusion technique can be beneficial here compared to a steel design. The reason for this is that aluminium alloys can be extruded to complex shapes with ease, a requirement of particular importance with a relatively expensive material. Also, different parts and features can be introduced into the section shape which increase the torsional stiffness and can provide additional functions, for example parts to connect multiple sections along the perimeter. Such features in a steel section would require joining and machining, thus adding to the cost and narrowing the gap between initial steel and aluminium costs.

Furthermore, this flexibility in design makes it easy, in most cases, to overcome the fact that aluminium and its alloys have only 1/3 the modulus of elasticity of steel. Since stiffness is dependent not only on the Young's Modulus E but also on the Second Moment Inertia I, it is possible to match the stiffness of the steel. This can be done by increasing the web-height of the beam, see Figure 3.7 The three beams have the same stiffness EI. For the first aluminium beam, the cross-sectional area is based on the maximum possible extrusion dimensions. The weight reduction compared to the steel variant is 57%. For the second aluminium beam, the height of the original steel beam is primarily considered. While it is not possible to increase the height of the beam to a large extend, the shape of the cross-sectional area is altered in order to increase the stiffness. The solution results in a 33% weight reduction, which is less than the first aluminium beam (Soetens F. et al., 2014).

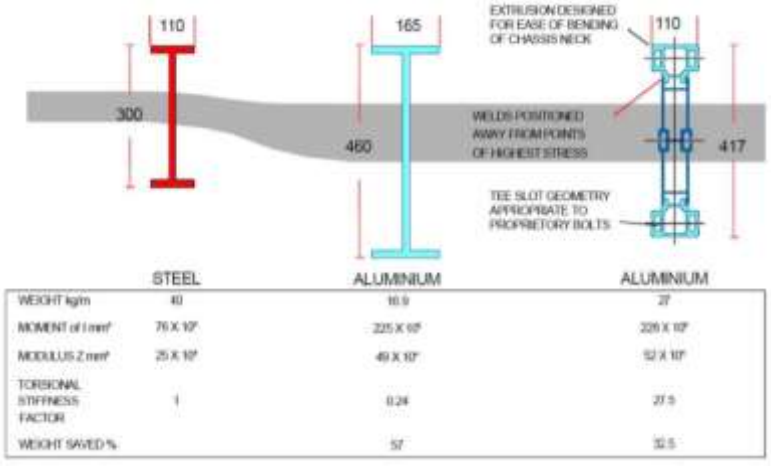

Figure 3.7. A comparison of cross-sectional areas considering the stiffness and weight (TALAT 1501, 1999)

The structural stiffness also influences stability. The lower Young's Modulus causes aluminium components to be more susceptible for instability phenomena, such as local buckling, global buckling and lateral-torsional buckling. Again, the cross-sectional area can be altered to counteract these phenomena: this decreases the slenderness of the structure or structural element (Soetens F. et al., 2014).

Profile section

Now the possibilities of the profile section will be looked into. It is important to take the limits of extrusion technique into account. There are several suppliers which produce large extrusion profiles. Three suppliers are featured below.

The first is SAPA. Their large profiles have a diameter of 320mm, 620x50 mm or 300x300 mm and a weight of 65 kg/m. Profiles in the larger range can sometimes be designed and extruded in thin wall thicknesses. SAPA's activities are spread over 6 establishments in the Benelux. Among these, there are two extrusion specialists for these large profiles, located in Harderwijk (NL) and Lichtervelde (BE) (SAPA, 2015a).

Another supplier is Nedal Aluminium, based in Utrecht. They have 3 extrusion presses (25MN, 40MN and 55MN). Figure 3.8 shows the limits of the three extrusion press mouths. Widths up to 650mm to a corresponding height of 200 with extrusion lengths up to 30000mm are possible (Nedal, 2015).

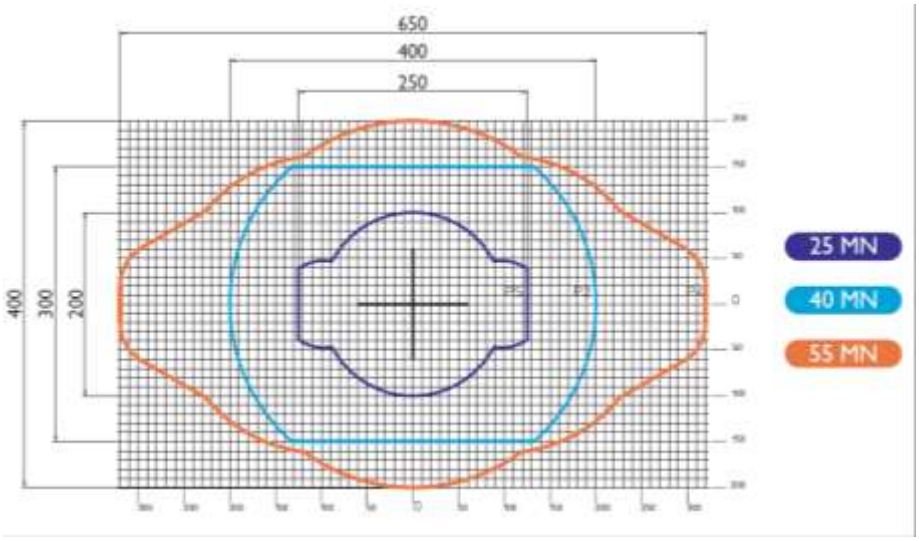

Figure 3.8. Limits for the extrusion press mouth (Nedal, 2015)

Then there is a supplier in China which had a 100MN extrusion press of which the extrusion sizes for different sections are listed in Table 3.3. The limits of the extrusion press mouth are shown in Figure 3.9. The 100MN extrusion press is designed to make large section aluminium extrusion profiles, with lengths up to 30000mm. In this case the sizes for the rectangular sections are of interest.

Table 3.3 Extrusion size of 100MN press (mm) (Horizon Aluminium, 2015)

Section	**Maximal size**
Flat bar	920 x 160
U-shape	800 x 300
Rectangular	700 x 200
Square tube	430 x 430
OD of seamless tube	Ø600
ID of seamless tube	Ø350

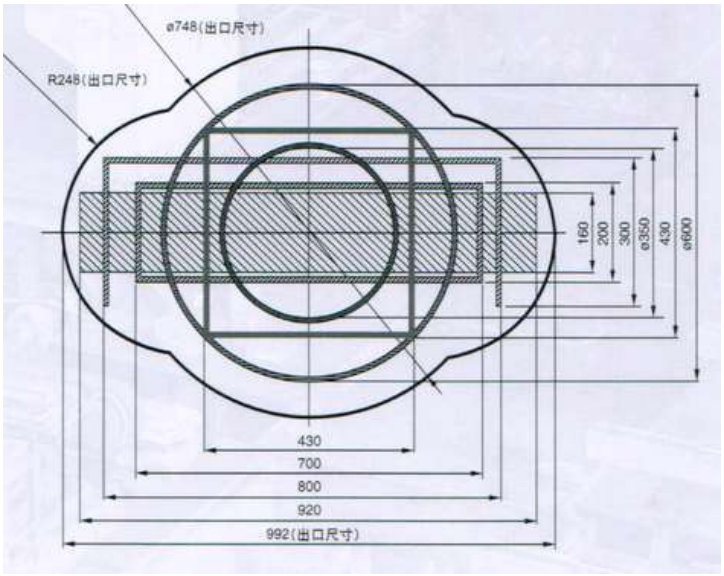

Figure 3.9 Limits for the extrusion press mouth (Horizon Aluminium, 2015)

When choosing an extrusion press and making an optimal design, transportation limits should be taken into account. For transportation on road, diameters up to 4,25m are possible and lengths up to 30m (with a trailer) (Gerritsen, 2015). When the tower is produced in Qingdao, China (near the seacoast), overseas transport is required. In this case, the dimensions are not limited. However, this is an expensive option. The best choice would be the using the 55MN extrusion press from Nedal Aluminium. The diameter of the tower can obviously not be extruded at once; the cross-section has to be divided in multiple equal extruded parts, connected radially as depicted in Figure 3.10. A width of 650mm with lengths of 30m requires the least connections to manufacture the tower's cross-section.

3.4 Joining methods

The extruded parts can be joined by adhesive bonding, mechanical fastening (bolts, rivets, etc.) or by using features that are integrated in the profile. Another way of joining two aluminium parts is by fusion welding or Friction Stir Welding. A combination of joining methods is also possible, the so called hybrid connections. The joining techniques are elaborated below; a short

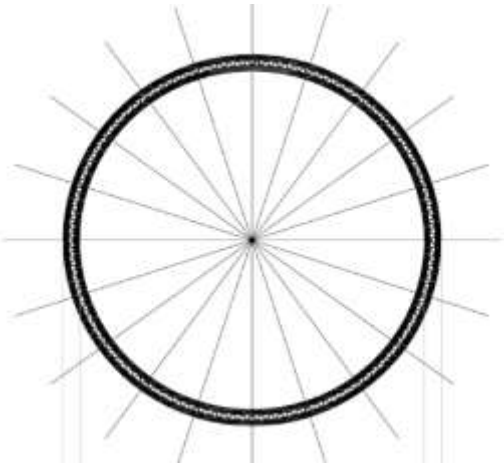

Figure 3.10 Tower cross-section divided radially for extrusion

description is given followed by an enumeration of the advantages and disadvantages. Hereafter, a consideration will be made for the best solution in this case.

Adhesive bonding

Adhesive bonding is defined as the process of joining parts using a non-metallic substance (adhesive), which undergoes a physical or chemical hardening reaction causing the parts to join together through surface adherence (adhesion) and internal strength of the adhesive (cohesion) (SAPA, 2015b).

The advantages of adhesive bonding are (Brockmann W., et al, 2008):

- Uniform stress distribution, in particular for cyclic loaded structures. This results in a longer lifetime for the structure.
- Possibility to join large surfaces.

The disadvantages are (Höglund T. et Al., 2014):

- The material and adhesive must come into good contact with each other.
- Not all types of bonds are so strong that they can withstand the effect of another medium, e.g. water. In corrosive environments this can cause boundary layer corrosion. When the bond is then subjected to minus temperatures, this can also lead to frost erosion in the boundary layer.
- The adhesives are more open to the influences of temperature and time than metals; increasing the temperature decreases the bond strength.
- Cleaning and surface preparation of the adherents is necessary in many cases.
- Specific clamping devices are often required to fix the joint.
- Unpredictable durability, this should be determined experimentally for each application.

Mechanical fastening

In primary structures, the most commonly used mechanical fasteners are either aluminium or steel bolts. Normally galvanised steel or stainless steel bolts are preferred because of their better mechanical behaviour compared to aluminium bolts. However, since the wind tower is located in an offshore environment, there is a risk of galvanic corrosion. This risk can be reduced by using material corrosion protection. However, one of the main advantages of aluminium compared to steel is not using corrosion protection. Using steel preloaded bolts can be an advantage above non preloaded bolts considering corrosion and fatigue resistance. However, preloaded bolts are more expensive. In comparison to welded joints, mechanical fasteners have the advantage that there is no softening of the materials since there is no influence of heat. Furthermore, mechanical fastening can be performed on-site whereas welding is an in-shop method. Thus, for mechanical fastening, on-site bolting is the preferred joining method (Höglund T. et Al., 2014).

Integrated features

Another method for joining extruding profiles is using integrated features. For latitudinal joining, the joints in Figure 3.11 could be considered which have snap-fits, which are easy to realise due to aluminium's high elasticity. Applying snap-fit joints will lead to a quicker assembly than, for example, bolted or welded joints. Besides, stiffeners or weld backings can be added to the cross-section, but are

mainly suitable for profiles with thin walls. In addition, they have low shear strength (Höglund T. et Al., 2014).

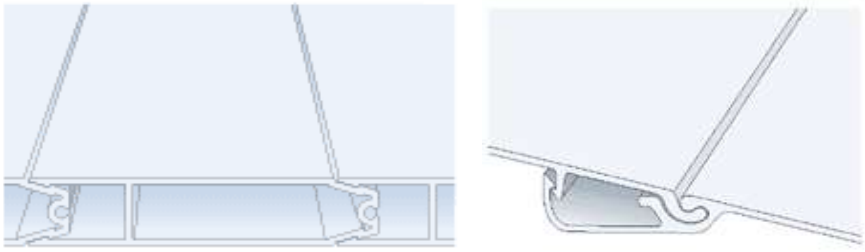

Figure 3.11 Latitudinal joining with snap-fits (Aluminium Design, 2015)

Welding

First some general information regarding welding techniques is given. Then four welding types will be explained, namely inert gas shielded arc welding, laser welding, friction welding and Friction Stir Welding. When welding with steel materials, a weld can be made as strong as the parent material. This is unfortunately not the case with aluminum. In almost all cases, the weld will be weaker than the parent material. In this case, a heat treated alloy will be used where the last heat treatment step heats the metal to approximately 200° C. But during welding, the temperature of the material around the weld becomes higher than 200° C so the material tends to lose some of its mechanical properties. Also, when no post-weld heat treatments are performed after welding, the area around the weld will become significantly (30-40%) weaker than the rest of the aluminum (Lincoln Electric, 2015). However, there are also advantages of welded connections, for example saving of work and material, absence of drilling and overlap, tight joints and no projection of crevice corrosion (SAPA, 2016)

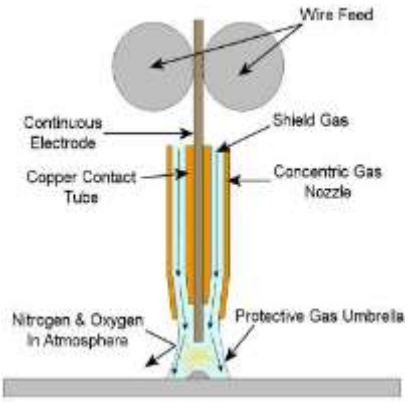

Figure 3.12 MIG welding (Engineer Student, 2014)

Inert gas shielded arc welding (TIG and MIG) are the most widespread welding techniques used for structural aluminium applications. **TIG welding** is only suitable for thin-walled materials, so in this case using MIG welding is more appropriate. **MIG welding** is suitable for parts that are 1mm or thicker and are in position. During MIG welding the arc is struck across the small gap between the wire electrode and the work piece, see Figure 3.12 (Höglund T. et Al., 2014).

The primary advantages of MIG welding are:

- Metal can be welded much more quickly than traditional with welding techniques (Weldguru, 2015).

- The gas shield protects the arc so there is very little loss of alloying elements as the metal transfers across the arc. Only minor weld spatter is produced, which can be removed easily.
- It can be operated semi- and fully automatic (Weldguru, 2015).
- Robotized MIG welding can be used with advantage in long production runs. This method noticeably increases productivity and is also advantageous from a work environment point of view. The position of the work piece is easy to control. This facilitates welding from the optimum position and gives good results (SAPA, 2016)

A disadvantage is that it cannot be used in the vertical or overhead welding positions due to the high heat input and the fluidity of the weld puddle (Weldguru, 2015). Furthermore, MIG welds are fatigue sensitive.

With **laser welding** is another type of welding which can be used for bonding aluminium parts. There are two types of lasers, namely solid-state lasers (Nd-YAG) and gas-discharge lasers (CO_2). The first operates at lower energy and is most suited for thinner materials, while the gas-discharge lasers operate at higher energy and are used for thicker materials (Höglund T. et Al., 2014).

Advantages of laser welding are:
- Compared to MIG welding, laser welding has a low heat application, leading to minor changes in microstructure. This leads to a lower strength reduction.
- No filler metals necessary.
- No secondary finishing necessary (Weldguru, 2015).

Disadvantages (Hanzlaser, 2015):
- The weldment position must be accurate; it should be controlled in the focusing range of the laser beam.
- Maximum welding thickness is 19mm, although when welding single pass in horizontal position, weld penetrations up to 38mm are possible.
- Rapid cooling rate may cause cracking.

Friction welding is a solid state welding process wherein joining is realized by friction heat combined with pressure. The heat is generated by the friction between two surfaces of the components, usually by rotation of one part relative to the other. The temperatures developed are below the melting point of the metals being welded but high enough to create plastic flow and intermolecular bonding (Zaman P.B., 2014).

The advantages of friction welding are (Zaman P.B., 2014):
- There is no gas or filler material present to cause imperfections. Also, no smoke, fumes and spatter are produced.
- Low power requirements.
- Once the welding parameters have been determined, the welding takes only a few minutes.
- Repeatability is reported as excellent and several jobs have been fully automated.
- The technique can be applied to irregularly shaped components using linear, angular, orbital or positional arrest variations.

The disadvantages are:

- The absence of a filler wire means that the process cannot easily be used for making fillet welds. It is limited to angular and flat butt welds (Weldguru, 2015).
- It can only be used for parts with a maximum length of 3,5m (Friction Welding Holland, 2015)

A more recently developed process is **Friction Stir Welding** (FSW). A specially shaped rotation pin moves between the adjoining faces of the joint and stirs the soft material, see Figure 3.13 The tool is moved along the joint line, forcing the plasticized material to merge behind the tool to form a solid-phase joint. The workpieces have to be clamped onto a backing bar and secured against the vertical, longitudinal and lateral forces which will try to lift and push them apart, thus making a support necessary (Höglund T. et Al., 2014).

The main advantages of FSW are (Threadgill, P.L. et al., 2009):

- There is no gas or filler material present to cause imperfections. Also, no smoke, fumes and spatter are produced.
- The process is tolerant to poor quality edge preparation: gaps up to 20% of plate thickness can be tolerated, although this will lead to a reduction in local thickness since no filler is added.
- It is very flexible, joining can be performed in one, two and three dimensions, it is applicable to butt, lap and spot weld geometries and it can be conducted in any position.
- The energy required lies between laser welding (which requires less energy) and MIG welding (which needs more energy).
- High welding speeds and joint completion rates: in thicker materials, FSW can be accomplished in a single pass (*e.g.* the 50 mm tool in *Fig.2d*), whereas other processes need multiple passes. This leads to higher joint completion rates for FSW, even though the welding speeds may be lower. Thick plates can also be joined by FSW on either side.
- The lengths of the elements are limited, but SAPA can weld parts up to3m in width and 14,5m in length.

The main disadvantages are (Threadgill, P.L. et al., 2009):

- The absence of a filler wire means that the process cannot easily be used for making fillet welds. It is limited to angular and flat butt welds.
- The fully mechanized nature of the process prevents its use for applications where access or complex weld shape is best suited to a manual process.
- The workpiece also needs to be restrained in well-designed steel support tooling, both to react to the forces applied, and to prevent the probe from pushing the workpiece materials apart. Joining two curved elements requires an expensive supporting tool and in combination with the large length, this would probably cause difficulties.

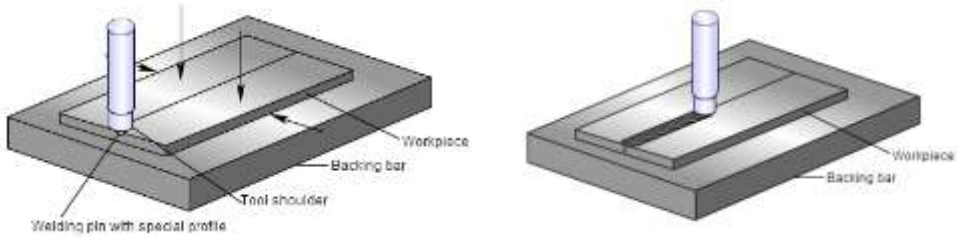

Figure 3.13 Friction Stir Welding (Höglund T. et Al., 2014)

Hybrid joints

In some applications different joining methods are combined. In primary structures, welding and bolting is a commonly used combination, see Figure 3.14.

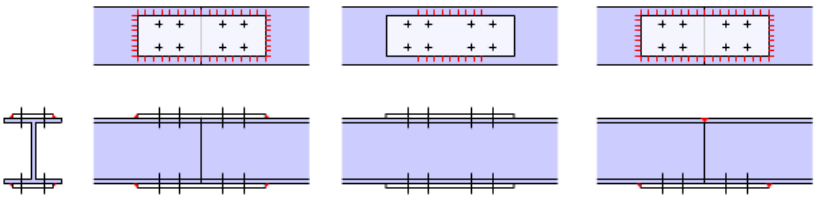

Figure 3.14 Hybrid joints (Höglund T. et Al., 2014)

Now all the joining methods have been briefly described, it is clear that by all means mechanical fasteners should not be considered. Adhesive bonding is not practical in offshore environments. Welding and integrated features are more suitable choices. Friction welding is limited to a length of 3,5m, this may not be practical when welding the wind turbine parts and laser welding cannot penetrate deep enough. That leaves MIG welding and Friction Stir Welding. FSW has a lower strength reduction in contrast to MIG welding, but joining large, curved elements is expensive and difficult. MIG welding has therefore the preference. Then there is joining using integrated features, which is a huge advantage of aluminium above steel. Applying this could make it easier to join the parts for welding. Therefore, the best method for joining aluminium parts for the wind turbine tower would be MIG welding in combination with integrated features.

4. Literature study on dynamics

An offshore wind turbine system can be seen as a number of coupled mass-spring-damper systems. A single degree of freedom mass-spring-damper system is shown in Figure 4.1. A short basic dynamics review will be provided.

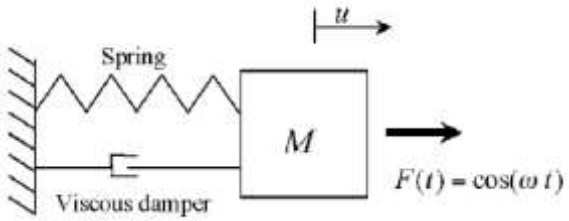

Figure 4.1. Single degree of freedom mass-spring-damper system (Tempel J. van der, 2006)

When a sinusoidal excitation force *F(t)* is applied to the mass, the magnitude and phase of the resulting displacement *u* strongly depend on the excitation frequency ω. Three response regions can be observed (Tempel J. van der, 2006):

Quasi-static

For frequencies of excitation below the natural frequency of the system, the response will be quasi-static as illustrated in Figure 4.2a: the displacement of the mass will follow the time varying force almost immediately. There is only a small phase lag, as if it were excited by a static force.

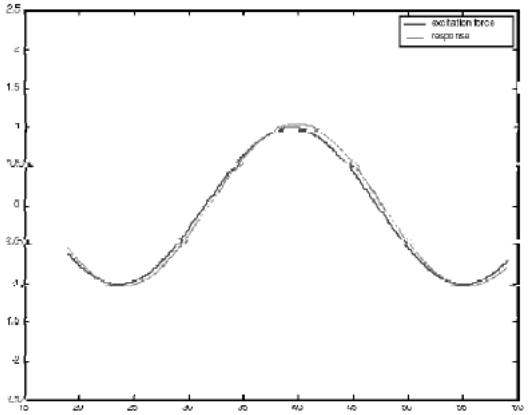

Figure 4.2a. Quasi-static response. Solid line: excitation force, dashed line: simulated response (Tempel J. van der, 2006)

Resonance

Figure 4.2b shows a typical response for frequencies of excitation within a narrow region around the system's natural frequency. The spring force and inertia force almost cancel, creating a response that is a number of times larger than it would be statically. The occurring amplitude is regulated by the damping present in the system.

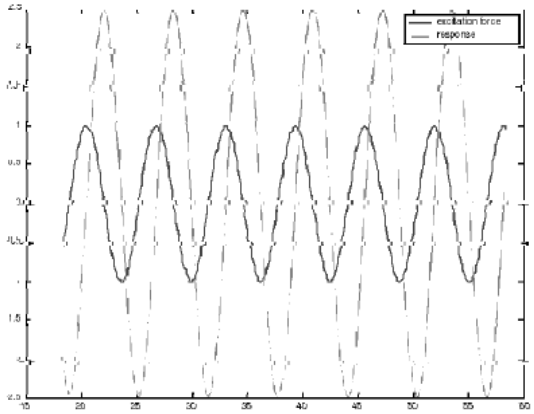

Figure 4.2b. Resonant response. Solid line: excitation force, dashed line: simulated response (Tempel J. van der, 2006)

Inertia dominated

For frequencies of excitation above the natural frequency, the mass cannot follow the movement any more. As a result, the response level is low and almost in counter-phase, as is illustrated in Figure 4.2c. Here, the inertia of the system dominates the response.

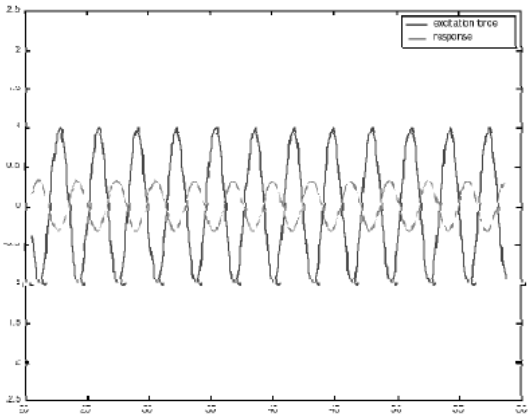

Figure 4.2c. Inertia dominated response. Solid line: excitation force, dashed line: simulated response (Tempel J. van der, 2006)

In the three figures, the magnitude of the excitation force is equal, but applied at different excitation frequencies. In general it can be said that, in steady state, sinusoidal inputs applied to a linear system generate sinusoidal outputs of the same frequency, although differ in magnitude and phase.

4.1 Schematization

Figure 4.3 shows a mass-on-pole system of an offshore wind turbine. It consists of a laterally loaded uniform beam with two masses, which is embedded in the soil. The two main forces with a harmonic character which are taken into account in the dynamic analysis are the wave and wind forces. The lateral loads must be in equilibrium with the soil resistance.

The upper mass m_2 represents the nacelle, hub and rotor mass, which is located at hub height. This mass will be loaded with a harmonic force due to the wind (F_2). The lower mass m_1 represents the mass of the support structure above the fixed support. In reality, the pile continues below the schematized support. This mass is not taken into account since it will not take part in the dynamic vibrations. The mass of the support structure is concentrated at mean sea level (MSL), since the harmonic wave load (F_1) is applied here.

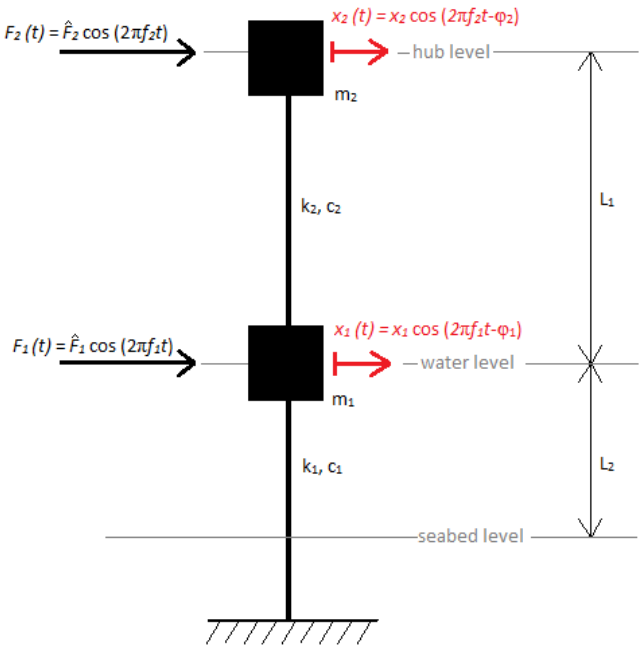

Figure 4.3. Mass-on-pole system (Wijngaarden M., 2013 - edited)

Figure 4.4 shows the reduction of the mass-on-pole system to an equivalent 2-mass-spring-damper system.

The equation of motion belonging to this model is the following:

$$[M]\frac{d^2u}{dt^2} + [C]\frac{du}{dt} + [K]u = [F]\cos(\omega t - \theta) \qquad (4.1)$$

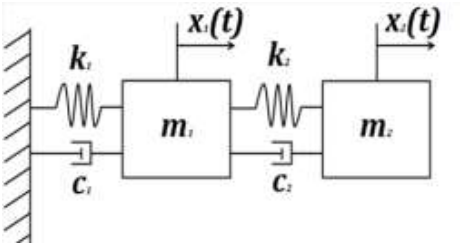

Figure 4.4. 2-mass-spring-damper system

Where:

M	=	mass matrix	[kg]
C	=	damping matrix	[Ns/m]
K	=	stiffness matrix	[N/m]
$\frac{d^2u}{dt^2}$	=	acceleration vector	[m/s²]
$\frac{du}{dt}$	=	velocity vector	[m/s]
U	=	displacement vector	[m]

The properties required to solve the equation of motion are the mass, the spring stiffness and the structural damping (Tempel J. van der, 2006).

Mass

The mass of the tower is divided over the two schematized masses, however not all structural mass will be equally excited. Depicted in Figure 4.3, the upper mass m_2, represents the top mass and a part of the tower structure. In the case of a uniform beam this mass is:

$$m_2 = m_{top} + 0{,}23m_{tower} \qquad (4.2)$$

which is obtained from the formula for the angular frequency of a cantilevered beam in Figure 4.5. However, in this case the mass of the tower is not uniformly distributed. The upper 0,23 part of the tower represents 15% of the total tower mass. So in this case, m_2 should be calculated with:

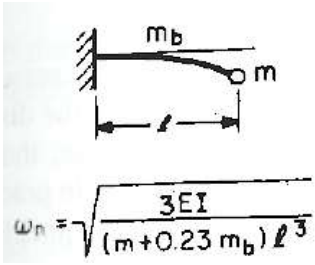

Figure 4.5. Baumeister's equation (Avallone E.A. and Baumeister T., 1996)

$$m_2 = m_{top} + 0{,}15m_{tower} \qquad (4.3)$$

The lower mass m_1 represents the remaining mass of the tower and the mass of the support structure:

$$m_1 = m_{ss} + 0{,}85m_{tower} \qquad (4.4)$$

Spring stiffness

During the preliminary design stage, only estimations are possible. This also applies for the 'apparent fixity length', which is the length below the seabed under which the pile is assumed to be rigidly clamped in order to achieve the same fundamental eigenfrequency as the flexible support pile. The value for this length is related to the soil type. In the offshore technology, rough approximations are often used, see Table 4.1.

Table 4.1. Indicative values of apparent fixity length for piles of oil and gas jacket platforms (Kühn, 2001)

Fixity length	Soil condition
3,5 *D* – 4,5 *D*	Stiff clays
7 *D* – 8 *D*	Very soft silts
6 *D*	General calculations

All calculations done by M. van Wijngaarden were based on a homogeneous sand layer with a schematized fixed support at a depth of 3,5·D_{pile} below seabed, see Figure 4.6. With this figure, the stiffness can be determined, which is one of the main parameters of the support structure. The lateral deflection u is defined at the top of the support structure. The displacement at water level can be calculated with the following two formulas:

$$u_1 = \frac{F_{current} {l_1}^3}{3EI} \tag{4.5}$$

$$u_2 = u_1 + \frac{F_{current} {l_1}^2}{2EI} + \frac{F_{wave} {l_2}^3}{3EI} \tag{4.6}$$

In order to calculate the bending stiffness EI, the mono pile is considered to be prismatic with a moment of inertia and section modulus of a thin walled cross-section:

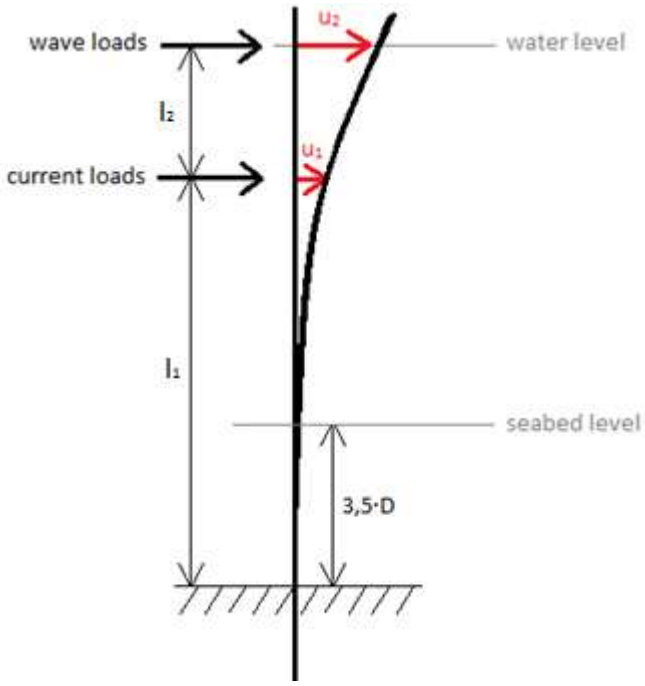

Figure 4.6. Lateral displacements of the support structure due to waves and current (Wijngaarden, M., 2013)

$$I = \frac{1}{8}\pi D^3 t_w \tag{4.7}$$

$$W = \frac{1}{4}\pi D^2 t_w \tag{4.8}$$

With $D = (D_{out} + D_{in})/2$

There are no standards for the total displacement, so this does not need to be checked. The dimensions are overall large enough to limit the displacements. Only a check needs to be done to ensure the rotor

blades do not approach the tower too closely. This will not be checked in this thesis since the rotor blades are left out of account.

In the schematization, the two masses are connected through linear springs. The spring stiffness of the support structure k_1 can be determined from the soil-structure interaction. The horizontal wave and current forces result in a static displacement u_2 of the support structure, from which the stiffness can be calculated:

$$k_1 = \frac{F_{wave} + F_{current}}{u_2} \tag{4.9}$$

The stiffness of the tower k_2 can be calculated with simple deformation formulas for a one-sided fixed beam:

$$k_2 = \frac{3EI}{{L_1}^2} \tag{4.10}$$

In which the moment of inertia is calculated using the formula for a thin walled cross-section with an average tower diameter.

Damping

Lastly, the damping of both connecting elements should be taken into account.

Damping is the means by which the response motion of a structural system is reduced as a result of energy losses. For convenience in structural design, damping is usually assumed as viscous in nature and is normally expressed as a percent of the critical damping c_{crit} (Stevenson, J.D., 1980). When the damping ratio $\zeta = \frac{c}{2\sqrt{mk}}$ equals 1, the system is said to be critically damped.

Four sources of damping are important for an offshore wind turbine, which are given in the order of decreasing relevance (Kühn, 2001):

- Aerodynamic damping
- Structural damping
- Soil damping
- Hydrodynamic damping

Aerodynamic damping is the most significant source of damping. The basics can be illustrated by considering a tower top in motion. When the tower top is moving forward, the blades experience a small increase of wind speed and will respond to it aerodynamically. The response is such that an extra aerodynamic force will counteract the tower top motion, so the eventual excursion of the tower top due to the induced tower top velocity will be less. When the tower top moves backward the aerodynamic force decreases, again reducing the tower top motions. As this effect is linked to the velocity term in the equation of motion, it is comparable to damping, hence the term aerodynamic damping (Cerda Salzmann D.J. and Tempel J. van der, 2005).

Structural damping is generated by internal material friction and bolted or welded joints, which is conveniently considered as modal damping. Typical values recommended for dynamic response analysis of wind loaded steel and concrete structures are given in Table 4.2.

In Kühn's research (Kühn, 2001) generally material damping is considered as 0,5% of critical damping for steel structures. However, according to DVN, the structural damping c_1 should be taken as 1% of the critical damping c_{crit}.

Table 4.2. Recommended structural damping ratios (Kühn, 2001)

Structure	Modal damping ratio (1st bending mode, as percentage of critical damping)
Steel lattice tower	
- all welded	0.2 %
- welded bracings	0.2 - 1. %
- bolted bracings	0.3 - 1.2 %
Steel chimneys (unlined)	
- welded	0.4 - 0.7 %
- bolted	0.6 - 1. %
Concrete chimneys	
- without internal flues	0.5 - 1.2 %
- with internal flues	1.2 - 2.5 %
Steel tubes and pipes	0.5 - 1 %

Soil damping of piled systems is low. Measurements gained by Kühn give an indication on the total structural and soil damping during shut-down and employment of the mechanical brake at two specific turbines. The results lead to an adequate number of 0,5% for the damping ratio, but further investigations at other mono pile structures are recommended.

Hydrodynamic damping is caused by the structural motion in the water. For offshore support structures, which are relatively stiff below the water surface, the effect is negligible.

Frequency

The support structure is likely to fail due to the large sinusoidal deformations resulting in fatigue. In order to prevent resonance, the natural frequencies of the 2-mass-spring-damper system needs to be determined and should stay well away from the frequencies of wave and wind loads.

From the equation of motion, the following equation can be obtained:

$$m_1 m_2 \omega^4 - \big(m_1 k_2 + m_2 (k_1 + k_2)\big)\omega^2 + k_1 k_2 = 0 \tag{4,11}$$

Now, four angular velocities can be determined, of which two will be negative and do not have any physical meaning. So two angular frequencies remain: ω_1 and ω_2 (rad/s). Then the two natural frequencies can be determined with:

$$f_{1,2} = \frac{\omega_{1,2}}{2\pi} \tag{4.12}$$

For the derivation of the equation, see Appendix A.

The system's natural frequency is governed by damping. As a result the amplitude and vibrations can be reduced. Therefore, any resonant problem can be counteracted with adequate damping controls, see Figure 4.7. This figure shows that as the excitation frequency gets closer to the natural frequency, the amplitude of the response gets larger. When the damping increases, the peak value reduces and

shifts slightly (Manwell J.F., Mcgowan J.G., and Rogers A.L., 2002). In dynamics, aside from the frequency of the force, the magnitude of the force is also crucial (Tempel J. van der, 2006). Resonant behavior can cause critical load cases, even failure is possible, but special attention should be paid to fatigue difficulties.

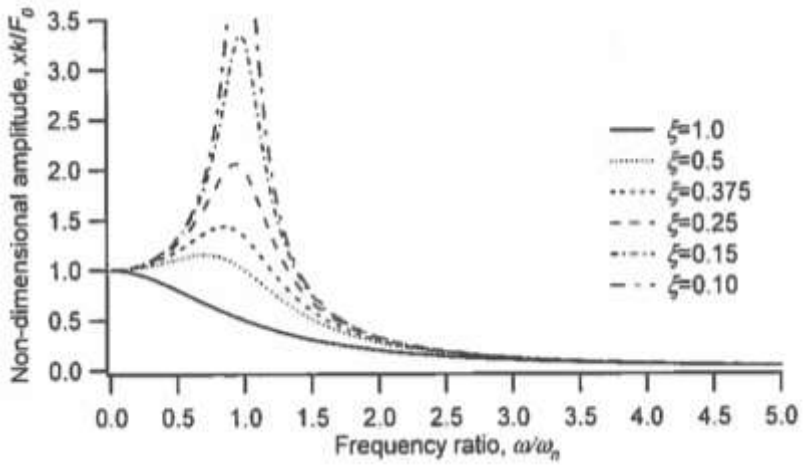

Figure 4.7. System responses to forced vibrations; x: non-dimensional damping ratio (Manwell J.F., Mcgowan J.G., and Rogers A.L., 2002)

4.2 Excitation frequencies

Four fundamental dynamic excitation frequencies affect the dynamic response of the structure, namely excitation by:

- Current 0.0003Hz to 0.04 Hz
- Waves 0.05Hz to 0.2Hz
- Rotor 0.07Hz to 0.356Hz
- Blade passing 0.22Hz to 1.07Hz

When the eigenfrequency approaches an excitation frequency, the lifetime of the structure will be influenced since the damage as a result of fatigue will be larger when the dimensions remain the same. This can lead to extra maintenance costs or a reduction in lifetime.

Excitation frequencies as a result of currents

When an object is located in a flowing medium, there is the possibility that the structure will vibrate as a result of fluctuating swirls (time-dependent turbulences) which arise behind the object. This occurs when the Reynolds number is between 300 and $3 \cdot 10^5$ which is commonly applied for hydraulic structures. Due to the fluctuating swirls behind the object, a varying load perpendicular to the current is applied on the object. The frequency of these eddy changes is (Aalst, W. van, 1984):

$$fs = \frac{uS}{D} \tag{4.13}$$

Where:

- u velocity of undisturbed current
- S number of Strouhal, describing the oscillation of liquids. With the aid of a graph and the Reynolds number $Re = \frac{U \cdot D}{\nu}$, the number of Strouhal can be determined. It can also be approached with the following formula: $S = 0{,}21 \cdot C_D^{-0{,}75}$
- D characteristic diameter of the cylinder

Excitation frequencies as a result of waves

Waves come with different frequencies, in general in a range below and in the 1P frequency range of the wind turbine, which is around 0,05HZ to 0,2Hz as indicated in Figure 4.8 with the curved line (Bhattacharya, S., 2014). The rest of the graph will be explained later on.

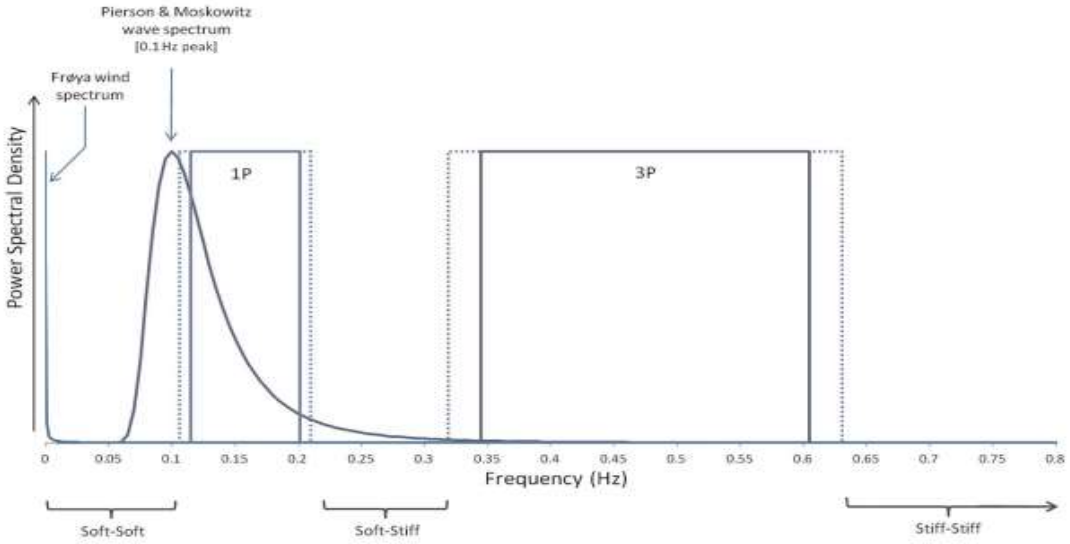

Figure 4.8 Frequency ranges of a wind turbine and waves (Bhattacharya, S., 2014)

Excitation frequencies as a result of the rotor and blades

The rotor frequency f_{1P}, also referred to as 1P, occurs as a result of the eccentricity of the rotor hub, see Figure 4.9. This means that the center of gravity is not situated exactly in the middle in relation with the axis, resulting in a dynamic force when the rotor rotates. The eccentricity could be a consequence of a small deviation in the rotor blades.

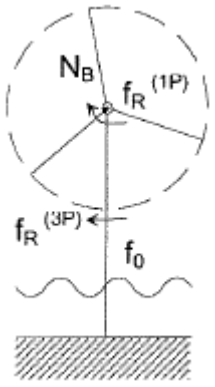

Figure 4.9. Rotor and blade passing frequenc (Ginhoven, J. van, 2006)

The blade passing frequency $f_B = N_B \cdot f_R$, occurs when a rotor blade passes the tower at a certain frequency which is N_B times larger than the rotor frequency. N_B represents the number of rotor blades.

The rotor frequency and blade passing frequency can be determined with the following formula:

$$f_{1P} = \frac{\lambda V_w}{\pi D_{rotor}} = \frac{V_{tip}}{\pi D_{rotor}} = \frac{rpm \cdot \pi \cdot D_{rotor}}{60 \cdot \pi \cdot D_{rotor}} = \frac{rpm}{60} \tag{4.14}$$

$$f_B = N_B \frac{\lambda V_{rated}}{2\pi R} \tag{4.15}$$

Where:			
	N_B	number of rotor blades	[-]
	R	radius of the rotor	[m]
	V_{rated}	the velocity of the wind	[m/s]
	λ	V_{tip}/V_{rated}	[-]
		V_{tip}: the velocity of the tip of the blades	[m/s]

The smallest frequencies are obtained during startup (3-4 m/s), then the frequency increases until the wind velocity is equal to the nominal wind velocity. From this moment on, the frequency is maximal and remains unchanged until eventually the shutdown velocity (25m/s) is reached (Ginhoven, J. van, 2006).

4.3 Natural frequency

Currently, most wind turbines have a variable rotor speed and therefore a 1P and 3P frequency range, as can be seen in Figure 4.8. This figure merely serves as a clarification of the frequency ranges, the values are not of importance here. To avoid resonance, the structure should be designed in such a way that its natural frequency does not coincide with either 1P or 3P frequencies. This creates three possible intervals and therefore three possible structures; a very stiff structure with a high natural frequency greater than 3P (stiff-stiff), a natural frequency between 1P and 3P (soft-stiff) and a very soft structure less than 1P (soft-soft) (Kühn, 2001). In literature, the term soft is commonly used for flexible turbine systems. In the first interval, the dynamic load occurs mostly due to waves with an eigenfrequency of 0,04Hz (25s) to 0,5 à 1,0Hz (2s à 1s). In the middle range, the dynamic load is mainly caused by wind.

During the design process of the support structure it is convenient to state allowed ranges for the lower eigenfrequencies which account for the exclusion bands due to rotor excitations e.g. 1P +- 10% and N_bP +- 20% (Kühn, 1997).

Stiff-stiff structures are problematic due to the increase of wind induced fatigue. So according to Kühn (1997), at least in the upper part flexibility should be introduced. In conctrast, soft-stiff support structures should be possible for most sites, but not for all generic concepts. Problems may occur if the design range for the fundamental eigenfrequency is not large enough or the overall height is too large

for the considered concept and stiffness. Soft-soft designs are economically interesting but susceptible to wave fatigue (see Figure 4.10) thus careful design is required. Relatively high stiffness in the foundation and submerged part of the support structure and a gradual decrease in stiffness from towards the top seem to be an possibility, certainly for locations with a moderate wave regime (Kühn, 1997).

5. Literature study on loads

5.1 Limit states and loads

A limit state is a condition beyond which a structure or structural component will no longer satisfy the design requirements. The following limit states are considered in the Det Norske Veritas (DNV) Offshore Standard for Design of Offshore Wind Turbine Structures (DNV, 2014):

- **Ultimate limit states (ULS)**, which correspond to the maximum load-carrying resistance. Examples are:
    - Loss of structural resistance (excessive yielding and buckling)
    - Loss of static equilibrium of the structure, or of a part of the structure, considered as a rigid body
    - Failure of critical components of the structure caused by exceeding the ultimate resistance or the ultimate deformation of the components
- **Fatigue limit states (FLS),** which correspond to failure due to the effect of cyclic loading.
    - Cumulative damage due to repeated loads
- **Accidental limit state (ALS)**, which corresponds to (1) maximum load-carrying capacity for (rare) accidental loads or (2) post-accidental integrity for damaged structures.
    - Structural damage caused by accidental loads (ALS type 1)
    - Ultimate resistance of damaged structures (ALS type 2)
    - Loss of structural integrity after local damage (ALS type 2)
- **Serviceability limit states (SLS)**, which correspond to tolerance criteria applicable to normal use.
    - Deflections that may alter the effect of the acting forces
    - Deformations that may change the distribution of loads between supported rigid objects and the supporting structure
    - Motions that exceed the limitations of equipment
    - Differential settlements of foundation soils causing intolerable tilt of the wind turbine

Load categories according to DNV are:

- **Permanent loads (G)** are loads that will not vary in magnitude, position or direction during the period considered. Examples are:
    - Mass of structure (rotor, hub, nacelle, tower, support structure and foundation)
    - Mass of permanent ballast and equipment
    - External and internal hydrostatic pressure of a permanent nature
    - Reaction to the above, e.g. articulated tower base reaction
- **Variable functional loads (Q)** are loads which may vary in magnitude, position and direction during the period under consideration, and which are related to operations and normal use of the installation. Examples are:
    - Actuation loads due to operation and control of the wind turbine
    - Loads on access platforms and internal structures such as ladders and platforms
    - Ship impacts from service vessels

  - Crane operational loads
- **Environmental loads (E)** are loads which may vary in magnitude, position and direction during the period under consideration, and which are related to operations and normal use of the structure. Examples are:
  - Wind loads
  - Hydrodynamic loads induced by waves and current
  - Earthquake loads
  - Tidal effects
  - Marine growth
  - Snow and ice loads

For the preliminary design stage, the variable functional loads will not be taken into account, only the permanent and environmental loads. There is also a fourth type of load, namely the accidental loads (A) such as dropped objects, ship collisions and explosions, which are not taken into account. Thus, the accidental limit state (ALS) will not be discussed any further. So only the ULS, FLS and SLS will be analyzed after the determination of the design inputs.

5.2 Load and resistance factors

The partial safety factor method is applied. DNV defines this as follows: a design method by which the target safety level is obtained as closely as possible by applying load and resistance factors to characteristic values of the governing variables and subsequently fulfilling a specifies design criterion expressed in terms of these factors and these characteristic values. The governing variables consist of:

- Loads acting on the structure or load effects in the structure
- Resistance of the structure or strength of the materials in the structure.

The safety level of a structure or a structural component is considered to be satisfactory when the design load effect S_d does not exceed the design resistance R_d.

The design load effect S_{di} is obtained by multiplication of the characteristic load effect S_{ki} by a specified load factor γ_{fi}: $S_{di} = \gamma_{fi} S_{ki}$

The design resistance R_d is obtained by dividing the characteristic resistance R_k by a specified material factor γ_m: $R_d = \frac{R_k}{\gamma_m}$

Table 5.1. Load cases with related factors γ_f for the ULS, SLS and FLS (DNV, 2014)

Limit State			Load factors γ_f	
			G	E
1	ULS	Extreme permanent loads and normal environmental loads	1,25	1,00
2	ULS	Normal permanent loads and extreme environmental loads	1,00	1,35

3	SLS	1,00	1,00
4	FLS	1,00	1,00

Table 5.2. Resistance factors γ_m for the ULS, SLS and FLS (DNV, 2014)

		Resistance factor γ_m
ULS		1,10
SLS		1,00
FLS	Depends on location of the element or joint	1,15

5.3 Load combinations for the ULS

According to DNV, there are 31 load cases to consider for wind turbine load conditions and their companion wave load conditions, current conditions and water level conditions. The load cases refer to design in the ULS and in the FLS and include a number of abnormal load cases for the ULS. The 31 load cases correspond to the 31 load cases defined in IEC61400-3 (offshore wind turbines) based on the load cases in IEC61400-1 (onshore wind turbines). The required combined load effects should be calculated with various directions of wind, wave and current loads for different return periods of these loads. In case of insufficient information to produce these calculations, there are 5 simplified environmental load combinations to be considered, including ice loads. When ice loads can be neglected regarding the location of the wind turbine, three load combinations remain (Wijngaarden, M., 2013). These three will be taken into account in this thesis, see Table 5.3.

Table 5.3. Proposed load combinations for simplified load combinations (DNV, 2014)

Load combination for ULS	Environmental load type and return period to define characteristic value of corresponding load effect			
	Wind	Waves	Current	Water level
1	50 years	5 years	5 years	50 years
2	5 years	50 years	5 years	50 years
3	5 years	5 years	50 years	50 years

For each load type in a particular load case, the table specifies the characteristic value specified in terms of the return period.

5.4 Wave and current loads

Wave is the oscillatory movement of water as reflected by the alternate rise and fall of the surface water while current is that part of the water that is moving continuously in a definite direction so the main difference is in direction (from www.answers.com).

Waves

To determine the extreme wave loads on a structure, the maximum wave for the site must be known. The location which is chosen is shown in Figure 5.1 with a red dot. The IJ-geul Munitiestortplaats 1 is the most nearby measuring station where Rijkswaterstaat measures wind and waves. This data is converted in site specific data, shown in Table 5.4.

Figure 5.1. Selected location in the North Sea (Wijngaarden, M., 2013)

Table 5.4. Water, wind, wave and current data for selected location (Wijngaarden, M., 2013)

Water depth (MSL)	20	[m]
HAT (high astronomical tide)	1.04	[m+ MSL]
MSL (mean sea level)	0.00	[m+ MSL]
LAT (low astronomical tide)	-1.03	[m+ MSL]
Storm surge 50 yr.	1.00	[m+ MSL]
Mean wave height	1.25	[m+ MSL]
Wave height 50 yr.	14.9	[m+ MSL]
Wave height 5 yr.	12.61	[m+ MSL]
Wave period 50 yr.	10.99	[s]
Wave period 5 yr.	10.02	[s]
Wind speed 50 yr.	42.04	[m/s]
Wind speed 5 yr.	35.95	[m/s]
Current velocity 50 yr.	2.1	[m/s]
Current velocity 5 yr.	1.0	[m/s]
Top transition piece	13.23	[m+ MSL]
Hub height	93.23	[m+ MSL]

For the calculation of the wave loads, the Morison formula can be used, as proposed in the DNV Offshore Standard. This is a formula to calculate the hydrodynamic loads on slender members per unit length, consisting of two parts: an inertia part, which is quadratic in D and a drag part, linear in the structural diameter D (Kühn, 2001). The velocity and acceleration have a 90° phase difference, so inertia and drag loads will also be out of phase. This means that in general the maximum load is not

equal to either maximum drag or maximum inertia load. For a conceptual design, the wave load can be defined as follows (DNV, 2014):

$$F_{wave} = F_I + F_D = C_I K_I H \rho_{water} g \pi \frac{D^2}{4} + C_D K_D H^2 \frac{1}{2} \rho_{water} g D \tag{5.1}$$

Where:

C_I	inertia coefficient	[-]
C_D	drag coefficient	[-]
K_I	correction coefficient for extent of inertia force	[-]
K_D	correction coefficient for extent of drag force	[-]
H	wave height	[m]
ρ_{water}	density water	[kg/m^3]
D	pile diameter	[m]

The four coefficients depend on the water depth d, the wave height relative to the breaking wave height (H/H_b), and the wave period T.

The ratio H/H_b can be calculated with Figure 5.2 by entering the graph at the horizontal axis, and determine the value at the vertical axis (with H = breaking height of the wave) at the intersection with the 'breaking limit' line. When the breaking wave height H_b is known, the ratio H/H_b can be calculated.

In deep water ($d > \frac{1}{2}\lambda$), waves break when $\frac{H}{\lambda}$ exceeds about 0,14. In shallow water ($d < \frac{1}{20}\lambda$), waves break when $\frac{H}{d}$ or, more accurate, when $\frac{H}{H_d}$ exceeds about 0,78 (DNV, 2014). For the chosen location, the value for shallow water should be taken. When breaking waves occur, the Morison formula cannot be used anymore since a breaking wave will exert a larger force on the structure. The accelerations of the water particles will be subordinate to the velocity of the water, and consequently the inertia force is negligible relative to the drag force.

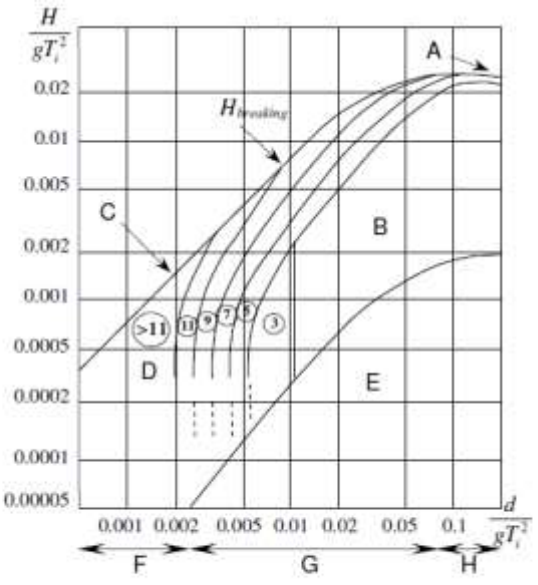

Figure 5.2 Regions of application of different wave theories (ISO 19901-1, 2005)

Formula 5.2 can be used to calculate the force of breaking waves on a rigid structure. So in this case, not all four coefficients from formula 5.1 need to be determined.

$$F_{breaking\ wave} = C_D{}^* K_D H_b{}^2 \frac{1}{2} \rho_{water} g D \tag{5.2}$$

Where:

$C_D{}^*$	drag coefficient in breaking waves = 2,5 · C_D	[-]
K_D	correction for extent of drag force	[-]
H_b	breaking height of the wave	[m]
D	pile diameter	[m]

Currents

Sea currents are mostly driven by the tides and ocean circulations, although the outflow of rivers, differences in temperature or salinity and storm surges may cause extra local currents (Tempel, J. van der, 2006).

The current velocity will cause a load on the submerged structure. The velocity varies over water depth, it will be highest at the surface level and zero at the seabed due to friction. The design guides usually present three basic current profiles over depth (see Figure 5.3), namely

- the linear profile
- the bilinear profile
- the power law profile

(Tempel, J. van der, 2006)

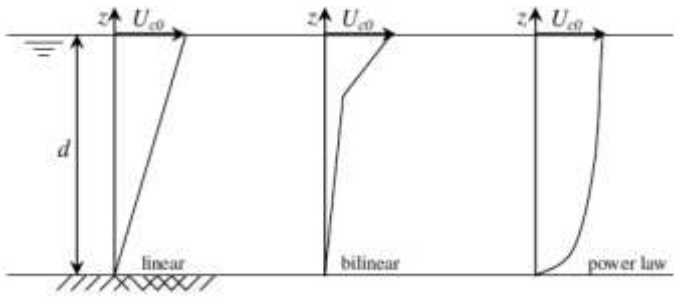

Figure 5.3. Different current distributions (Tempel, J. van der, 2006)

For ease of calculation, a linear distribution will be assumed. Therefore, the point of action of the current load is on 2/3 of the water depth, calculated from the bottom.

Table 5.4 shows the current velocities with a return period of 5 and 50 years. The resulting load can be derived using a formula for flow around slender structures, which consists of a static and a dynamic part of the drag force (Ginhoven, J. van, 2006):

$$F_D = \frac{1}{2} \rho_{water} u^2 (C_D + C_D') A \tag{5.3}$$

Where:

ρ_{water}	density water	[kg/m³]
u	extreme current velocity	[m/s]
C_D	static drag coefficient	[-]

C_D'	dynamic drag coefficient	[-]
A	area facing water flow	[m²]

5.5 Wind loads

Wind-generated loads on the rotor and the tower shall be considered, which include wind loads produced directly by the inflowing wind as well as indirect loads that result from the wind-generated motions of the wind turbine and the operation of the wind turbine. The direct wind-generated loads consist of:

- Aerodynamic blade loads
- Aerodynamic drag forces on tower and nacelle

(DNV, 2014)

Wind speed and wind shear

First, some background information regarding wind loads is given. The current generation of wind turbines usually starts operating at 3-4 m/s wind speed and will shut down at around 25 m/s. Because the wind speed is constantly changing, the main feature of wind speed is its mean. Either over short intervals called gusts (3-10s) or as 10 minute means, daily means, monthly means or yearly means. When taking a longer measurement period, the time varying character of the wind can be captured in a wind spectrum, covering frequency ranges from years to seconds. This spectrum is shown in Figure 5.4. The frequencies on the left side represent the yearly changes, pressure systems and diurnal changes. On the right, the turbulence is visible. The solid line represents high turbulence during a period of high wind speeds, the dotted line stands for the reduced turbulence at lower wind speeds. The last notable point is the gap around the 1-hour period, which is known as the 'spectral gap'. It separates the slowly changing and turbulent ranges. Because in this frequency range the wind speed does not change, the mean over a period of 10 minutes to 1 hour can be considered constant: the instantaneous wind speed changes with turbulence, but the mean wind speed stays constant over the interval (Tempel, J. van der, 2006).

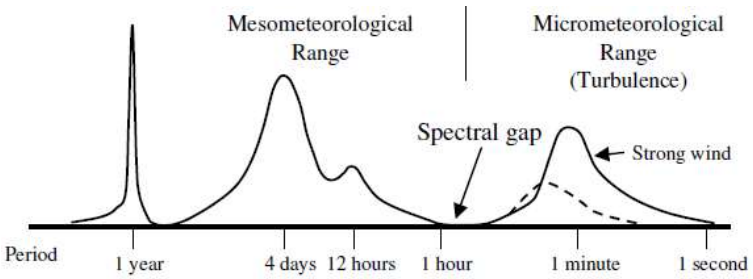

Figure 5.4 Wind speed spectrum over a broad range of frequencies (Tempel, J. van der, 2006)

The wind velocity measured in the wind field shows variations in space, time and direction. A momentary representation of a typical wind speed distribution is shown in Figure 5.5. The figure shows that the mean wind speed

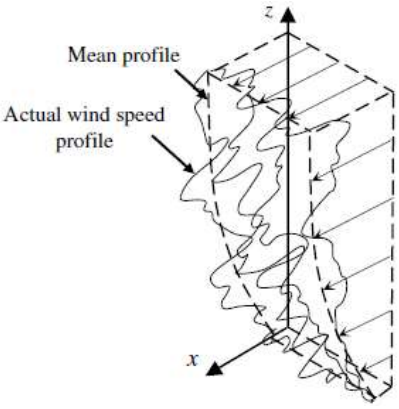

Figure 5.5 Actual wind speed profile (Tempel, J. van der, 2006)

increases with height. The reason for this is that the wind speed in the lower 2 km of the Earth's atmosphere is affected by friction with the Earth's surface. This phenomenon is called wind shear. Furthermore, the actual wind speed at any location varies in time and direction around its mean value due to the effect of turbulence.

To describe the shear effect on the mean wind speed at a certain elevation, two main models are commonly used: the logarithmic profile and the power law profile. Both profiles are fitted curves to measured wind shear effects. The logarithmic profile and the power law profile are described by the following equations:

$$V_w(z) = V_{w,r} \frac{\ln\left(\frac{z}{z_0}\right)}{\ln\left(\frac{z_r}{z_0}\right)} \tag{5.4}$$

$$V_w(z) = V_{w,r} \left(\frac{z}{z_r}\right)^{\alpha_{shear}} \tag{5.5}$$

Where:			
	$V_w(z)$	mean wind speed at height z	[m/s]
	$V_{w,r}$	mean wind speed at the reference height z_r	[m/s]
	z_r	reference height	[m]
	z_0	surface roughness length	[m]
	α_{shear}	power law coefficient	[-]

DNV advises the use of z_0 = 0,05m for offshore terrain. No real difference exists for either wind shear model.

Wind calculations

Now the aerodynamic behavior will be analyzed by considering the simplest model of a wind turbine, the so-called actuator disc model. In this model, the turbine is replaced by a circular disc through which the airstream flows with a velocity U_∞ and across which there is a pressure drop from p_u to p_d as illustrated in Figure 5.6. The actuator disc model is based on the following ideal assumptions: no frictional drag, homogeneous, incompressible, steady state fluid flow, constant pressure increment or thrust per unit area over the disc, continuity of velocity through the disc and an infinite number of blades.

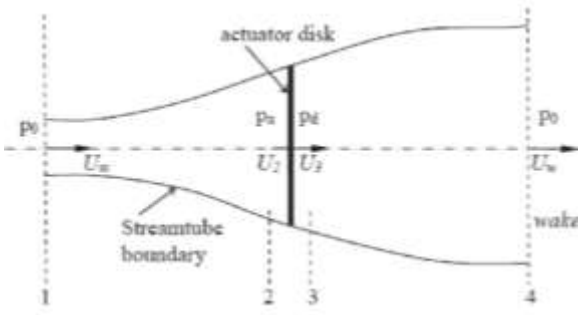

Figure 5.6. Actuator disc model (Kulunk, E. 2011)

The analysis of the actuator disc theory assumes a control volume in which the boundaries are the surface walls of a stream tube and two cross-sections. Four sections are made where the control

volume is analyzed: 1) free-stream region, 2) just before the blades, 3) just after the blades, 4) far wake region. The mass flow rate remains the same throughout the flow. It is assumed that the velocity through the disc is continuous, thus: $U_2 = U_3 = U_R$ (Kulunk, E. 2011).

The thrust coefficient of the rotor C_T can be determined with the following equation (Ginhoven, J. van, 2006):

$$C_T = \frac{T}{\frac{1}{2}\rho U^2 A} = \frac{2Aa\rho(1-a)U^2}{\frac{1}{2}\rho U^2 A} = 4a(1-a) \tag{5.6}$$

Where:

T Thrust which is, under unideal conditions, dependent on the dimensions of the rotor and the aerodynamic design versus settings of the rotor blades.

a Axial induction factor $a = \frac{U_\infty - U_R}{U_\infty}$, which represents the relative variation of the undisturbed wind speed from the free-stream region up to just after the blades.

The following applies under ideal conditions: $U_R = \frac{2}{3}U_\infty$, this leads to an induction factor of $a = \frac{1}{3}$. Now the value for the thrust coefficient C_T can be obtained (Ginhoven, J. van, 2006):

$$C_T = 4a(1-a) = 4 \cdot \frac{1}{3}\left(1 - \frac{1}{3}\right) = 0{,}89$$

Under non-ideal conditions, this value depends on the dimensions of the rotor and the aerodynamic design. The maximum drag coefficient is reached when the rated wind speed is assumed, and not the cut-out wind speed. When the latter would be the case, the flow velocities would be larger which leads to a decrease in drag since the angle of attack of the rotor blades will be smaller to remain constant revolutions of the blades for a constant energy production.

Now the value for the horizontal load exerted by the rotor blades can be calculated with the following formula:

$$F_{wind,rotor} = \frac{1}{2} C_T \rho_{air} A_{rotor} {v_r}^2 \tag{5.7}$$

Where:

C_T	thrust coefficient of the rotor	[-]
ρ_{air}	density air	[kg/m^3]
A_{rotor}	swept area	[m^2]
v_r	rated wind speed	[m/s]

The wind flow also exerts a force on the cylindrical tower. In order to calculate this force a value for the shape drag coefficient C_w needs to be determined. This can be done with the aid of Figure 5.7: h/d = 70/4= 17,5. Interpolating gives a value for C_w of 0,85. The cut-out wind speed of the turbine results in the highest wind load on the tower, thus a wind speed of 30m/s is assumed.

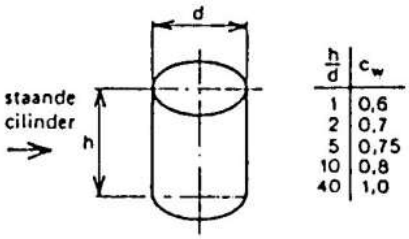

Figure 5.7 Drag coefficient for a cylinder (Hydromechanica 1, 2005)

The horizontal load on the tower as a result of the wind can be determined with the following formula:

$$F_{wind,tower} = \frac{1}{2} C_w \rho_{air} A_{tower} {v_c}^2 \tag{5.8}$$

Where:

C_w	shape drag coefficient	[-]
ρ_{air}	density air	[kg/m^3]
A_{tower}	area facing wind flow	[m^2]
v_c	cut-out wind speed	[m/s]

6. Literature study on fatigue

6.1 Fatigue in general

Wind turbines are continuously subjected to varying loads. Because of this, a fatigue analysis is an important feature in designing wind turbines. In EN 1999-1-3, fatigue is defined as: 'weakening of a structural part, through crack initiation and propagation, caused by repeated stress fluctuations.' In other words: damage caused by repeated application of stresses. The more cycles occur, the lower the stress (range) required till failure. The damage caused by fatigue is cumulative; the material does not recover itself. Three important aspects are (Soetens, F., et al, 2014):

- The stress range *S*;
- The number of cycles *N*;
- (To a lesser extent) the mean stress $\sigma_m = \frac{\sigma_{min}+\sigma_{max}}{2}$ or the stress ratio $R = \frac{\sigma_{min}}{\sigma_{max}}$. The fatigue strength provided in EN 1999-1-3 is based on a relatively high mean stress.

The fatigue life consists of three phases, see Figure 6.1 (Soetens, F., et al, 2014):

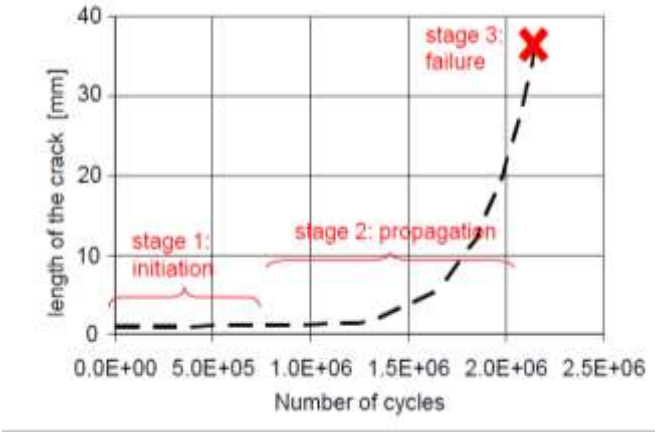

Figure 6.1. The three stages of fatigue life (Soetens, F. et al, 2014)

Initiation

This phase is characterized by the formation of slip bands, resulting in intrusions and extrusions at the specimen surface which can be considered as microcracks. Subsequently, these microcracks merge, thereby forming small cracks, typically in the order of several grains. During this stage, it is impossible to observe degeneration of the material on macroscopic level.

Crack propagation

As the microcracks grow, the stress state at the crack tip becomes more severe so that crack growth advances progressively both in length and width direction. In this stage the crack propagates approximately perpendicular to the direction of local maximum principal stress range. In this stage, the crack is detectable using special techniques, or even by the naked eye if the crack has grown to a large size.

Failure

As the crack grows, the remaining ligament decreases and at a certain point it may no longer be able to bear the loads due to interaction of yielding and fracture. The latter aspects are a function of the maximum applied stress, the crack size, the 0,2% proof stress of the material and the fracture toughness of the material.

The following items have a negative impact on the fatigue resistance (Ginhoven, J. van, 2006):

- Corrosion and a rough surface
- Grooves or sharp welded joints
- Internal forces

Furthermore, components which are loaded in tension decrease the fatigue life of the structure while compression increases it.

6.2 Safe life design

EN 1999-1-3 states: 'The aim of designing a structure against the limit state of fatigue is to ensure, with an acceptable level of probability, that its performance is satisfactory during its entire design life, such that the structure shall not fail by fatigue nor shall it be likely to require undue repair of damage caused by fatigue during the design life.'

The design of aluminium structures against the limit state of fatigue may be based on the following three design methods: damage tolerant design, design assisted by testing or safe life design, which is the most commonly used method to check fatigue failure (Soetens, F., et al, 2014).

The safe life design method involves prediction of the stress histories at potential initiation sites, followed by counting of load cycles with the associated stress ranges and compilation of stress spectra. From this information an estimate of the design life is made using the appropriate stress range endurance data for the constructional detail concerned (EN 1999-1-3, 2007).

To ensure sufficient resistance of the component or structure, the safe life design method may be based on the linear damage accumulation calculation (Palmgren-Miner's summation). In this procedure, the damage value (D_L) for all cycles should fulfil the condition:

$$D_L \leq D_{lim} \tag{6.1}$$

Where:

D_{lim} tolerable value of the fatigue damage. A recommended maximum value is 1,0.

D_L $= \sum \frac{n_i}{N_i}$

Where:

n_i = number of stress cycles $\Delta\sigma_i$

N_i= predicted number of stress cycles till failure of stress range $\Delta\sigma_i$

The number of cycles n_i involves counting the number of stress cycles that will occur during the element's expected lifetime. For constant-amplitude cycles it may not be difficult to obtain the number of cycles during lifetime. In variable-amplitude cycles occur more frequently. To be able to obtain the number of variable-amplitude cycles during lifetime, a cycle counting method such as the rainflow or the reservoir method can be used. The first method is more suited for numerical implementation

whereas the last mentioned method is easier to visualize. The result of both methods is the same (Soetens, F., et al, 2014).

As briefly mentioned before, when the predicted number of cycles to failure increases the stress range for fatigue design decreases. The generalized form of this relationship is shown in Figure 6.2, plotted on a logarithmic scale. This so-called S-N curve, giving the characteristic number of cycles to failure N, as a function of the stress range $\Delta\sigma$, is split into two parts: one part in the range between 10^5 to $5x10^6$ cycles (part I) ($2x10^5$ for plain material), the other part in the range between $5x10^6$ to 10^8 cycles (part II). The stress range at the transition between part I and part II, $\Delta\sigma_D$, is referred to as the constant amplitude fatigue limit (CAFL). Range II only applies in case of a variable amplitude load with at least some stress ranges above $\Delta\sigma_D$. In case of a constant amplitude load with stress ranges below $\Delta\sigma_D$, or a variable amplitude load with all stress ranges below $\Delta\sigma_D$, an infinite life results according to the dotted curve in Figure 6.2. Further, stress ranges below $\Delta\sigma_L$ are considered non-damaging even in case of a variable amplitude loading. The contribution to damage caused by these stress ranges is so small that it does not have to be considered (Soetens, F., et al, 2014).

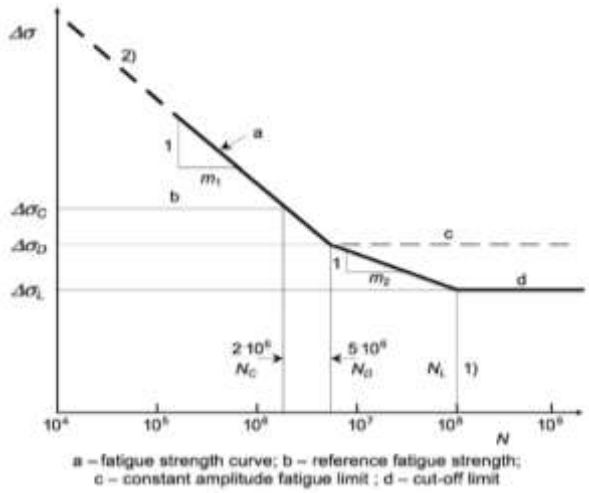

Figure 6.2. Logarithmic fatigue strength curve (EN 1999-1-3, 2007)

6.3 Fatigue concerning offshore wind turbines

The fatigue limit state claims that the design fatigue lifetime has to be longer than the design lifetime, which is expressed in the number of stress cycles. In this thesis, the design lifetime of a wind turbine is assumed to be 20 years. The number of cycles in 20 years depends on the period of the loading. Loads due to wind and waves and dynamic response due to resonant effects are the main sources of stress fluctuation concerning offshore wind turbines.

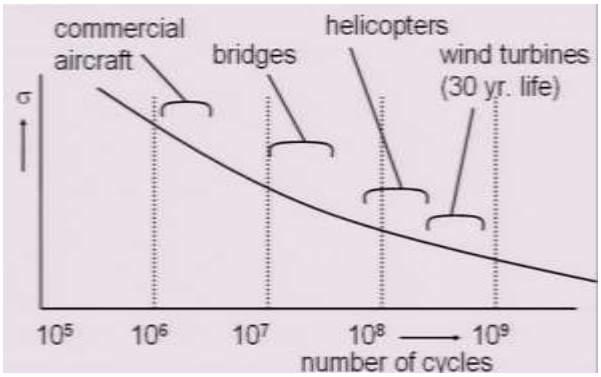

Figure 6.3. Number of cycles for different structures (Bussel, G.J.W. van, 2009)

Figure 6.3 shows that wind turbines experience an extreme amount of cycles. Thus, wind turbines typically require long service lives in order to be cost effective. Although this figure shows a wind turbine with a lifetime of 30 years, a turbine with a lifetime of 20 years will also be in the range of 10^8 – 10^9 cycles (Bussel, G.J.W. van, 2009).

Fatigue prone locations on the wind turbine are the hinged connection between tower and nacelle, the mechanic components in the nacelle and the rotor blades (Ginhoven, J. van, 2006). Of course, the tower itself is also prone to fatigue. In this thesis will only be checked if the tower is resistant against fatigue.

The recognized standard for the fatigue analysis of wind turbines is the Palmgren-Miner linear damage rule, commonly called Miner's Rule, which has already been explained in *Paragraph 6.2 Safe life design*. Now it shall be discussed more extensively. The damage law may be written in the following form:

$$\sum_{i}^{M} \frac{n_i}{N_i} = \frac{n_1}{N_1} + \frac{n_2}{N_2} + \frac{n_3}{N_3} + \cdots . + \frac{n_M}{N_M} = D \tag{6.2}$$

Where the total damage D is sustained by a structure that undergoes n_1 stress cycles at stress level σ_1, n_2 stress cycles at stress level σ_2, and so on for all stress levels through the final level of M. N_i is the number of cycles to failure at stress level σ_i. It is a measure of the material's ability to endure stress cycles. The number of cycles n_i is usually taken to be the number of full cycles, but the number of reversals (two reversals for each full cycle) or the number of 'cross-overs' (zero-crossings) are also possible. The stress level is usually taken to be the amplitude or range at a given R value or mean stress.

Miner's Rule assumes that structural failure will occur when the damage equals one. It appears that over a wide range of references the computed damage D at failure varies between 0,79 and 1,53. When dealing with wind turbines, additional uncertainties arise from the variation in material properties and applied loads. Thus, differences of a factor of 2 between damage predictions and measured lifetimes are not only common in wind turbine application; they should be expected (Sutherland, H.J., 1999).

Three sets of information are required to estimate the service lifetime of a wind turbine: the fatigue load cycles on the turbine as a function of the inflow conditions, the S-N behavior of the material(s) being analyzed, and the annual wind speed distribution.

7. References

ALUMINIUM DESIGN (2015) *Joining Aluminium* and *Corrosion Resistance* www.aluminiumdesign.net/design-support/

AALCO (2015) *Introduction to Aluminium and its alloy* www.aalco.co.uk/datasheets/

AHLSTRÖM A. (2002) *Simulating Dynamical Behaviour of Wind Power Structures*, Licentiate Thesis, Royal Institute of Technology; Department Mechanics

ALCOA (2015) *General Engineering Plates*, Alcoa Global Commercial Transportation, Industrial and Specialties

ANCONA D. AND MCVEIGH J. (2001) *Wind turbine – Materials and Manufacturing Fact Sheet*, Princeton Energy Resources International LLC

ASCE 7-05 (2006) *ASCE Standard for Minimum Design Loads for Buildings and Other Structures,* The American Society of Civil Engineers

AVALLONE E.A. AND BAUMEISTER T. (19996) *Mark's Standard Handbook for Mechanical Engineers*

BROCKMANN W. ET AL (2008) Adhesive Bonding: Adhesives, Applications and Processes - Materials, Applications and Technology

BUSSEL, G.J.W. VAN (2009) *Introduction to Wind Energy,* online reader 3TU course

CERDA SALZMANN D.J. AND TEMPEL J. VAN DER (2005) *Aerodynamic Damping in The Design of Support Structures for Offshore Wind Turbines*, Duwind, Faculty of Civil Engineering and Geosciences, Delft University of Technology

CHEN B. (2012) *Introduction to Wind Turbine* www.bindichen.co.uk/post/Wind%20Turbine/Introduction%20to%20Wind %20Turbine.html

CLAUSEN A.V. (2012) *Tips for Offshore Wind Corrosion Protection,* Hempel A/S www.renewableenergyworld.com/rea/news/article/2012/12/tips-for-offshore-corrosion-protection

DNV (2014) *Design Of offshore Wind Turbine Structures*, Det Norske Veritas Offshore Standard, May 2014

EN 1999-1-3 (2007) *Eurocode 9: Design of aluminium structures - Part 1-3: Structures susceptible to fatigue*

ENGINEER STUDENT (2014) *MIG Welding (Metal Inert Gas)* www.engineerstudent.co.uk/mig_welding.php

FISCHER T., DE VRIES W., SCHMIDT B. (2010) *Upwind Design Basisl WP 4: Offshore Foundations and Support Structures,* Endowed Chair of Wind Energy (SWE) at the Institute of Aircraft Design Universität Stuttgart

FRICTION WELDING HOLLAND (2015) *The perfect weld for piston rods, tubes and forgings,* Friction Welding Holland B.V.

http://www.frictionweldingholland.com/friction-frictionwelding-welding-frictionweld.html

GAMESA (2010) *Design and Manufacture; Manufacturing and assembly process* www.gamesacorp.com/en/products-and-services/wind-turbines/design-and-manufacture/manufacturing-and-assembly-process.html

GERRIITSEN (2015) *Lengte transport* www.gerritsentransport.nl/packaging/129.html

GERVEN (2011) *Optimising the Design of a Steel Substructure for Offshore Wind Turbines in Deeper Waters,* MSc thesis, Delft University of Technology, Faculty of Civil Engineering & Geosciences

GINHOVEN, J. VAN (2006) *Het effect van erosie en grondeigenschappen op het dynamische gedrag van offshore windturbines, betreffende stalen en betonnen mono paal funderingen,* M.Sc. rapport offshore windturbines, Delft University of Technology, Faculty of Civil Engineering & Geosciences

HANZLASER (2015) Advantage & disadvantage analysis of laser welding machine

www.hanzlaser.com/service/laser-knowledge/311.htm

HÖGLUND T. ET AL. (2014) *AluMATTER* www.aluminium.matter.org.uk/

HORIZON ALUMINIUM (2015) *Products; Custom Shape* www.aluhorizon.com/custom_shape.html

HYDRODYNAMICA 1 (2005) Dictaat mt501, Delft

JONKMAN J.M. (2007) *Dynamics Modeling and Loads Analysis of an Offshore Floating Wind Turbine*, Technical rapport, National Renewable Energy Laboratory, pp 1-2

KÜHN (1997) *Soft Stiff; A Fundamental Question for Designers of Offshore Wind Energy Converters,* EWEC '97

KÜHN (1999) *Design Optimisation of an Offshore Wind Energy Converter by Means of Tailored Dynamics,* EWEC '99

KÜHN (2001) *Dynamics and Design Optimisation of Offshore Wind Energy Conversion Systems*

KULUNK, E. (2011) *Aerodynamics of Wind Turbines, Fundamental and Advanced Topics in Wind Power,* Rupp Carriveau (Ed.), InTech

LINCOLN ELECTRIC (2015) Aluminum Welding Frequently Asked Questions

www.lincolnelectric.com/en-us/support/welding-solutions/Pages/aluminum-faqs-detail.aspx

MANWELL J.F., MCGOWAN J.G., AND ROGERS A.L. (2002) *Wind Energy Explained- Theory, Design and Application,* Rogers, University of Massachusetts, Armherst, USA

MATWEB (2015) *Aluminum Alloy Heat Treatment Temper Designations*, Material Property Data www.matweb.com/reference/aluminumtemper.aspx

MMS (2006) *Technology White Paper on Wind Energy Potential on the U.S. Outer Continental Shelf,* Minerals Management Service, Renewable Energy and Alternate Use Program, U.S. Department of the Interior, May 2006

MTI (2013) *Friction Stir Welding*
www.mtiwelding.com/friction-stir-welding.html

NEDAL (2015) Nedal Aluminium
www.nedalextrusion.com/

NEN-EN-IEC 61400-3 (2009) *Wind turbines - Part 3: Design requirements for offshore wind turbines*

NICHOLSON J.C. (2011) *Design of wind turbine tower and foundation systems- optimization approach,* MS thesis, University of Iowa

SAPA (2013) *Meeting design challenges of turbines,* SAPA Group
www.sapagroup.com/en/sapa-profiler-ab/news/2013/meeting-desing-challenges-of-turbines/

SAPA (2014) *Handboek voor ontwerpers; Succes met Aluminium Profielen,* SAPA Group

SAPA (2015a) *SAPA Extrusion Benelux*
www.sapagroup.com/nl/sapa-extrusion-benelux/wie-is-sapa/profiles-nederland/

SAPA (2015b) *SAPA Bonding of Aluminium*
www.sapagroup.com/upload/Sapa_Bonding_Aluminum.pdf

SAPA (2016) *Joining aluminium*
http://www.aluminiumdesign.net/design-support/joining-aluminium/

SOETENS F. ET AL. (2014) *Aluminium Structural Design; Lecture handbook 'Aluminium Structures'* Eindhoven University of Technology, Department Architecture, Building and Planning, Unit Structural Design, Chair Aluminium Structures

STEVENSON, J.D. (1980) *Structural Damping Values as a Function of Dynamic Response Stress and Deformation Levels*, Nuclear Engineering and Design 60 211-237

SUTHERLAND H.J. (1999) *Fatigue Analysis of Wind Turbines,* Sandia National Laboratories

TALAT 1302 (1994) *Aluminium Extrusion: Alloys, Shapes and Properties,* Training in Aluminium Application Technologies (TALAT) Lecture 1302

TALAT 1501 (1999) *Aluminium: Physical Properties, Characteristics and Alloys,* Training in Aluminium Application Technologies (TALAT) Lecture 1501

TEMPEL J. VAN DER (2006) *Design of Support Structures for Offshore Wind Turbines;* Proefschrift april 2006

TEMPEL J. VAN DER AND MOLENAAR D. (2002) *Wind Turbine Structural Dynamcis – A Review of the Principles for Modern Power Generation, Onshore and Offshore,* Wind Engineering Volume 26, No. 4, 2002

THREADGILL, P.L. ET AL. (2009) *Friction Stir Welding of Aluminium Alloys*, International Materials Review, vol.54. no.2. March 2009. pp. 49-93.

www.twi-global.com/technical-knowledge/published-papers/friction-stir-welding-of-aluminium-alloys/

URAZ E. (2011) *Offshore Wind Turbine Transportation & Installation Analyses; Planning Optimal Marine Operations for Offshore Wind Projects*, Gotland University, Department of Wind Energy

WELDGURU (2015) *Welding methods*
www.weldguru.com

WIJNGAARDEN M. VAN (2013) *Concept Design of Steel Bottom Founded Support Structures for Offshore Wind Turbines*, Bachelor Thesis, Delft University of Technology, Faculty of Civil Engineering and Geosciences

WORLD STEEL (2012) *Steel Solutions in the Green Economy; Wind Turbines*, World Steel Association

WWEA (2014) *Components of a Wind Turbine,* World Wind Energy Association
www.wwindea.org/technology/ch01/en/1_2.html

ZAMAN, P.B. (2014) *Other Welding Process*
www.coursehero.com/file/8724349/L4-Other-Welding-Process/

Appendix A

Natural frequencies (Wijngaarden, M., 2013)

A main parameter in the design of support structures for offshore wind turbines is the natural frequency of the turbine/support-structure system. This can be determined with the schematized 2-mass-spring-dashpot system of Figure 4.4.

First of all, the mass, damping and stiffness matrix have to be determined to solve the differential equation. This is done by analyzing the free body diagram of the 2-mass spring damper system with Newton's law of motion, see figure below.

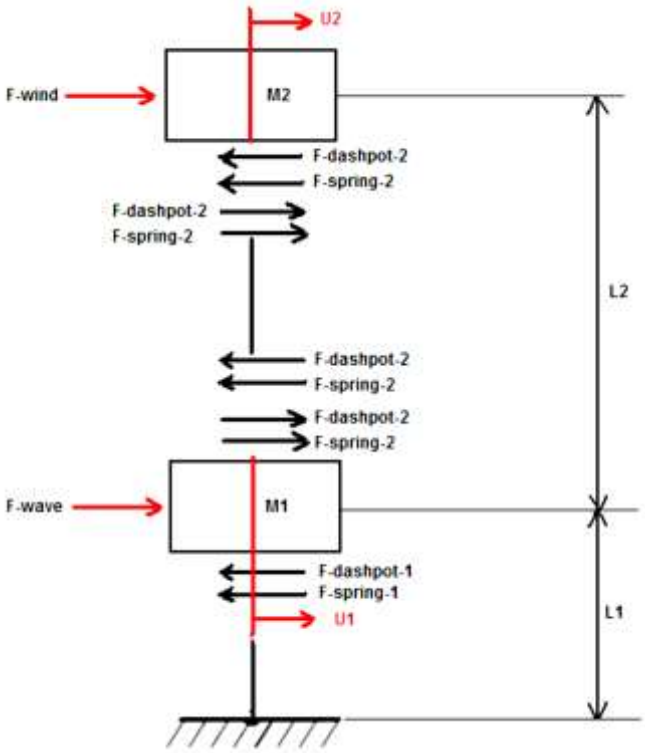

Figure A1. Free body diagrams of both masses (Wijngaarden, M., 2013)

For mass m_1 the law of motion results in:

$$m_2 \frac{d^2u_2}{dt^2} = F_{wind} - F_{dashpot\,2} - F_{spring\,2}$$

$$m_2 \frac{d^2u_2}{dt^2} + c_2\left(\frac{du_2}{dt} - \frac{du_1}{dt}\right) + k_2(u_2 - u_1) = F_{wind}$$

For mass m_2 this results in:

$$m_1 \frac{d^2u_1}{dt^2} = F_{wave} + F_{dashpot\,2} + F_{spring\,2} - F_{dashpot\,1} - F_{spring\,1}$$

$$m_1 \frac{d^2u_1}{dt^2} - c_2\left(\frac{du_2}{dt} - \frac{du_1}{dt}\right) - k_2(u_2 - u_1) + c_1\frac{du_1}{dt} + k_1u_1 = F_{wave}$$

This system of coupled equations can be rewritten in matrix form

$$\begin{bmatrix} m_1 & 0 \\ 0 & m_2 \end{bmatrix}\begin{bmatrix} \ddot{u}_1 \\ \ddot{u}_2 \end{bmatrix} + \begin{bmatrix} c_1 + c_2 & -c_2 \\ -c_2 & c_2 \end{bmatrix}\begin{bmatrix} \dot{u}_1 \\ \dot{u}_2 \end{bmatrix} + \begin{bmatrix} k_1 + k_2 & -k_2 \\ -k_2 & k_2 \end{bmatrix}\begin{bmatrix} u_1 \\ u_2 \end{bmatrix} = \begin{bmatrix} \bar{F}_{wind} \\ \bar{F}_{wave} \end{bmatrix}\cos(\omega t - \theta)$$

Now the mass, damping and stiffness matrix are determined and can be filled with the values of the individual springs and dashpots. In order to determine the natural frequencies of the 2-mass-spring-dashpot system, the right hand side is set at 0. The displacement will be of a harmonic type with

amplitude $\bar{u}$, radial velocity ω and phase angle θ. The first and second derivative can be determined, and put into the matrix equation:

$$u(t) = \bar{u}\cos(\omega t - \theta)$$

$$\dot{u}(t) = -\bar{u}\,\omega\sin(\omega t - \theta)$$

$$\ddot{u}(t) = -\bar{u}\,\omega^2\cos(\omega t - \theta)$$

Which leads to the following matrix equation:

$$\begin{bmatrix} -m_1\omega^2 + k_1 + k_2 & -k_2 \\ -k_2 & -m_2\omega^2 + k_2 \end{bmatrix}\begin{bmatrix}\bar{u}_1\\ \bar{u}_2\end{bmatrix}\cos(\omega t - \theta) + \begin{bmatrix} -\omega(c_1 + c_2) & \omega c_2 \\ \omega c_2 & -\omega c_2 \end{bmatrix}\begin{bmatrix}\bar{u}_1\\ \bar{u}_2\end{bmatrix}\sin(\omega t - \theta) = \begin{bmatrix}0\\0\end{bmatrix}$$

This equation can be solved with an in-phase ($\cos(\omega t-\theta)$) and out-of-phase ($\sin(\omega t-\theta)$) part. The in-phase ($\cos(\omega t-\theta)$) part leads to an equation from which the natural frequency can be determined. Therefore, only the in-phase part is relevant in this case. The dampening is neglected, as this will have a minor influence on the natural frequency. A trivial solution can directly be seen, namely when the amplitude of the harmonic equation is 0, which is not very interesting. In that case the structure will not move at all. The in-phase part can only satisfy the 0 vector, if the determinant of the matrix on the left hand side is 0, because the harmonic time-function cannot be 0 for all of the time. The determinant of the left hand side matrix can easily be determined, which yields an equation from which the natural frequency can be determined:

$$m_1 m_2\omega^4 - \omega^2(m_1 k_2 + m_2(k_1 + k_2)) + k_1 k_2 = 0$$

From this equation four angular velocities can be determined, but two will be of a negative sign and do not have any physical meaning, so only two angular frequencies remain: $\boldsymbol{\omega}_1$ and $\boldsymbol{\omega}_2$ (rad/s). Now the two natural frequencies can be determined as well:

$$f_{1,2} = \frac{\omega_{1,2}}{2\pi} \qquad [\text{Hz}]$$

The two masses and two stiffness parameters have been determined as well, and are shown below:

m_1 [tons]	m_2 [tons]	k_1 [N/m]	k_2 [N/m]
6.5*10^3	5.3*10^2	1.64*10^8	1.08*10^6